Development and Design of Self-Sensing SMAs using Thermoelectric Effect

Vijaya Venkata Narasimha Sriram Malladi

Thesis submitted to the Faculty of the
Virginia Polytechnic Institute and State University
in partial fulfillment of the requirements for the degree of

Master of Science
in
Mechanical Engineering

Pablo A. Tarazaga, Chair
Daniel J. Inman
Andrew J. Kurdila

20^{th} May, 2013
Blacksburg, Virginia

Keywords: Shape Memory Alloys, Sensorless Control, Seebeck Coefficient, Thermoelectric Effects, ANFIS, Postion Control, ANN

Development and Design of Self-Sensing SMAs using Thermoelectric Effect

Vijaya Venkata Narasimha Sriram Malladi

Abstract

Active research of SMAs has shown that its Seebeck coefficient is sensitive to its martensitic phase transformation and has the potential to determine the SMAs state of transformation. The combination of Shape Memory Alloys, which have a positive Seebeck coefficient, and Constantan which has a negative Seebeck coefficient (-35 mV/K) results in a thermocouple capable of measuring temperature. The work presented in this thesis is based on the development and design of this sensor.

This sensor is used to study the hysteretic behaviour of SMAs. Although Shape Memory Alloys (SMAs) exhibit a myriad of nonlinearities, SMAs show two major types of nonlinear hysteresis. During cyclic loading of the SMAs, it is observed that one type of hysteretic behavior depends on the rate of heating the SMAs, whilst the variation of maximum temperature of an SMA in each cycle results in the other hysteretic behavior. This later hysteretic behavior gives rise to major and minor nonlinear loops of SMAs. The present work analyzes the nonlinearities of hysteretic envelopes which gives the different maximum temperatures reached for each hysteretic cycle with respect to stress and strain of the SMA. This work then models this behavior using Adaptive Neuro Fuzzy Inference System (ANFIS) and compares it to experimental results. The nonlinear learning and adaptation of ANFIS architecture makes it suitable to model the temperature path hysteresis of SMAs.

वागर्थाविव सम्पृक्तौ वागर्थप्रतिपत्तये ।

जगतः पितरौ वन्दे पार्वतीपरमेश्वरौ ॥

Meaning: In search of knowledge of words and their meanings, I pay homage to Parvathi and Paramesvara, the parents of the Universe who are inseparably blended together like the word and its meaning.

Acknowledgements

I wish to express my gratitude and deepest appreciation to my advisor, Professor Pablo A. Tarazaga for his great interest and assistance in the pursuit of scientific research during these years. I acknowledge his strategic guidance concerning the development and implementation of this work. As my supervisor he gave me the freedom to experiment and swim across this research ocean with great patience.

I would also like to thank my committee members, Prof. Daniel J. Inman and Dr. Andrew J. Kurdila. I always knew that I could turn to you for the insight and advice I needed in the course of my research.

I wish to thank my colleagues Bryan Joyce, Jeremy Kolansky, Dragan Avirovic, Mohammad Albakri, Ravi Anant, Joseph Hamilton, Ethan Robinson and Mathieu Vandaele for many fruitful discussions that have directly or indirectly lead to the completion of my work. I would specially thank Carlos E Garcia for helping and bearing with me throughout his time at Virginia Tech. I wish to thank my friends and roommates for making my time in the USA pleasant and enjoyable.

The help and guidance of many people have brought me to this position. I cannot forget to thank Vanessa Tarazaga for helping me edit this thesis. I cannot thank Justin Farmer enough for all his help and assistance with things inside and outside the lab. He has been the final solution for all my problems with lab equipment. I would also like to take this opportunity to thank Beth Howell for the time she has taken to help me take care of my paper work. She has made my time in CIMSS pleasant and hassle free.

I believe that "*A person who thanks his mother and father is the worlds greatest fool*". In one life-time, it is impossible for any person to count and acknowledge the sacrifices made by these people. I fail to find words to express my gratitude towards these "*first* "teachers. I humbly bow my head at the feet of my parents,

Dr. Varalakshmi Malladi and B.V.L.N.Swamy Malladi. I would love to thank my sister, Satya Sarvani Malladi, for the love and friendship we have developed as siblings. I am grateful to my aunt Dr. Padmavathi Garimella for motivating me to pursue the path of research.

But none of this is possible with out the love of Almighty.

ఎవ్వనిచే జనించు జగమెవ్వని లోపల నుండు లీనమై,
యెవ్వని యందు డిందుఁ బరమేశ్వరుఁ డెవ్వఁడుమూలకారణం,
బెవ్వఁ డనాదిమధ్యలయుఁ డెవ్వఁడు సర్వముఁ దానయైనవాఁ,
డెవ్వఁడు వాని నాత్మభవు నీశ్వరు నే శరణంబు వేడెదన్.

Meaning: I pay my obeisance to such God by whom this universe is created; in whom it is contained; into whom it is dissolved; who is the supreme ruler; who is the root-cause of this universe; who neither has beginning nor end; who takes the forms of all the animate and the inanimate, the visible and the invisible.

Contents

List of Figures

List of Tables

Nomenclature

Acronyms

ANFIS	Adaptive Neuro-Fuzzy Inference System
ANN	Artificial Neural Networks
FIS	Fuzzy Inference System
FLS	Fuzzy Logic System
GENFIS	Generalized Fuzzy Inference System
GRNN	Generalized Regressive Neural Networks
MF	Membership Function
MISO	Multi-Input Single Output
RMSE	Root Mean Squared Error
SMA	Shape Memory Alloy
SMART	Shape Memory Alloys in Real Time

Chapter 1

Introduction

1.1 Motivation

The dawn of the 21^{st} century has witnessed a relentless pursuit of development of actuators and sensors based on Smart Materials. Shape Memory Alloys (SMAs) is one such material which has been in focus for its superior physical characteristics and better power to weight ratio. Although the potential properties of this material were discovered in the 1960's by the US Naval Ordance Laboratory (Buehler et al. [1963]), it is this last decade which has seen a enormous interest in utilizing these mechanical properties as a viable actuator. Engineers in various industries ranging from aerospace (Hartl and Lagoudas [2007]) and naval (Shinjo and Swain [2004]) departments, to surgical (Morgan [2004]) and medical sectors (Chen et al. [2004]), have worked towards converting thermal energy into mechanical work through the use of SMAs.

Research (Ryhänen [1999]) has shown that Ni-Ti based SMAs have a non-toxic and non-irritant response towards muscular tissues. This work has shown that the bio-compatibility of Ni-Ti is similar to, or better than other materials presently used in medical applications. The mechanical properties of this material make it possible to develop a self-locking, self-expanding and self-compressing medical equipment. With optimal surface treatment, this work has shown that SMAs can be utilized in long-term implants. The elevation of SMAs as a bio-material has created a new wave of research in integrating exo-skeleton structures within the human body. Although several designs (Bundhoo et al. [2009]; De Laurentis and Mavroidis [2002]; Esfahani and Elahinia [2010]; Price et al. [2007]) of SMA based actuators

aimed at mimicking the kinematics of a human hand have been developed, it has proven difficult to track the biological trajectories of hands. Inherent complexity and non-linearity of martensitic phase transformation of SMAs has made it difficult to control SMA wires.

The "shape memory effect"of SMAs has facilitated the use of thin wires in various actuator configurations. Different shapes and designs of SMA springs (Menciassi et al. [2002, 2004]) have been utilized in robotic applications for enhancing and adapting the properties of SMA based actuators. The force and displacement developed by heating SMA wires has to be discretely controlled in some of these shape set structures, particularly those used in instruments engaged for minimal invasive surgeries (Maeda et al. [1996]). In such applications, the constantly changing temperature of the foreign environment severely complicates the energy required from an external heat source needed to compensate for heat transfer by conduction. In these applications, monitoring the change in shape of these structures due to multiple sources of temperature, is critical in order to control them. Micro and mini devices working in such space constraint situations, require an actuator capable of sensing the effective temperature profile which regulates the motion of the structure.

When designing an SMA based actuator for a mechanism, one has to first decide on the heating source for the SMA element. In certain specialized applications (Morgan and Yaeger [1985]), the temperature of the surrounding medium can be used as a source of heat.This method provides an excellent option when designing mechanisms that regulate the temperature of the actuator element. If the control temperature required to initiate and complete the phase transformation changes, the whole SMA element has to be changed and a new setup has to be assembled. Even though research in material properties of SMAs (Kohl et al. [2000]) is looking into adjustable material properties, it is not practically feasible to cover the whole temperature domain. External and intentional heating of SMAs is the only solution for this problem.

In course of using SMAs, for the purpose of actuation, various methods of heating SMAs have been researched and tested. One of the traditional ways of heating SMAs is by utilizing the concept of Joule heating (Hirose et al. [1988]). When electric current flows through the SMA wires, the power dissipated due to the electric resistance of the material raises the temperature of the structure and activates it. The demand of various applications has led to experimentally actuating SMA wires with a laser (Avirovik et al. [2013]). This work uses

energy from the ultraviolet region of light spectrum to heat the SMA wires. In another study Thermo-Electric Devices (TEDs) (Selden et al. [2006]) have been used to transfer heat energy into SMA wires by conduction. There are many other applications(Elzey et al. [2005]) where resistive heating of SMAs is not practicable and new heating methods have been implemented.

Although the electrical resistivity measurement approach is popular, there are some advantages and some disadvantages of engaging ohmic heating over unconventional modes of heating. In this, electrical resistance can be used to sense and relate it to the temperature change of the SMAs. One of the major advantage of this is method is the possible use of resistivity measurements of SMA wires for closed loop feed-back applications. But the resistance measurement across the terminals of a wire, reflects the temperature averaged throughout the length of the wire. The level of phase transformation along the length of a wire depends on the actual temperature distribution rather than on any average measurement. Thus, in applications where the actual stress or strain profile of the SMA wire is required, this feedback approach is limited.

Another disadvantage of using resistivity of SMAs to feedback the level of phase transformation is that it is restricted to those cases where SMAs are heated by ohmic methods. A closed electrical circuit is required to measure the changes in resistance of SMA wires. This is possible in cases whre SMA wires have been heated by electric current and resistance. The other limitation of Joule's resistive heating approach is its large electric power requirement for achieving complete phase transformation. The electrical efficieny of this mode of heating is less than 10 precent. As this factor plays a major role in one-dimensional systems, it is impractical to scale this method of heating into activating two- dimensional structures like SMA ribbons (Barbarino et al. [2009]) or films (Craciunescu and Wuttig [2000]; Krulevitch et al. [1996]). As the focus is increasingly shifted to harnessing the physical properties of these 2D structures (Hassan et al. [2004]) as actuators, there is now a need for non-traditional modes of heating to actuate these structures. Although different applications might lead to different methods of heating SMAs, the major feature of these modes of actuation would be to directly raise the temperature of the SMA system. So, to develop future SMA based actuators, a methodology which can detect the temperature of SMA which can be adapted to any mode of heating, is required.

With this understanding of all the limitations and the present research in SMA actuators, a sensor capable of determining the change in temperatures was designed based on the thermoelectric properties of SMAs. A thermocouple was built by paring a positive Seebeck Coefficient material, Shape Memory Alloy, with a negative Seebeck coefficient (-35 mV/K) material, Constantan. The bi-material junction of this sensor utilizes the relative thermoelectric properties of this compound system to sense the tip temperature.

One of the advantages of the developed technique is that it can be adapted to any mode of heating. When multiple Constantan wires are welded onto a single SMA wire, numerous bi-material contacts are formed. This hybrid configuration is a potential source of sensing temperature at different locations at the same time. This gives a more viable temperature distribution at different points contrary to the average measurements in conventional feedback practices. Although the concept put forward in this work is applicable to higher dimensional systems, the present work is confined to one-dimensional system of wires. The proposed technique is applicable for higher dimensional systems with complex dynamics due to the geometric independence of Seebeck voltage. The proposed concept is equally useful in thin structures, such as wires and ribbons, and in 2D-structures, like membranes and plates.

1.2 Previous Work

The rapid boom in developing applications using SMAs has produced a considerable amount of research in studying and modeling SMA wires and structures. Many soft-computing methodologies have been developed deriving inspiration from nature. The following sections will focus on previously completed work covering SMAs and artificial intelligence methods. A brief introduction on soft-computing methods used in the present work are also presented.

1.2.1 Shape Memory Alloys

Shape memory alloy actuators, which have the ability to return to a predetermined shape when heated, and has the potentia to be used in numerous applications. On the other hand, there has been little success in accurately controlling the motion of SMAs since the inherent systems dynamics are highly nonlinear and a unified model is unable to simulate

these properties. This problem has been attacked in various fronts including deterministic methods and non-deterministic methods. Some of these advances are presented in this section.

Many applications of SMAs require a precise model to study changes in their mechanical behavior with phase transformation. Researchers have tried to understand the mechanics behind these changes and to develop a precise, theoretical or constitutive model of SMAs. This type of modeling approach has been significantly challenging due to their nonlinear thermo-mechanical behavior. Substantial research has been conducted over the past three decades with the aim of developing constitutive models that can predict SMA thermo-mechanical behavior. The basis for the development of present research in this field is based on the models proposed by Bertram [1983]; Birman [1997]; Brinson [1993]; Liang and Rogers [1990]; Tanaka [1986]. One way of theoretically modeling macroscopic behaviors of SMAs is by studying micro-structural changes based on the principles of micro-mechanics(Lagoudas et al. [2006]; Levitas and Ozsoy [2009]; Patoor et al. [2006]; Petryk and Stupkiewicz [2010]). These models require substantial computational effort in order to analyze the dynamic crystallographic changes of SMAs, and then relate them to a macroscopic effect. The other type of theoretical modeling considers, global effects, like the energy potentials defined over the entire homogenized material volume, or thermo-mechanical loading paths. This type of modeling is called phenomenological modeling (Chemisky et al. [2011]; Christ and Reese [2009]; Popov and Lagoudas [2007]; Ziolkowski [2007]).

These theoretical models developed over last few decades have been able to simulate and predict the complex and hysteretic behavior of SMAs, but most of them are case specific and are limited by the constitution of the SMA material and thus cannot predict over a wide range of material dynamics. These models cannot be directly used because of the different type of diverse behaviors of SMAs.

To resolve some of the problems that arise when using these constitutive methods of modeling, various soft computing methodologies capable of capturing the hysteretic behavior have been tested. This type of approach, in which models are generated based on adaptive training of input-output data without actually studying the material, is called a black-box approach. Artificial Neural Networks (ANNs) is one such method which has been popular for the last two decades. The nonlinear adaptive function mapping property of ANNs makes it a

forerunner for learning nonlinear problems. Literature shows that inverse models developed using ANNs have been able to determine the control voltage required to actuate SMA wires (Lee et al. [2013]; Tai and Ahn [2012]; Tan and Baras [2005]). One of the problems of modeling hysteresis using these soft-computing methods is the identification of the factors effecting these inputs. But present advances in the application of neural networks is unable to capture the non-linearities and model multi-loop hysteresis.

Another method which has given promising results in modelling this hysteretic behavior is the hybrid technique based on neural networks and fuzzy logic. One such technique called the ANFIS technique was used to track a desired trajectory for a single loop hysteresis curve with position and velocity as inputs (Kumagai et al. [2000]). The time histories of the inputs were used to learn and capture the nonlinear hysteretic behavior. In another work (Kilicarslan et al. [2008]) that uses this techniques multiple loops of varying frequency, has been modeled in order to capture strain characteristics of SMAs. One factor that needs to be considered in determining the level of generalization of these black box models is the choice of the feedback variable. As multiple inputs are generally required for dynamically complex system like SMAs, there is a need for at-least two inputs. There has been a wide search and applicability of different inputs for modeling the path dependence of these systems. Electrical resistivity is one of the most common methods for sensing the state of SMAs during actuation. In most cases, one of the inputs has been the resistance and for the other input there has been a variety of options, like a artificial tag signal (Song et al. [2003a,b]) or current and time (Grigorie and Botez [2010]), or time delayed signals (Kilicarslan et al. [2011]).

Variation of electrical resistance for predicting and capturing the nonlinear hysteresis as SMAs has been investigated for a long time. The nonlinear behavior of SMAs is traditionally considered to depend on the fractional ratio of austinite to martensite phase (Wayman et al. [1972]). This transformational change is related to the temperature of the material and can be evaluated by noting the change in its resistance (Uchil et al. [1998]). Numerous attempts have shown that the electrical resistance of an SMA can be used as feedback for strain of thin SMA wires in actuators (Ma et al. [2004]). Despite years of research of electrical resistance of SMA wires, the complex relationship of resistivity with thermo-mechanical properties of SMAs is not fully understood and the results are not consistent. This measure of feedback

cannot be confidently used as a feedback sensor in actuation applications.

1.2.2 Artificial Neural Networks

It is well known that biological nervous system can communicate and perform complex tasks without resorting to complex quantitative calculations (Hebb [2002]; Rosenblatt [1962]). In particular, biological neurons have a capacity to generalize the response of a human body to external stimuli by learning it (McCulloch and Pitts [1943]). Such learning capabilities of nervous system has attracted researchers to design an artificial network of neurons capable of processing and learning the dynamic relationship between complex data sets (Levenberg [1944]).

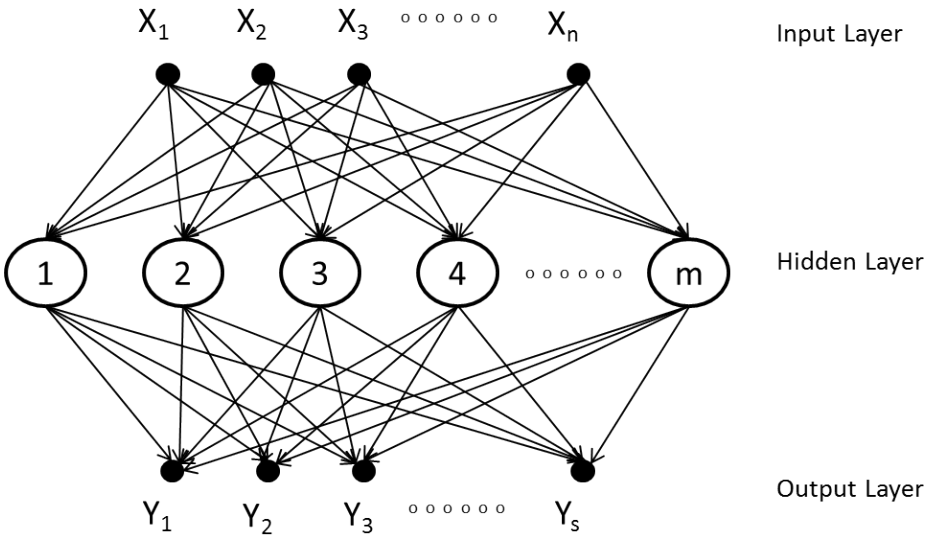

Figure 1.1: Architecture of a simplified Artificial Neural Network

Artificial Neural Networks (ANN) are computational models motivated from our understanding of biological nervous systems (Lippmann [1987]). A neural network is a collection of simplified mathematical replications of biological neurons. An incoming, informative signal is computationally processed in the connection that links between two neurons. A simplified representation of ANN is shown in Figure 1.1. Each neuron in hidden layer received is

processed with a proper weight and bias. This information is added in this layer.

$$F_{1i} = \sum_{j=1}^{n} iw_{ij} X_j + hB_i \tag{1.1}$$

where X is the input matrix, n is the number of input variables, iw is the initial weight matrix and hB is the bias of the network. The output of this hidden layer, A is calculated by a suitable transfer function, TF, as

$$A_{1i} = TF(F_{1i}) \tag{1.2}$$

The output of this layer is the input of the next layer. The selection of different transfer functions is critical in determining the converging dynamics of the model. Wide selections of transfer functions are present in the literature, ranging from linear functions to nonlinear functions, like sigmoid or radial basis type functions. Depending on the requirement and complexity of the data set, multiple hidden layers can be included in the model. In this section, a single hidden layer model is explained. The input to the output layer is a combination of output response signals from the hidden layer.

$$F_{2k} = \sum_{i=1}^{m} hw_{ik} A_{1i} + oB_k \tag{1.3}$$

where hw is the hidden layer weight matrix,oB is the bias, m is the number of neurons in the hidden layer. Assuming a linear transfer function at the output layer the outputs can be given by:

$$Y_k = F_{2k} \tag{1.4}$$

The mathematical derivation previously shown assumes that for an optimum set of bias and weight values of the networks, the trained output of the neural network is identical, or near to, the targeted output. In order to find these parameters of the network, the training error is computed in each cycle. Specifically, the learning problem can be defined as

$$
\begin{aligned}
T &= \{(X^p, Y^p), p = 1, ..., N\} \\
X^p &= (X_1^p, X_2^p, ..., X_n^p) \in \Re \\
Y^p &= (Y_1^p, Y_2^p, ..., Y_s^p) \in \Re
\end{aligned} \tag{1.5}
$$

To train the model, the experimental data set is randomly divided into a training set and testing set. The training data set is used to adjust the weights and biases of the neural network with n input nodes and s output neurons with a hidden layer of m neurons. Different learning algorithms are available in literature to optimize the learning capabilities of the neural network (Chen et al. [1991]; Elman [1990]; Hopfield [1982]; Widrow and Lehr [1990]). One such learning algorithm called Levenberg – Marquardt back propagation algorithm (Hagan and Menhaj [1994]; Marquardt [1963]) is employed in determining the optimum parameters of the system.

1.2.3 Adaptive Neuro-Fuzzy Inference System

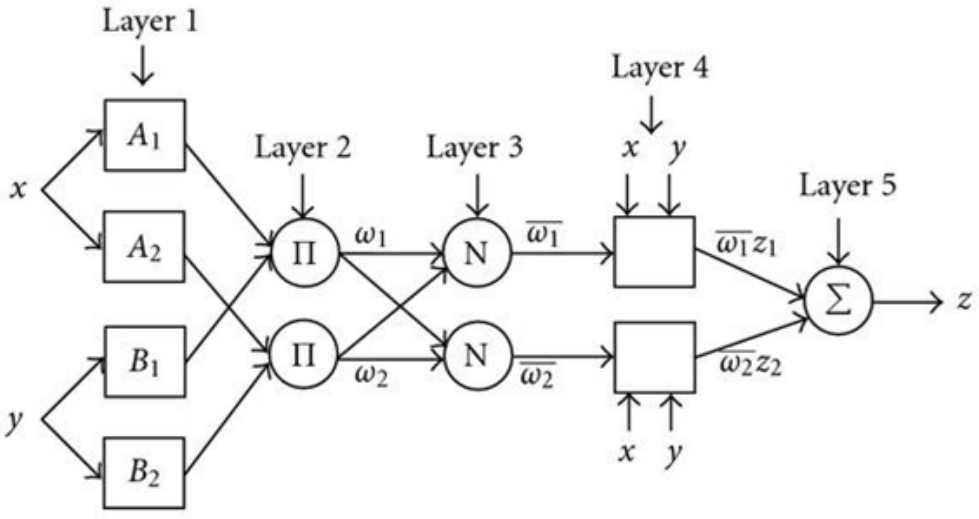

Figure 1.2: Architecture of an Adaptive Neuro-Fuzzy Inference System

Fuzzy set theory (Zadeh [1965]) generalizes classical set theory and widens the range of the membership degree of a variable by inclusion of all values between 0 and 1 and do not restrict it to a crispy set of $\{0, 1\}$. The linguistic sets (Zadeh [1975]) and fuzzy relations between them form a Fuzzy Logic System (FLS) (Zadeh [1973]). The relationship between different membership functions is established by simple linguistic rules called Fuzzy IF-THEN rules (Bellman and Zadeh [1970]; Mamdani and Assilian [1975]). Fuzzy if-then rules have an ability to capture the imprecise modes of reasoning that play an essential role in the human ability to make decisions in an environment of uncertainty and imprecision. In order to relate physical variables with fuzzy membership functions, both inputs and output are first fuzzified, i.e. converted from crisp numbers to a fuzzy set. The relationship between the fuzzified input membership functions with the output membership function is defined using if-then rules. The fuzzy sets computed by the fuzzy inference as the output of each rule are then composed and defuzzified (i.e., converted from a fuzzy set to a crisp number).

The connection of fuzzy systems with an artificial neural network is called a neuro-fuzzy system. Similar to neural networks, wherein information is stored in connection weights, fuzzy if-then rules are tuned to contain the data in a neuro-fuzzy system. There are many versions of fuzzy neural networks in literature (Gupta and Rao [1994]; Horikawa et al. [1992]). Adaptive network based fuzzy inference system, ANFIS (Jang [1993]) is one of them. A simplified architecture with two inputs, x and y, and one output with two Sugeno's –Takagi fuzzy-if -then rules, is considered for studying ANFIS model (Jang et al. [1997]). The ANFIS architecture is shown in Figure 1.2. The fuzzy rules based on the linguistic variables A_1 and A_2 of Input 1 and B_1 and B_2 of Input 2 are given by

$$Rule\,1:\ If\,x\,is\,A_1\,and\,y\,is\,B_1\,then\,f_1 = p_1x + q_1y + r_1 \tag{1.6}$$

$$Rule\,2:\ If\,x\,is\,A_2\,and\,y\,is\,B_2\,then\,f_2 = p_2x + q_2y + r_2$$

Where f_i is output and p_i, q_i and r_i are the parameters utilized in the training algorithm of ANFIS. The circles in the figure represents a fixed node while the square node denotes an adaptive node. The output of i^{th} node of a layer l is given by O_i^l.

- Layer 1: The membership function μ_{A_i} of linguistic variable, A_i, is given by O_i^1.

$$O_i^1 = \mu_{A_i}(x) \tag{1.7}$$

- Layer 2: In this layer, at each node denoted by Π the input signals are multiplied and the product is sent out.

$$\begin{aligned} O_i^2 &= w_i \\ &= \mu_{A_i}(x) \times \mu_{B_i}(y) \; i = 1, 2 \end{aligned} \tag{1.8}$$

- Layer 3: In this layer, normalized firing strength is calculated by using the ratio of outputs of the previous layer, i.e. the firing strength of each rule to the sum of all of them.

$$\begin{aligned} O_i^3 &= \bar{w}_i \\ &= \frac{w_i}{w_1 + w_2}, \; i = 1, 2 \end{aligned} \tag{1.9}$$

- Layer 4: The adaptive node function determining the output of this layer is given by

$$\begin{aligned} O_i^4 &= \bar{w}_i f_i \\ &= \bar{w}_i (p_i x + q_i y + r_i), \; i = 1, 2 \end{aligned} \tag{1.10}$$

  where p_i,$q_i$and r_i are the consequence parameters.

- Layer 5: In this layer the summation of all incoming signals is computed in this layer.

$$\begin{aligned} O_i^5 &= \sum_i \bar{w}_i f_i \\ &= \frac{\sum_i w_i f_i}{\sum_i w_i} \end{aligned} \tag{1.11}$$

This can be expanded as

$$\begin{aligned} Output &= \frac{w_1}{w_1 + w_2} f_1 + \frac{w_2}{w_1 + w_2} f_2 \\ &= \bar{w_1}(p_1 x + q_1 y + r_1) + \bar{w_2}(p_2 x + q_2 y + r_2) \end{aligned} \tag{1.12}$$

parameters p_1,q_1,r_1,p_2,q_2 and r_2 are updated in each epoch to map input membership functions with output membership function.

There are many methods to update these parameters. Some of them would be the gradient decent method (Guély and Siarry [1993]), the least squares method and the hybrid learning algorithm (Rutkowska [2002]).

1.3 Research Objectives

With growing interest in developing actuators based on SMAs for various applications, it is necessary to understand and study the temperature response of SMAs. In order to fully examine the non-linear dynamics of this material, and develop an actuator capable of multi-step activation, a closed feedback control loop is required. Therefore, the principle objective of this study is to develop a sensor capable of detecting the multi-phase transformations of this material and correlate this crystallographic change with the non-linear hysteretic response of SMA wires. To achieve these end goals, the following objectives need to be addressed

- **Study relative thermoelectric sensitivity:** Thermoelectric sensitivity, or the Seebeck voltage of SMAs, is capable of converting temperature changes into easily measurable electric voltage. This property has a potential to be harnessed to detect temperature changes in the system. A material is to be selected capable of magnifying the voltage signal from the proposed sensor.
- **Fabricate and develop a SMA based sensor:** A suitable fabrication methodology has to be selected to form a bi-material junction capable of measuring temperature. The developed sensor has to be tested and the different parameters that are required to

characterize the sensor have to be identified. Once the influence of all the parameters on the sensor is studied, a calibrated relationship has to be established.

- **Study the strain characteristics of SMA wires:** In order to study the stress characteristics of thin SMA wires, an experimental setup will be built. A SMA wire has to be constrained using fixed support at both ends. A weight will be suspended on the SMA wire to maintain uniform and constant stress in the wire. The response of this wire, with change in temperature will be recorded by measuring the displacement of the weight by employing a laser displacement sensor.

- **Model the position response of SMA wires:** A hysteretic relation is expected between the displacement and temperature change of the SMA wire. In order to verify this, two different soft-computing methods are studied to capture the dynamics of the system; a single loop curve to modeled first. Then the effect of amplitude and frequency of voltage applied on the displacement characteristics is to be studied. This data will be utilized to model an ANFIS and ANN model to learn the dynamics of the system.

- **Experimentally validate the developed models:** In order to prove the concept of a closed loop system experimental validation of the developed models is required.

1.4 Dissertation structure

The research in this dissertation is organized and presented in the following manner. Chapter 1 lays out the motivation for developing a thermoelectric based SMA sensor and briefly discusses various soft computing techniques employed in the present work. Previous work is presented along with research objectives. Chapter 2 presents the design and development of an SMA-Constantan thermocouple. This chapter identifies the variables affecting the sensor and models a relationship to predict the tip temperature of the bi-material system. Chapter 3 discusses the experimental setup built to study the position characteristics of SMA wires. Various ANFIS and ANN models developed using the data collected through experiments are presented in this chapter. The effect of time-shift on the prediction capabilities of ANFIS models developed to better understand the strain characteristics are discussed in Chapter

4. The possible applications of the present work in developing a novel collocated sensor is presented as an idea in Chapter 5.

Chapter 2

SMA-Constantan Thermocouple

2.1 Introduction

Active materials have been on the forefront of research in actuation and sensing applications. Shape Memory Alloys (SMAs) are a unique type of smart material that is engaged in a wide range of applications, in order to make use of its stress and strain characteristics associated with micro-structural behavioral changes (Degeratu et al. [2009]). The changes in the lattice structure of SMAs have a signature effect on their thermoelectric properties (Yoshida et al. [2000]). Thus, as the Seebeck coefficient of an SMA is sensitive to the phase transformation of an SMA, it can be exploited to determine the level of its Martensitic transformation. Using this property, a thermocouple is built by paring Shape Memory Alloys which has a positive Seebeck coefficient, with a negative Seebeck coefficient (-35 mV/K) material, Constantan. The bi-material junction of this sensor utilizes the relative thermoelectric properties of the compound to sense temperature. The effect of room temperature on this novel thermocouple is discussed and an Adaptive Neuro-Fuzzy Inference Model (ANFIS) is developed to replicate the Seebeck voltage characteristics of the thermocouple.

In this chapter the SMA-Constantan thermocouple is characterized and modeled. The procedures adopted in joining SMAs and Constantans to form a bi-material junction is explained in section 2.2. Although SMAs exhibit an inherent non-linearity in Seebeck coefficients, the Seebeck Voltage of the thermocouple developed shows a linear relationship with tip temperature. The experimentally determined linear fit is discussed in section 2.3. The dependence of this equation on ambient temperatures is studied in section 2.4 and is

modeled in section 2.6. As thermocouples quantify temperature changes, a reference viz. an ice-bath is used to determine the actual temperature. An ergonomic approach in attacking the problem of having an ice-bath is discussed and modeled in section 2.7.

2.2 Fabrication of SMA-Constantan Thermocouple

The Seebeck coefficient, or the thermoelectric sensitivity of the material, reflects the ease with which the valence electrons of a material polarize upon enforcing a thermal gradient. A thermocouple utilizes this principle and magnifies the effective voltage output by engaging a pair of dissimilar materials. The relative Seebeck coefficient (S_{AB}) of materials with individual Seebeck coefficients S_A and S_B is given by:

$$S_{AB} = S_A - S_A = \frac{\Delta V_B}{\Delta T} - \frac{\Delta V_B}{\Delta T} \tag{2.1}$$

where ΔV_A and ΔV_A are the thermoelectric voltages developed across the terminals of materials A and B due to a temperature gradient of ΔT. The sensitivity of the thermocouple is magnified by a prudent choice of materials, one having a positive Seebeck coefficient and the other with a negative Seebeck coefficient. Previous research (Yoshida et al. [2000]), has shown that an SMA has a positive thermoelectric sensitivity (or Seebeck coefficient) all throughout its phase transformation cycle. Figure 2.1 shows a thermocouple formed when a negative Seebeck Coefficient (-35mV/K) material Constantan is paired with a Flexinol wire (from Dynalloy [2011]). Flexinol and Constantan wires of equal diameters have been welded using a capacitive discharge spot welder to form a bimetallic junction. The bare terminals of both the materials have been welded with copper wires.

The thermoelectric electromotive force (emf) developed in one copper wire, due to the temperature gradient, is nullified with the emf generated by the other copper wire. Hence, the voltage generated across the free copper terminals is the difference between the emfs generated across the SMA and the Constantan wires. This is the Seebeck Voltage of the SMA-Constantan thermocouple. A reference temperature is required at the other end of the thermocouple wires to measure the temperature at the SMA-Constantan junction. The reference temperature junctions in Figure 2.2, namely, the SMA-Copper and the Constantan-Copper junctions, are maintained at 0^o C at the terminal block by an ice and water bath.

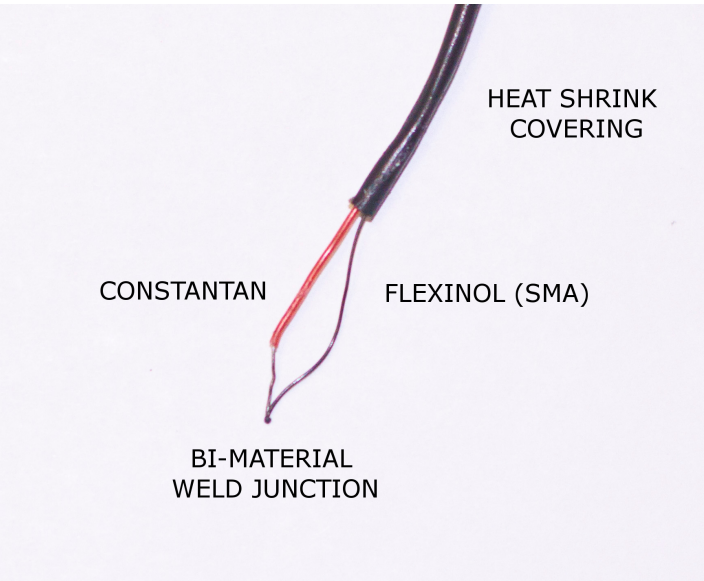

Figure 2.1: SMA-Constantan thermocouple

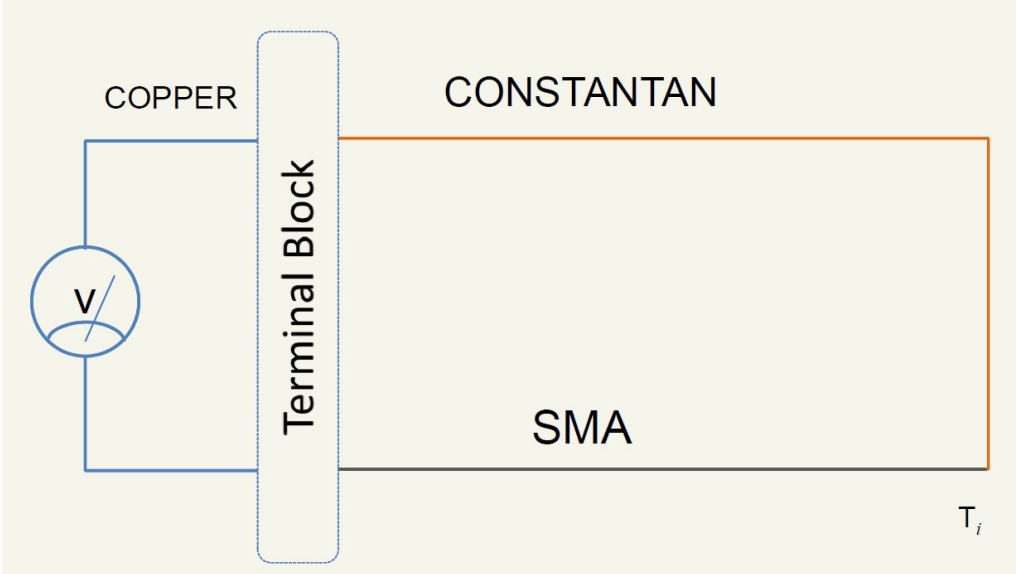

Figure 2.2: Electrical circuit using SMA-Constantan thermocouple

The voltage developed due to the temperature gradient across the dissimilar materials is measured at the bare copper terminals.

2.3 Linear characteristics of Thermocouple

The next step is to characterize the thermocouple and establish a relationship between the tip temperature of the thermocouple and the terminal voltage of the thermocouple. In a preliminary study performed in order to determine the required range of temperature measurement, it is observed that the transformation temperatures of Flexinol lie within the temperature range of [293K 298K] at a stress-free state. The thermoelectric voltage and temperature characteristic is measured by heating the tip of the bi-material thermocouple.The SMA-Constantan junction is inserted in a cold water bath and the water is heated from 283 K to 358 K using a heat pan. Repeatability of the Seebeck voltage-temperature trend is observed with different rates of heating water and with different diameter thermocouple pairs. To confine the transformation of NITINOL (a Nickle - Titanium alloy) to the thermocouple junction, the SMA-Constantan junction is placed just below the water surface. A K-type thermocouple is also placed at the same horizontal level as the tip of the SMA-Constantan thermocouple pair to avoid the effect of thermal gradient in the water. Throughout the experiment, the temperature of the reference junction is maintained at 273 K.

The thermoelectric voltage of the SMA-Constantan thermocouple is recorded along with the temperature obtained from the K-type thermocouple. The SMA-Constantan thermocouple characteristic relation is plotted in Figure 2.3. The heating curve (red) corresponds to the relationship between the thermocouple voltage and temperature during thermal loading, and the cooling curve (blue) gives relationship during the thermal unloading. The water is cooled by placing the setup in an ice water bath. Negligible effect on the thermoelectric voltage characteristic due to the rate of heating or cooling is recorded. The slope of the thermoelectric voltage temperature characteristic gives the relative Seebeck coefficient of SMA-Constantan pair as seen in Figure 2.4.

A slight hysteric behavior is observed in the thermoelectric voltage characteristic of the SMA-Constantan thermocouple. In this case, to avoid the chaotic motion at the surface of the water, a small portion of the thermocouple is inserted in water. Thus, as the tip of the SMA-Constantan thermocouple is heated and rest of the room temperature is maintained

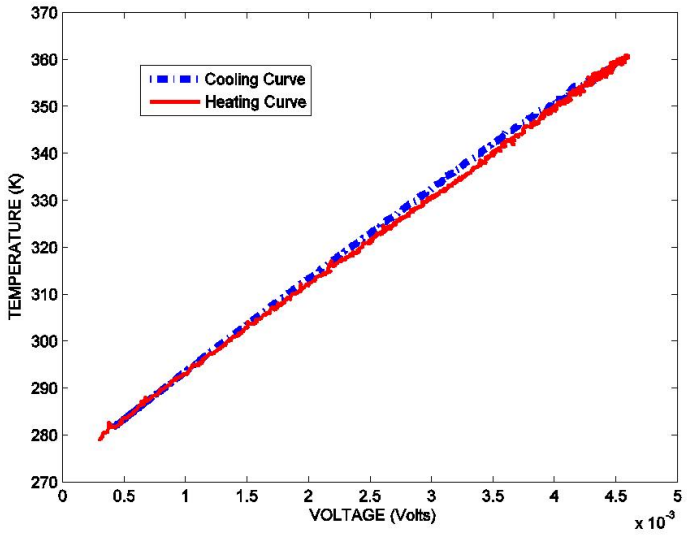

Figure 2.3: Thermoelectric Voltage vs. Temperature

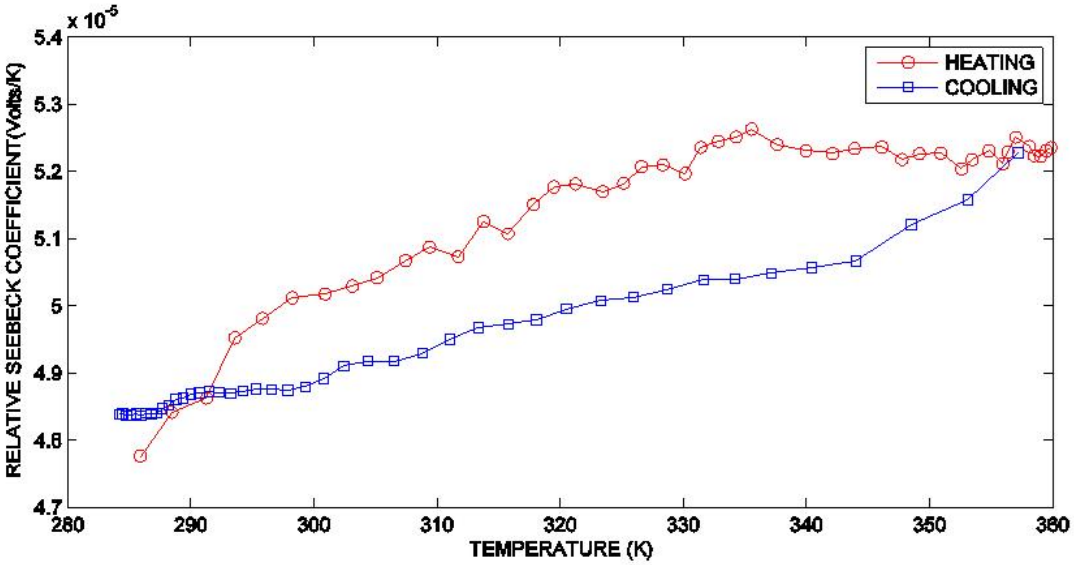

Figure 2.4: Relative Seebeck Coefficient Characteristic

at a constant room temperature, a negligible hysteretic behavior is observed.The shorter the SMA wire is in the water the closer the heating and cooling curves. It was later observed that a heat shrink rubber tube, used to insulate the SMA-Constantan thermocouple from the change in room temperature, efficiently insulates the SMA-Constantan thermocouple. It protects the electrical circuit made out of the SMA-Constantan thermocouple from being grounded. Electrical contact of SMA or Constantan bare wires, at any other place other than the tip of the thermocouple results in change in Seebeck voltage. With the help of the MATLAB curve fitting tool box (MATWORKS [1998]) a linear fit and a quadratic fit are obtained for the data for different cycles and the best set of equations are presented here. The linear fit corresponding to Heating curve is given by

$$T = 18810V_{sma} + 274.277. \tag{2.2}$$

The linear fit corresponding to Cooling curve is obtained by

$$T = 19430V_{sma} + 273.950. \tag{2.3}$$

The linear fit corresponding to Average of Heating and Cooling curves is given by

$$T = 19120V_{sma} + 2734.1139. \tag{2.4}$$

where T is the temperature corresponding to the Seebeck voltage V_{sma}. The quadratic fit corresponding to heating curve is obtained by

$$T = -3.978 \times 10^5 V_{sma}^2 + 2.106 \times 10^4 V_{sma} + 272.8985. \tag{2.5}$$

The quadratic fit corresponding to cooling curve is obtained by

$$T = 9.276 \times 10^3 V_{sma}^2 + 1.886 \times 10^4 V_{sma} + 274.234. \tag{2.6}$$

The quadratic fit corresponding to average of heating and cooling curves is obtained by

$$T = -2.035 \times 10^5 V_{sma}^2 + 1.996 \times 10^4 V_{sma} + 273.566. \tag{2.7}$$

as before T is the temperature corresponding to the Seebeck voltage V_{sma}.

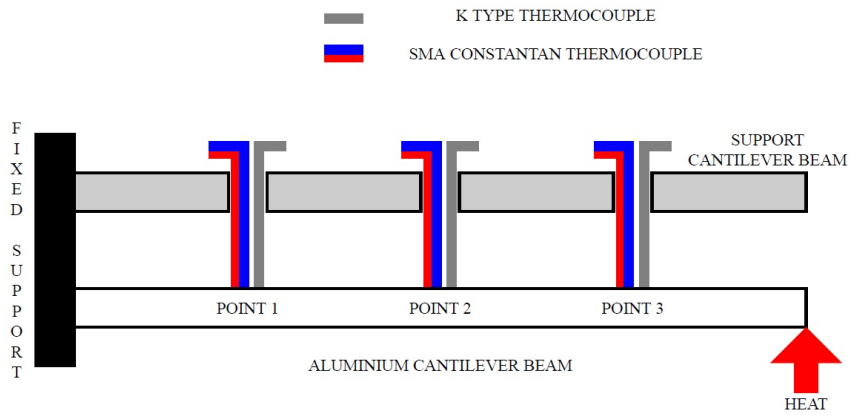

Figure 2.5: Experimental setup for validation of Seebeck Voltage relation

To validate the thermoelectric Voltage-Temperature characteristic of the SMA-Constantan thermocouple the temperature, distribution at three points along the length of an aluminum cantilever beam is measured. The cantilever beam is heated at one end with the help of a heating pan. Both the SMA-Constantan thermocouple and the K-type thermocouple are put in place with the help of another supporting cantilever beam. The temperature measured using a K-type thermocouple is used as a reference for comparison with an SMA-Constantan thermocouple. The thermocouples are positioned such that only the tips of the thermocouple lie on the beam to be heated. An ice-water bath is taken to be one of the reference temperatures for the SMA-Constantan thermocouple. The beam is heated from room temperature to 363K and allowed to cool back to room temperature naturally. Three different points are selected along the length of the beam and the temperature is measured, as shown in Figure 2.5. The temperature of the pan is raised at several intervals.

The temperature of the cantilever beam is computed from the Seebeck voltage of the SMA-Constantan thermocouple pair using the linear fit and quadratic fit. The heating, cooling and average of the heating and the cooling relations for the linear fits are compared with the temperature obtained by the K-type thermocouple and the results are plotted in

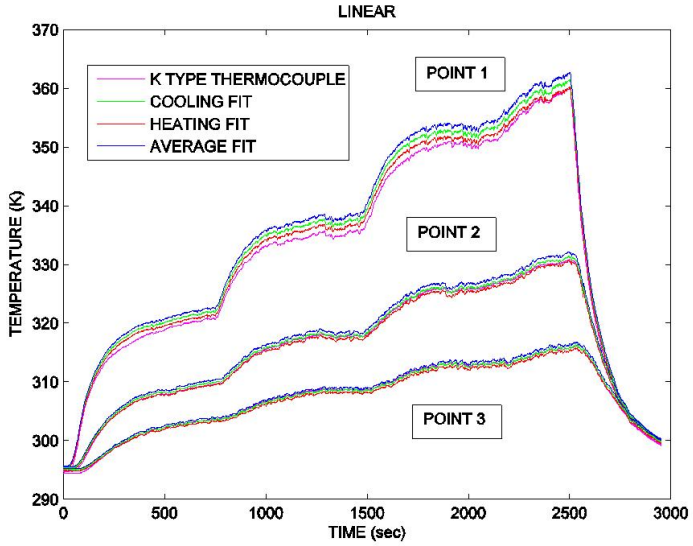

Figure 2.6: K-type thermocouple and linear fit validating the Seebeck Voltage -Temperature relationship

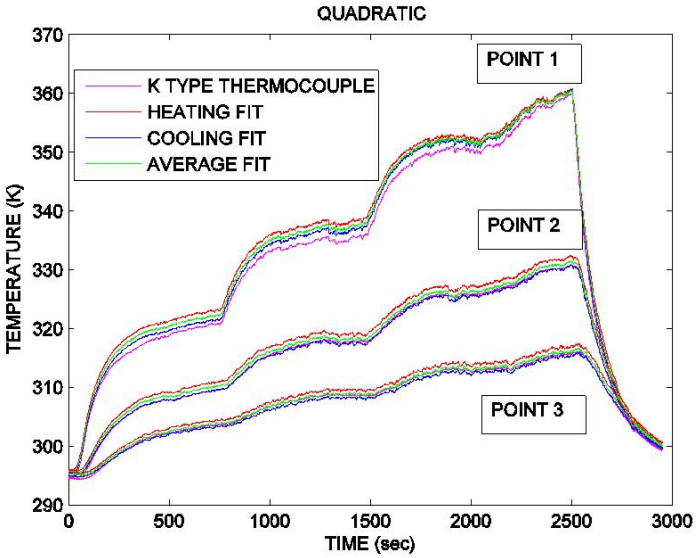

Figure 2.7: K-type thermocouple and quadratic fit validating the Seebeck Voltage - Temperature relationship

Figure 2.6 [1]. It can be seen from this plot that the heating relationship predicts a temperature much closer to the actual temperature measured using a K-type thermocouple. Similar plot for the quadratic fit can be seen in Figure 2.7 [1]. Contrary to the linear fit, the cooling relationship predicts a better temperature than the heating and average relationships.

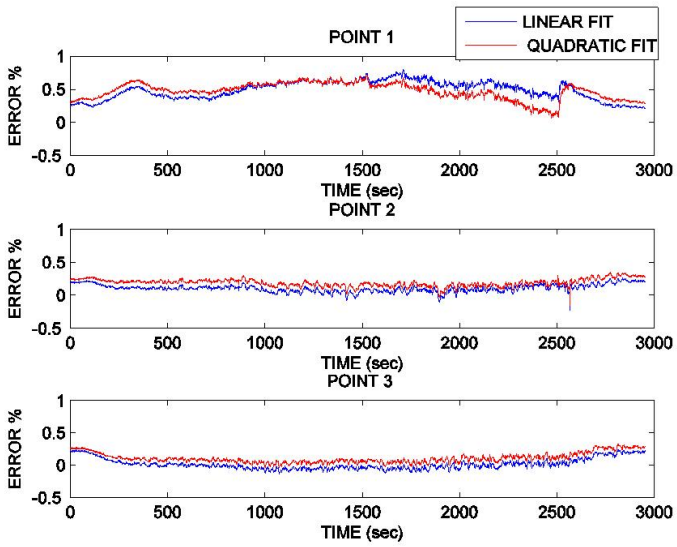

Figure 2.8: Comparison of error % between linear average fit and average quadratic fit

Upon comparing the error percentage of linear and quadratic fits for average relationship in Figure 2.8 [1], it can be deduced that the linear fit has less of an error than the quadratic fit for all points. The maximum error for both the linear and quadratic fits is less than 0.8% for POINT 1, and less than 0.4% for the other two points. This shows that the the Seebeck Voltage of an SMA-Constantan thermocouple can be approximated with a linear relationship with temperature.

Among linear relationships it is observed that the heating relationship fits much better than the cooling relationship or the average relationship for POINT 1 and POINT 2. But for POINT 3 the average relationship gives a better temperature prediction. As a temperature reference, K-type thermocouples are placed near each SMA-Constantan thermocouple; both

[1]For interpretation of the references to color in this figure legend, the reader is referred to the web version of this article.

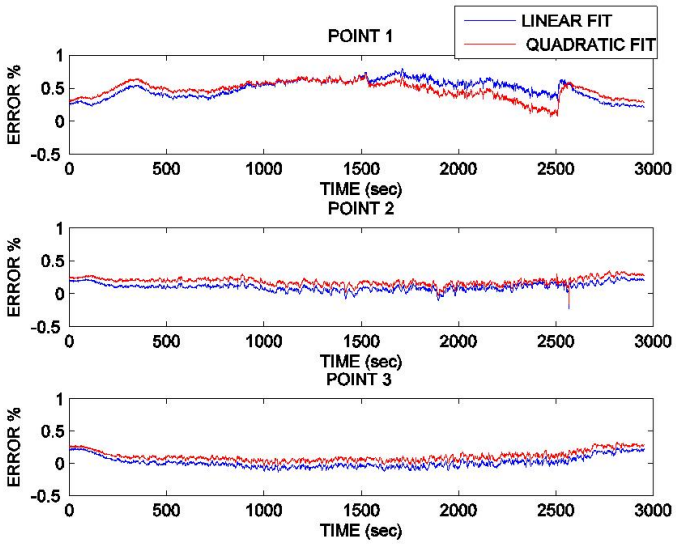

Figure 2.9: Comparison of error % between heating, cooling and average fits for linear relation

these thermocouples are placed at the same longitudinal distance from the heating source. These results show that the transient temperature variation along the width of the beam is more prominent at the point nearer to the heating source (i.e POINT 3) than other points. The error percentage range of the heating relationship is [-0.2% 0.4%] and that of cooling relation is [0.1% 1.1%] as can be seen in Figure 2.9 [1]. This experiment shows that the linear relationship of the heating relationship gives the best result among all the relationships.

In another experiment, the tip temperature of the thermocouple is varied from 268 K to 375 K to test and validate the equation for an extrapolated range of temperatures.The data obtained from the K -type thermocouple and the temperature predicted using the linear SMA-Constantan relation is plotted in Figure 2.10 [1]. A green shade and a yellow shade emphasize the portion of data which is outside the range of the Seebeck voltage-temperature characterization. From the plot, it can be inferred that the linear fit is predicted in the lower temperature with an error of less than 0.4 %, and in the higher temperature ranges with an error less than 0.7 %. This shows that the linear relation obtained can be extended for lower and higher temperatures with an acceptable error.

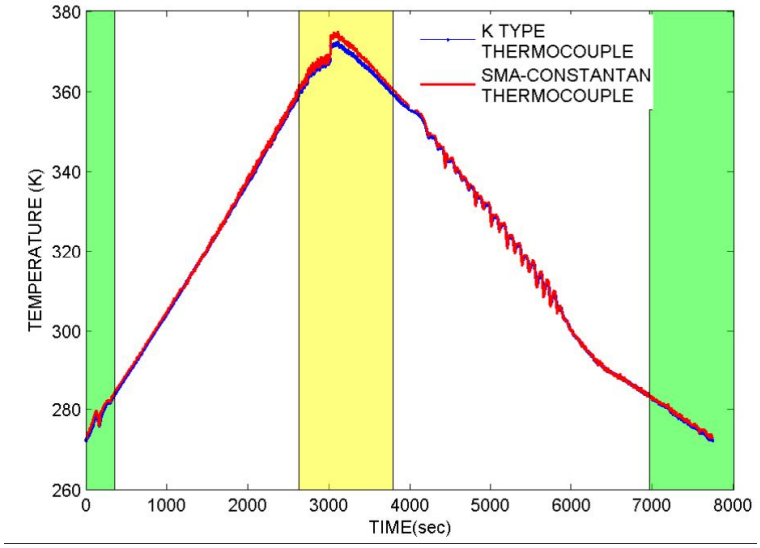

Figure 2.10: Checking the extrapolation of fit

2.4 Non-linearities due to ambient temperature

Contrary to the general laws of thermocouples, the room temperature plays an important role in the case of an SMA augmented thermocouple pair. Ambient temperature of SMA wire plays an important role in the phase transformation and thereby thermoelectric sensitivity of SMA. The effect of change in the material properties of an SMA on the thermoelectric laws of an SMA-Constantan thermocouple are discussed next.

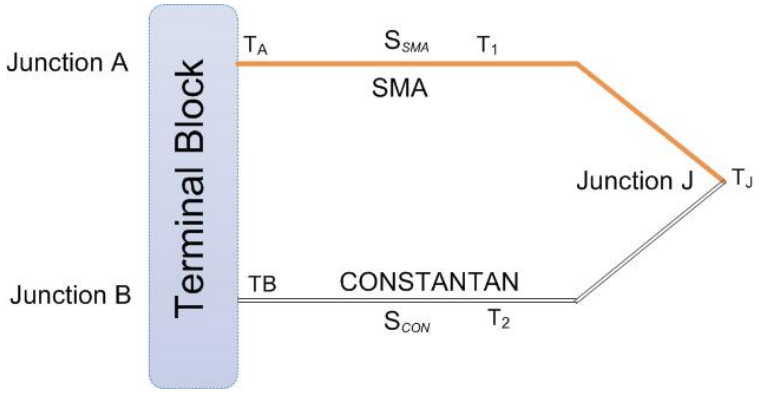

Figure 2.11: Schematic of a SMA-Constantan thermocouple

Consider an SMA –Constantan thermocouple with junction J and terminals A and B as shown in the Figure 2.11. The voltage developed across a wire with terminal temperatures T_A and T_J, with a linear Seebeck voltage vs. temperature relationship is given by

$$V_{AJ} = \int_{T_J}^{T_A} S_{ambient}\, \mathrm{d}t \tag{2.8}$$

where $S_{ambient}$ is the Seebeck coefficient of a small length of wire Δl having a temperature gradient Δt at ambient temperature. Neglecting the heating effects of the thermocouple due to conduction at its terminals, the Seebeck voltage (S_{SMA,T_1}) developed across junctions A and J at an ambient temperature T_1 can be simplified into:

$$V_{AJ} = S_{SMA,T_1}(T_A - T_J) \tag{2.9}$$

The potential difference generated across the terminal A and B is given by:

$$V_{AB} = S_{SMA,T_1}(T_A - T_J) - S_{Con,T_2}(T_B - T_J) \tag{2.10}$$

Assuming that the terminal temperatures are $T_A = T_B = T$, and the Seebeck coefficient variation of Constantan is independent of ambient temperature, the above equation can be rewritten in terms of a relative Seebeck coefficient as:

$$V_{AB} = (S_{SMA,T_1} - S_{Con})(T - T_J) = S_{rel,T_1}(T - T_J) \tag{2.11}$$

The relative Seebeck coefficient of the compound system is dependent on the ambient temperature; i.e as the ambient temperature changes, the Seebeck voltage vs. temperature relationship shifts from the calibrated equation. If the reference temperature is at 0°C, the above equation can be further simplified into:

$$V_{AB} = -S_{rel,T_1} T_J \tag{2.12}$$

An SMA-Constantan thermocouple fails to follow the conventional laws of thermocouple for homogeneous materials. The law of successive or intermediate temperatures is not applicable for this case and poses a challenge.

2.5 Experimentation

In the previous section, we have shown that the tip temperature of the developed sensor depends on the ambient temperature. In this section, we experimentally investigate and model this relationship. To detect the effect of ambient temperature on this sensor, the thermocouple is placed inside a temperature controlled environmental chamber (Teenney environmental chamber, Model: 36ST). A schematic of this experiment is presented in Figure 2.12 and the details of the different equipment used are shown in Figure 2.13.

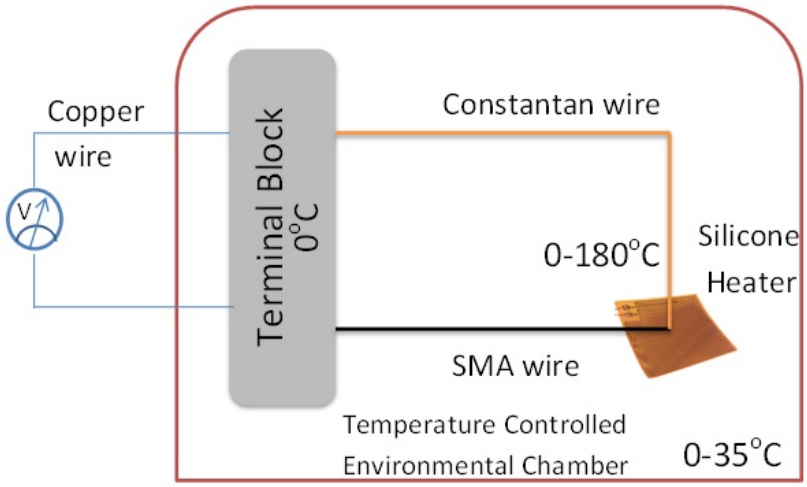

Figure 2.12: Schematic of an experiment varying the ambient temperature of a SMA-Constantan thermocouple

Initially the temperature in the chamber is set to a desired value and then the experiments on the thermocouple is conducted. When the chamber temperature has reached a steady state, the tip temperature of the thermocouple is varied from 0^oC to 180^oC using a silicone -type flexible heater (SILICONE RUBBER HEATER-Omega Model: SRFG-102/10). The ends of this thermocouple are connected to a terminal ice block maintained at 0^oC. Due to the change in temperature at the tip of the thermocouple, the Seebeck voltage is generated at its terminals. This is measured by a data acquisition system (National Instruments PXI, Model: PXI 1031,PXI-4472,PXI-6259,PXI-6115). This experiment is repeated at different chamber temperatures and both the Seebeck voltage developed and the chamber

temperature is recorded. In Figure 2.14, it can be observed that the slope of the relationship, between Seebeck Voltage and junction temperatures, is altered with different ambient temperatures.

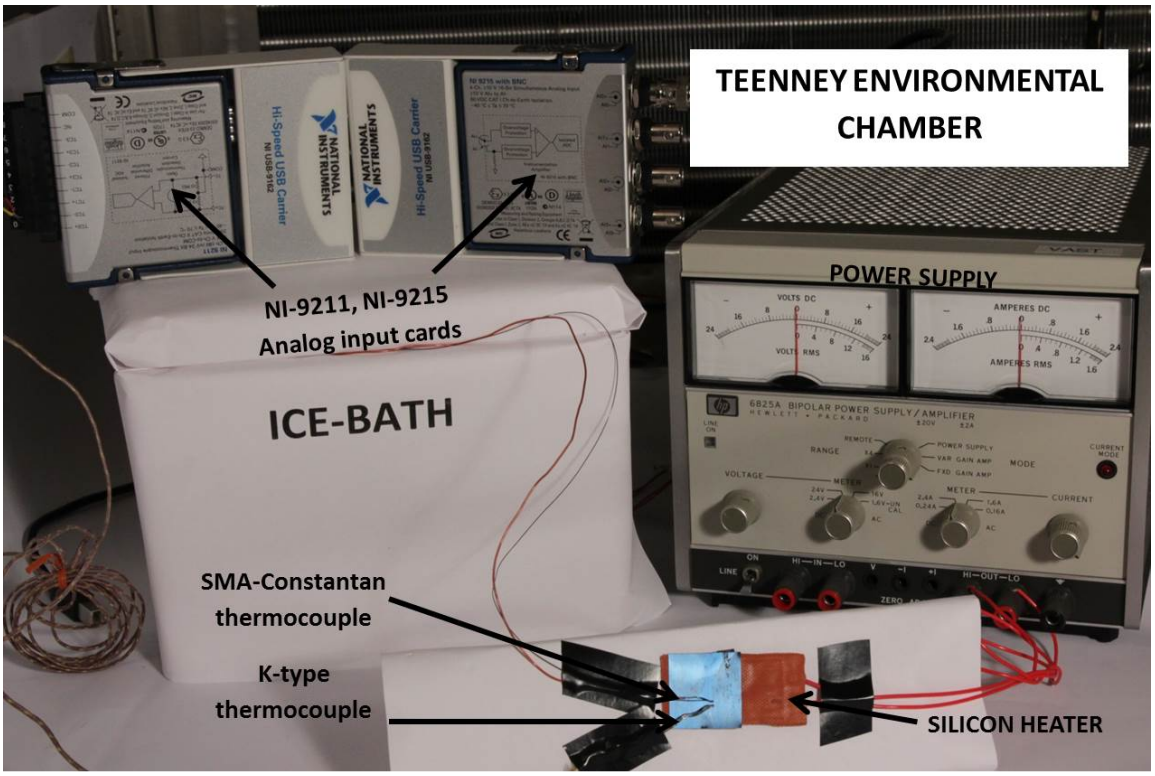

Figure 2.13: Experimental setup varying the ambient temperature of a SMA-Constantan thermocouple

If any one of the phase transformation temperatures lie in the range of a change in the room temperatures, the ratio of Martensitic phase to Austinite phase in SMA is liable to change with ambient temperature of the thermocouple. In order to determine the tip temperature of the SMA –Constantan thermocouple, the relationship between the relative Seebeck coefficient and ambient temperature has to be determined. Although the Seebeck coefficient of an SMA has a nonlinear hysteretic behavior with temperature, the temperature of the atmosphere surrounding the thermocouple is assumed to be constant during the experiment. Even when the ambient temperature is varying, the slow rate at which the SMA wire heats up or cools down due to this change, supports the assumption of having a

Seebeck coefficient as a constant value.

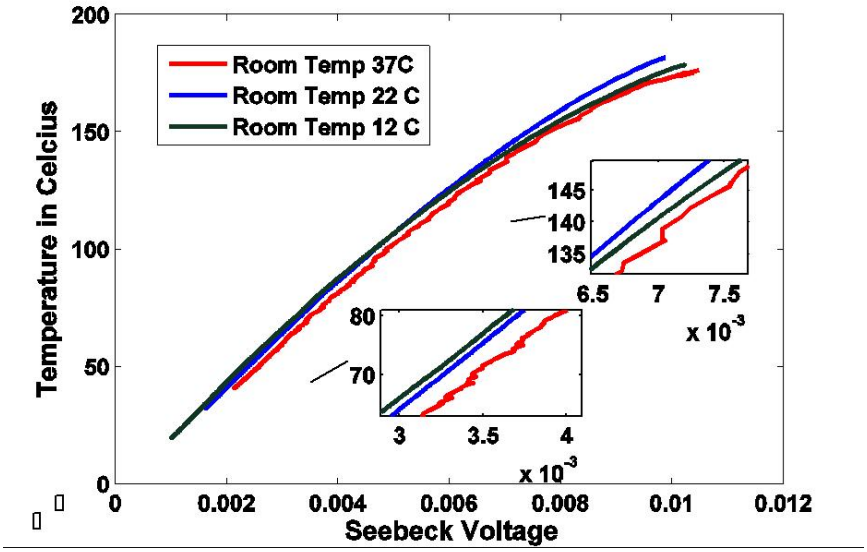

Figure 2.14: Variation of Seebeck Voltage with Temperature

2.6 ANFIS - Forward Model

This section models the tip temperature of the thermocouple using the Adaptive Neuro Fuzzy Inference System (ANFIS). Fuzzy models, in which the parameters of the model are adaptively updated with iterations using Adaptive Neural Networks (ANNs), form the architecture of ANFIS. An input-output mapping reflecting the nonlinear distributions of inputs and outputs is constructed based on the experimental data. This black box technique has Seebeck voltage and room temperature as inputs and, the SMA-Constantan tip temperature as output. Initially, using suitable input-output data pairs, membership functions covering the whole input-output space are computed. The initial untrained nonlinear Gauss membership functions have been computed using subtractive clustering functions in MATLAB. The parameters of this set of membership functions are updated using the gradient descent back propagation algorithm.

The number of fuzzy subspaces created by the membership functions determines the capability of the ANFIS model to capture the nonlinearities in the input-output space. In

order to determine the number of membership functions, the size of the cluster is varied, and the error resulting from that configuration is computed. Based on the RMSE errors obtained from those preliminary models, the cluster size with the least predictive error is chosen. The cluster radius determines the number of membership function generated by the genfis2 function. The inputs, the Seebeck voltage and the room temperature, and the output tip temperature, are normalized before feeding them into the subtractive clustering algorithm.

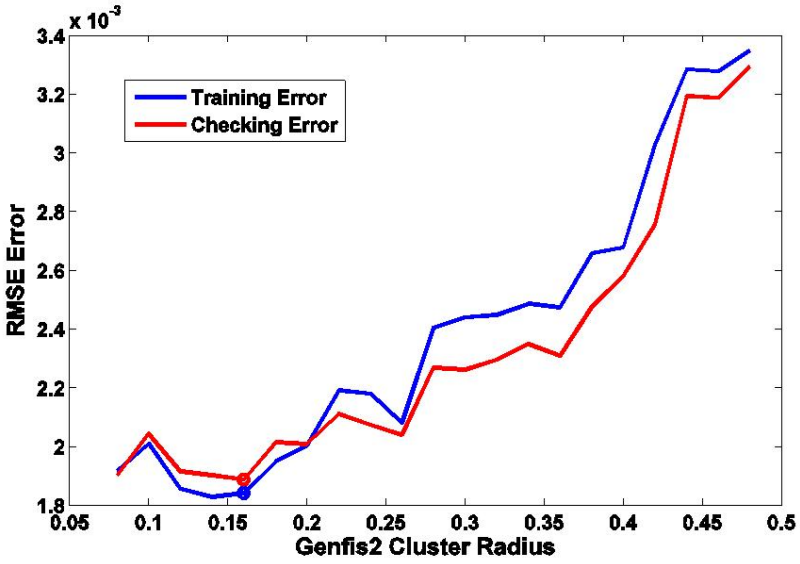

Figure 2.15: Optimum membership functions for ANFIS forward model

In order to choose the optimum number of fuzzy rules and antecedent membership functions, the cluster radius has been varied from 0.07 to 0.5, and each model has been tested for sets of training data and checking data for 50 epochs. Genfis2 uses least squares estimation to determine each rule's consequent equations. The effect of increasing the cluster radius on the training RMSE and checking RMSE is plotted in Figure 2.15. At a cluster radius of 0.1, a model of 31 rules and membership functions is observed to give a lower training and checking RMSE. As a large number of data points have been fed into the model, the comparatively higher fuzzy membership functions do not lead to over fitting of the data.

A Sugeno – type Fuzzy Inference System (FIS) structure is modeled by a hybrid learning

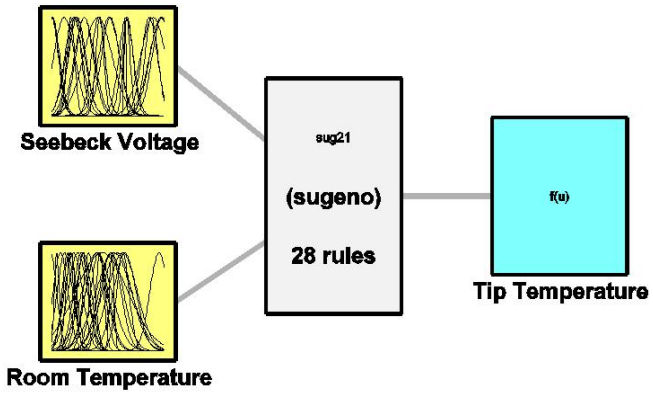

Figure 2.16: ANFIS forward model for SMA-Constantan thermocouple

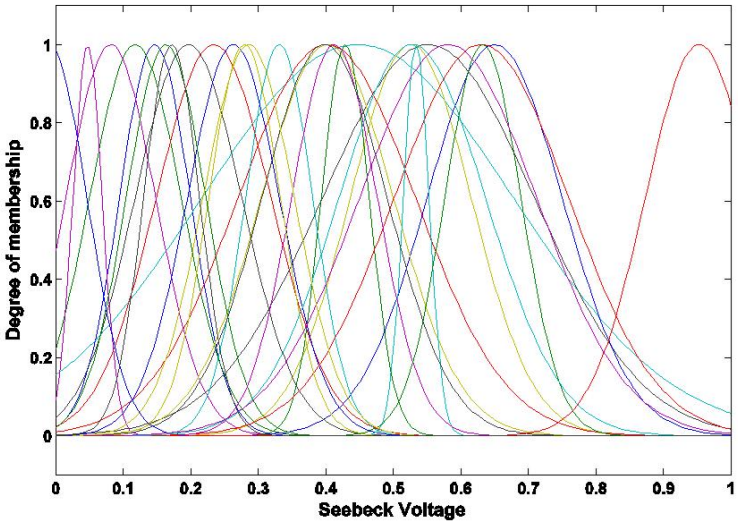

Figure 2.17: Tuned Seebeck voltage input membership function of ANFIS forward model

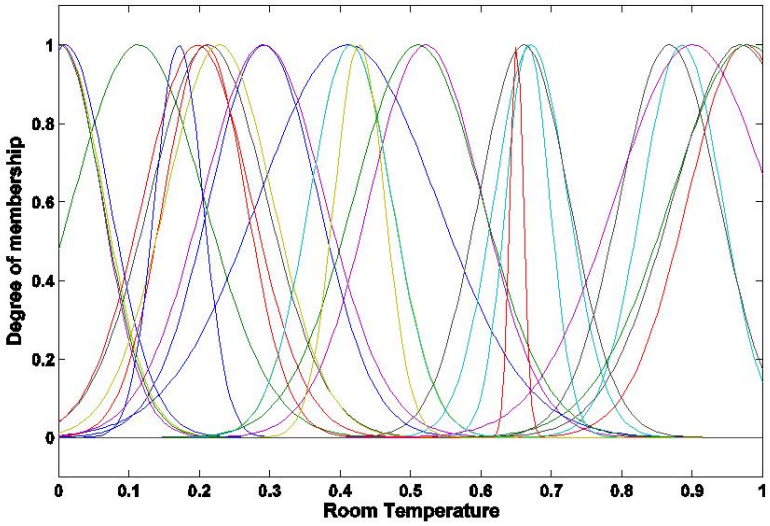

Figure 2.18: Tuned Room Temperature input membership function of ANFIS forward model

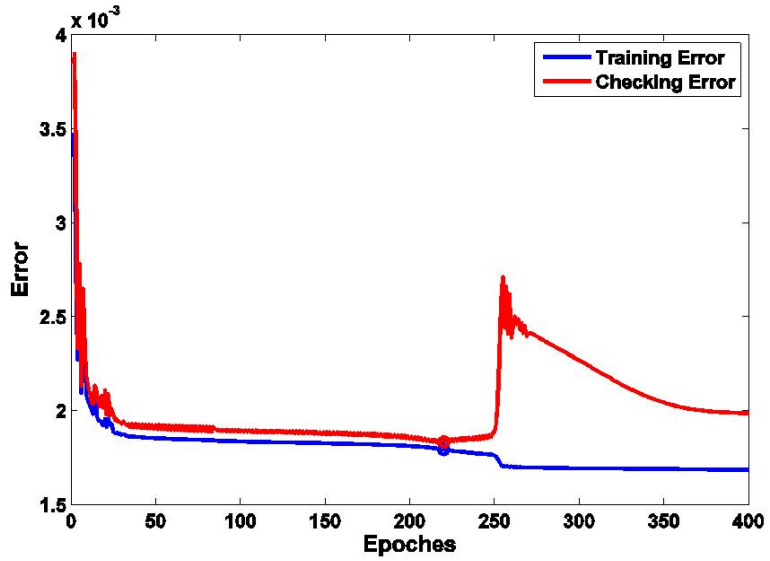

Figure 2.19: Change in RMSE with epoches ANFIS forward model

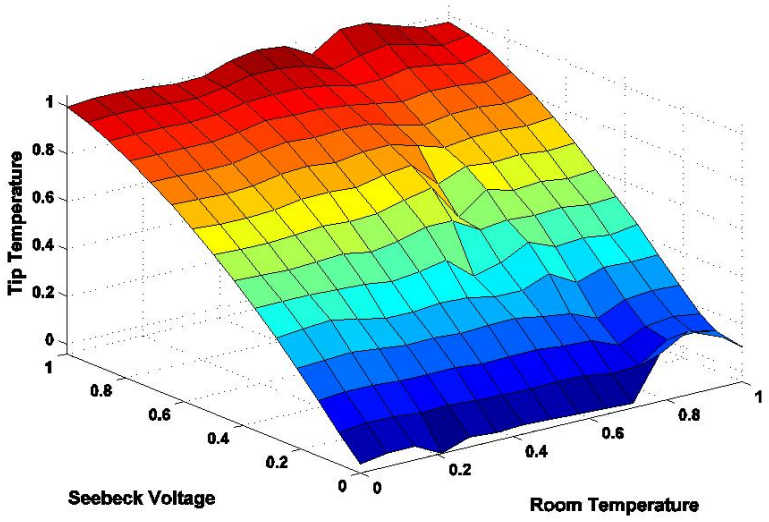

Figure 2.20: The final fuzzy rule surface

procedure using the initial membership functions developed. The structure of this model is shown in Figure 2.16. The ANFIS command in MATLAB iterates a hybrid of least squares estimation -method and gradient descent algorithm until the desired performance criteria are met.

The tuned input membership functions of Seebeck voltage and ambient temperature are plotted in Figure 2.17 and Figure 2.18. The final rule base formed by the ANFIS forward model is given by Figure 2.20. The change in training error and testing error with each epoch can be seen in Figure 2.19. As expected from an iterative learning algorithm, the RMSE reduces with training and the generalizing capability is verified using the checking error. The final training RMSE is 0.3638^{o}C and the final checking error is 0.3701^{o}C. The prediction capabilities of the ANFIS model for the training data of the case when the room temperature is 12^{o}C, can be seen in Figure 2.21. The correlation coefficient for this case is 0.998 and the corresponding plot is shown in Figure 2.22.

The prediction model developed from these limited data points should allow the utilization of this information to generalize the nonlinear behavior over the entire domain, and applied in any dynamic situation. The ANFIS model was trained with data at eight different room temperatures from 10^oC to 35^oC and a tip temperature ranging from 0^{o}C to 180^{o}C.

In order to test the generalization capabilities of the model, the data at room temperatures different from those used in training, is fed into the model. The error for room temperatures 17^o and 22^o are plotted in Figure 2.23. The model is capable of predicting the validating error with an accuracy under $\pm 2^o$.

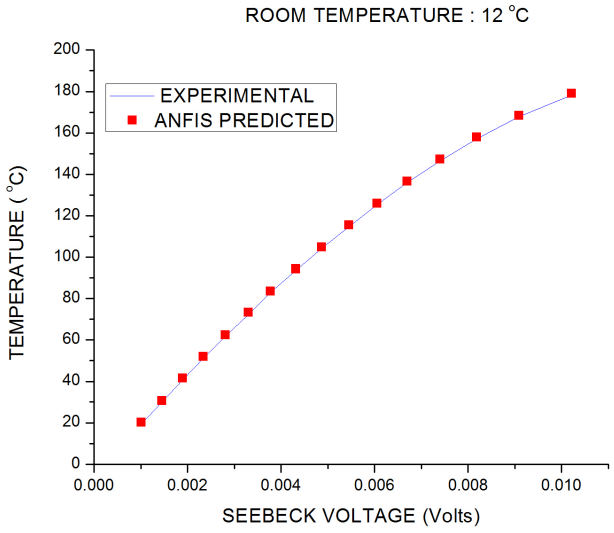

Figure 2.21: Training data of ANFIS forward model

2.7 ANFIS - Inverse Model

In order to have a reference temperature for the system, the terminals of the thermocouple are placed in an ice-water bath. The use of an ice-water bath is not practically feasible in space constraint applications. In order to replace this ice-water bath, the differential Seebeck voltage, due to the change in terminal junction temperature, has to be compensated.

From equation 2.11, the voltage across an SMA-Constantan thermocouple can be written as a sum of an SMA Constantan thermocouple and a zero compensation voltage.

$$V_{AB} = S_{rel,T_1}(-T_J) = \underbrace{S_{rel,T_1}(0 - T_{room})}_{\text{Inverse ANFIS model}} + \underbrace{S_{rel,T_1}(T_{room} - T_J)}_{\text{SMA-Constantan thermocouple}} \tag{2.13}$$

The zero-compensated differential voltage is obtained from an inverse ANFIS model,

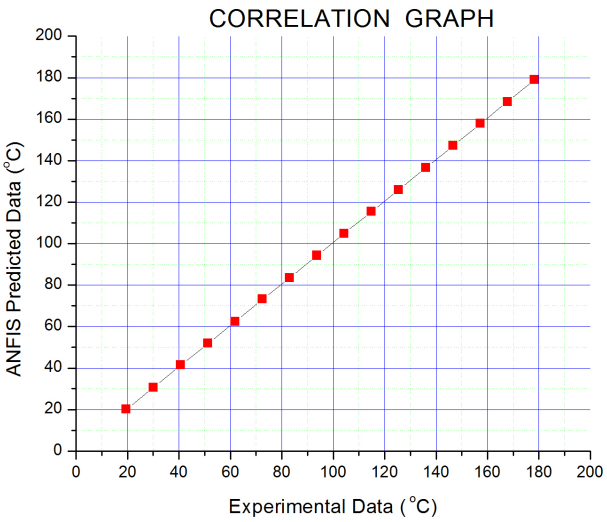

Figure 2.22: Correlation plot corresponding to the training data and ANFIS predicted data

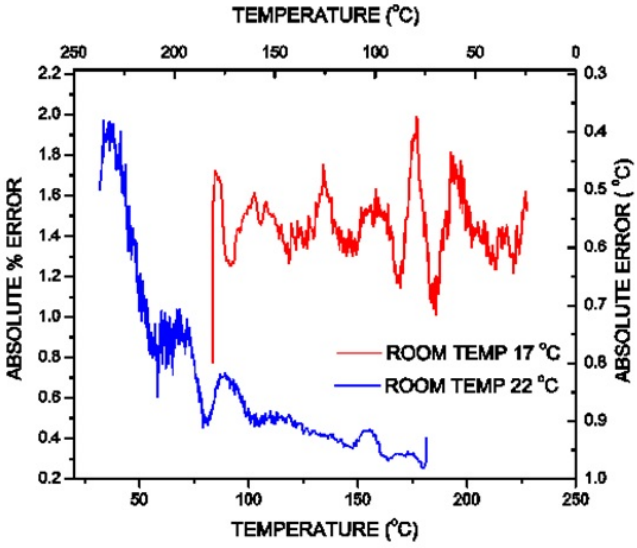

Figure 2.23: Validation of ANFIS forward model

where room temperature is an input and the Seebeck voltage is an output. Because an ANFIS model inherently requires two inputs, a two-column room temperature matrix is fed into the model as an input. An inverse ANFIS model with eight Gaussian membership functions is trained using 8,700 data points. Similar to the other ANFIS models, the membership functions have been obtained using the subtractive -clustering method. The optimum cluster radius is 0.5 for this case. The model has a training RMSE of 1.5084×10^{-5} Volts and a checking RMSE of 1.5565×10^{-5} Volts. The correlation graph is plotted in Figure 2.25.

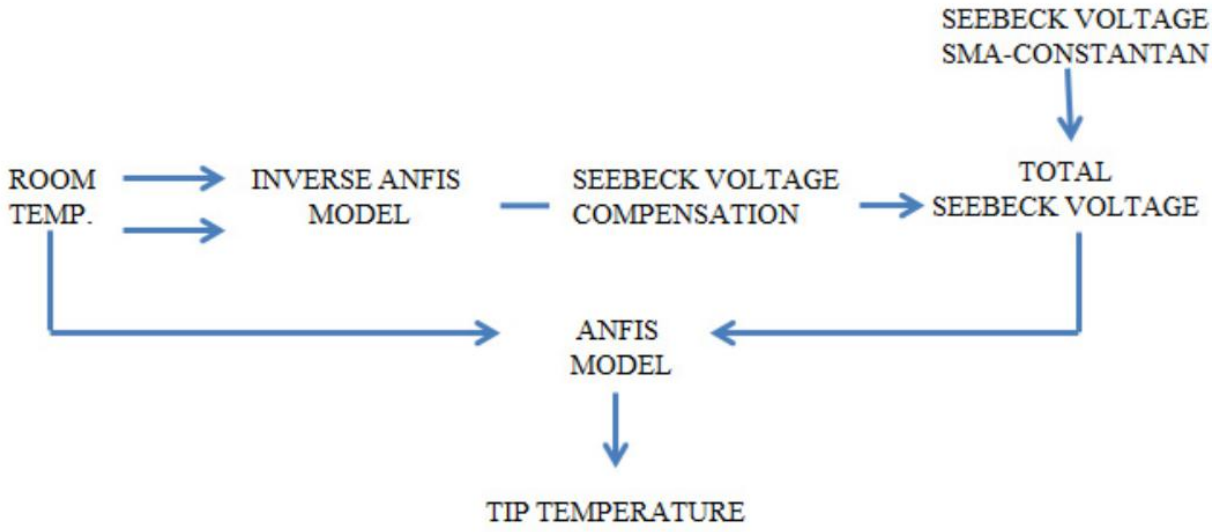

Figure 2.24: Flowchart for working model of thermocouple

The flow process involved in determining the tip temperature of an SMA-Constantan thermocouple when integrating inverse ANFIS model with forward ANFIS model is presented in Figure 2.24. As can be seen in this flowchart, the room temperature obtained from a K-type thermocouple, or an internal thermistor, is sufficient in determining the tip temperature of the SMA-Constantan thermocouple. In order to obtain the actual Seebeck voltage if there had been a reference ice -bath, the Seebeck voltage compensated for the reference temperature is added with the Seebeck voltage. This total Seebeck voltage and the room temperature is fed into the forward ANFIS model to determine the tip temperature.

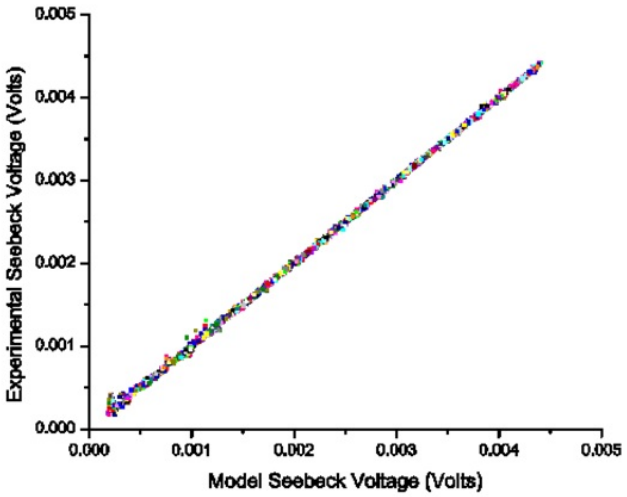

Figure 2.25: Co-relation plot of Inverse ANFIS model

2.8 Conclusion

In order to determine the state of SMA wires during actuation, a sensor that measures the temperature using a bi-material junction was developed. Wires of SMA and Constantan are brought together to form a thermocouple. The Seebeck voltage developed across the thermocouple due to the change in tip temperature, can be characterized using a linear relationship at a constant room temperature. In this section, the dependence of room temperature on the Seebeck voltage –tip temperature relationship is studied. The output of the developed ANFIS model shows a good correlation with the experimental data. In order to simplify the use of the sensor, an inverse ANFIS model was developed to eliminate the reference temperature.

Chapter 3

Study of Strain Characteristics of SMAs

3.1 Introduction

Despite the unique ability of SMAs to recover strain upon application of heat, SMAs have highly complex nonlinear dynamics that limit applicability and utility of SMAs to simple actuation tasks (Ruoff [1985]). It is not easy to control the degree of strain in an SMA wire. New mechanisms and techniques need to address the nonlinear problems associated with the actuation of SMA wires. The design and development of a sensor that can detect temperature, which is critical to the degree of phase transformation is discussed in the last chapter. The focus of this chapter, is the application of various black-box modeling techniques to understand the nonlinear behavior of SMAs. Various models based on soft-computing methods were developed using experimental data. The prediction capabilities of these models are compared and studied in this chapter.

3.2 Closed - Loop Feedback

Directly or indirectly, a change in temperature is required to actuate any SMA device. The speed of actuation of this device is dependent on the rate at which the temperature of the SMA wire changes, whereas the degree of actuation depends on the magnitude of the temperature change. In order to control the level of actuation of such devices, the hysteretic relationship between the source of temperature and the strain characteristics of SMA is to be established.

The cause-effect relationship between the temperature and strain of an SMA wire makes temperature a critical variable in analyzing the strain characteristics of SMAs. The thermoelectric voltage measurements from the SMA-Constantan thermocouple gives feedback of the changes in tip temperature of the thermocouple. The potential difference created across the ends of an SMA wire results in a change in its temperature. An SMA-Constantan thermocouple in contact with this actuator can read these changes in temperature. A relationship between the temperature and strain characteristics of the SMA wire is required to predict the dynamics of this system.

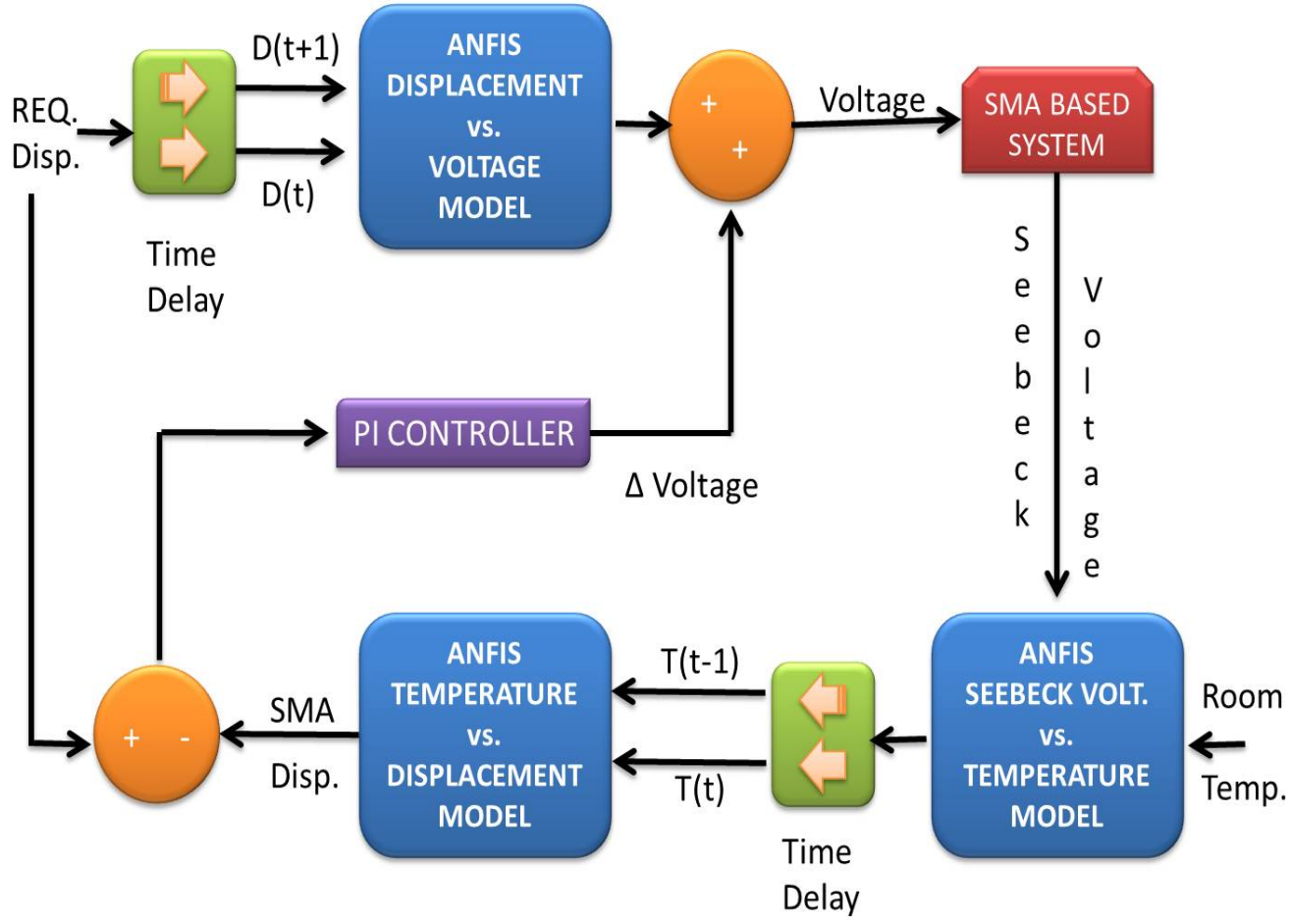

Figure 3.1: Closed loop position tracking system

The variables related to the strain characteristics of SMAs and the approach required

to model these nonlinearities is discussed in this chapter. The ANFIS and ANN modeling methodologies are used to understand and learn the path dependence of SMAs. Based on these models an algorithm is designed to control the actuator characteristics of any SMA device. The block diagram in Figure 3.1 shows a closed-loop system based on ANFIS models. The different ANFIS models involved in monitoring the present position of the system, and then realizing the voltage required to track a predefined path, are listed and described below:

- Desired Displacement vs. Output Voltage model: The system in the block diagram corresponds to an SMA device. Depending on the required position of the system, this model predicts the required voltage to be applied across the terminals of the SMA. The desired displacement-output voltage relationship of this model is a nonlinear hysteresis. A time-delay input is introduced in the control-loop to predict the path dependent output-voltage of this model. Displacements at times t and $t+1$ are considered as the inputs to this model.

- Temperature vs. displacement model: The next step is to determine the change in position of the system. This model predicts the position of the system of SMA wires from the feedback temperature of the activated SMA obtained from the Seebeck voltage vs. temperature model discussed in the previous chapter. As the strain of the SMA wires is a path dependent hysteric behavior, the input should also include time in the form of a delayed variable. This model represents the non-linear map of an SMA temperature at times t and $t-1$ with the strain of the SMA wires.

3.3 Experimental Setup

Experimental data is required to build and validate the proposed modeling approaches. Figure 3.2 shows the experimental setup utilized to record the strain characteristics of an SMA wire. A Flexinol SMA wire of diameter 0.005 inches and a length of 14 inches is considered in this experiment. To maintain a constant stress, a weight of 200 grams is suspended on a SMA wire that is secured at both ends to a non-conductive frame.

In order to capture the strain variation of the SMA with temperature, the terminals of the SMA wire are subjected to a periodic sinusoidal voltage. The NI DAQ system is used to vary the amplitude and frequency of the sinusoidal voltage generated. This voltage signal is

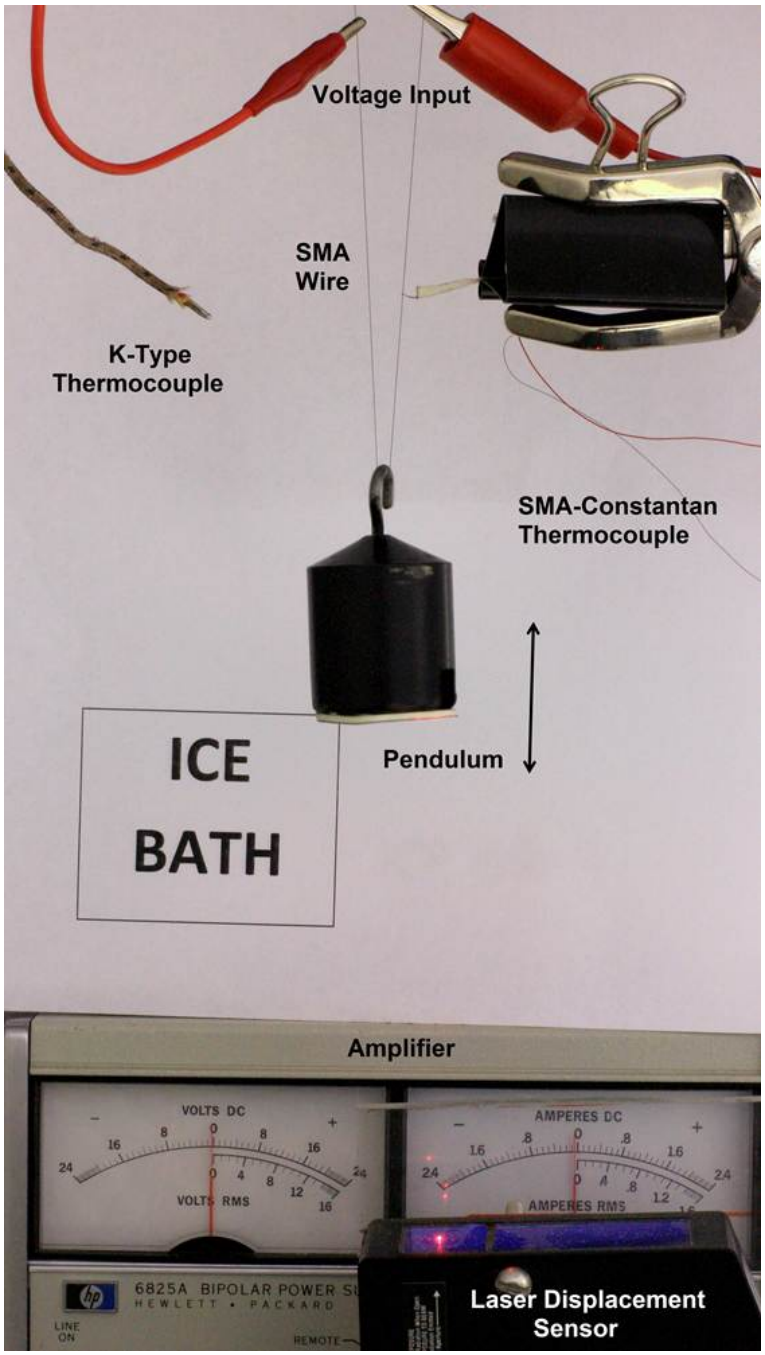

Figure 3.2: Experimental setup for studying strain characteristics of SMAs

amplified by a HP 6825A bipolar amplifier before it is applied to the SMA wire. This input indirectly heats and cools the SMA wire periodically allowing the SMA to transform from Martensitic state to an Austinite state, and vice versa.

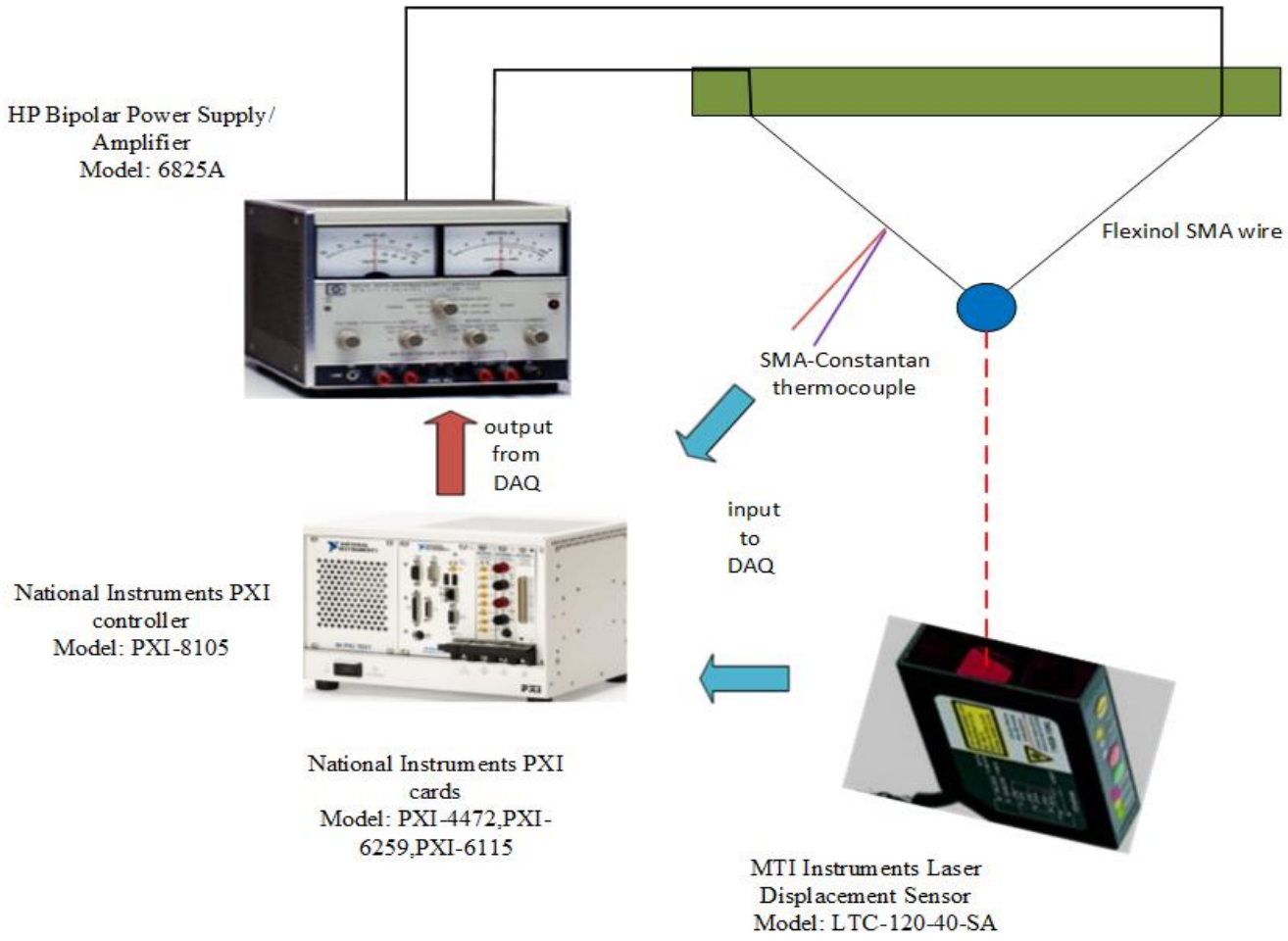

Figure 3.3: Schematic of the different equipment utilized in this experimental setup

The alternate rise and fall in temperature of an SMA results in the contraction and expansion of the SMA wire, which causes a periodic displacement of its weight. The contraction of the SMA wire is obtained by measuring the displacement of the suspended weight with the help of a laser displacement sensor.

The change in temperature of this SMA wire is captured through the Seebeck voltage of an SMA-Constantan thermocouple. SMA and Constantan wires with diameter of 0.005

inches are selected, and a bi-material junction is formed by a capacitive discharge-welding machine. As the Seebeck voltage of a thermocouple is generated due to a temperature gradient across the terminals of a thermocouple, the free ends of this sensor are placed in an ice-water bath. This gives rise to the Seebeck voltage generated due to the actual temperature of the bi-material junction. A K-type thermocouple is employed to measure room temperature.

The characteristic response of an SMA wire is affected by variation of both amplitude and frequency of excitation. The variation of either one of these values result in multiple hysteresis loops. The influence of these factors on the nature of actuation is studied by conducting experiments at different values of amplitude and frequency of sinusoidal voltage. Experiments were conducted by varying the input voltage from 6 to 10 volts in steps of 0.1 volts, and frequencies from 0.01 Hz to 0.2 Hz in steps of 0.01 Hz. The Seebeck voltage and the displacement measurements are recorded by NI PXI data aquisition system. The different equipment used in the experimental setup is shown in Figure 3.3

3.4 Single-Loop Hysteresis

SMAs display highly complex hysteretic curves which are difficult to model. In such situations, the applicability of the soft computing methods which handle hysteretic path dependent nonlinearities has to be verified. The predictive capabilities of the neuro-fuzzy and the neural networks techniques are tested on a simpler model consisting of a single-loop hysteresis. As detailed in the previous section, two major relationships, the Temperature vs. displacement and the Displacement vs. Output Voltage models will be discussed for a single hysteresis-loop. The experimental data required to build these models is obtained by activating the SMA wire with a sinusoidal voltage of amplitude 6.9 volts and frequency of 0.05Hz. The displacement of the weight is measured by the laser sensor and the Seebeck voltage is recorded by the thermocouple.

3.4.1 Desired Displacement vs. Output Voltage Model

The hysteretic nonlinearities present in strain characteristics of SMAs are path dependent. Hence, the voltage required for the pendulum to maneuver a trajectory at time t is assumed to depend on the displacements of the pendulum at time t and time $t+1$. The displacement

measurements at time t and time $t+1$, plotted in Figure 3.4, are fed as inputs to train both ANFIS and ANN models.

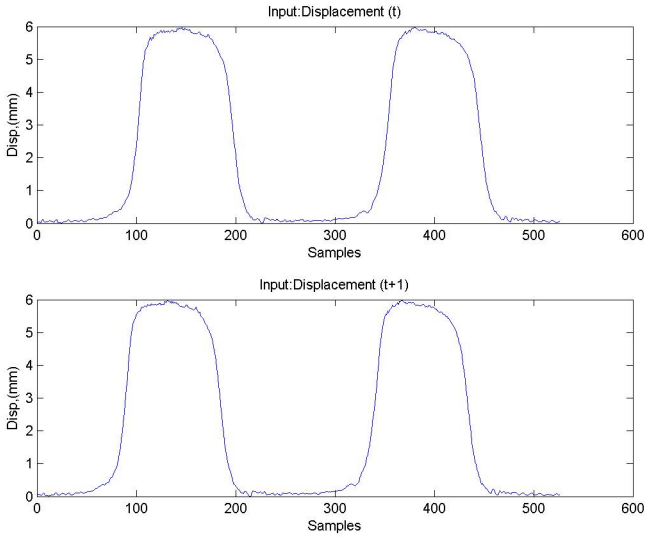

Figure 3.4: Input vectors to predict voltage for single loop hysteresis models

3.4.1.1 ANFIS model

The first step in modeling using an ANFIS method is to construct a set of membership function. Initial membership functions are obtained by feeding input-output data pairs into a grid clustering algorithm. The effect of the number of membership functions and the prediction capabilities is studied. Figure 3.5 shows that as the number of membership functions in the ANFIS model increases, the RMSE decreases. For 526 sets of data points, genfis1 function in MATLAB results in 11 Gauss membership functions with 121 fuzzy if-then rules. Using this set of rule base, the parameters of the model were tuned using neural networks. The change in RMSE with epoches is plotted in Figure 3.6. The final model has a RMSE error of 0.2922. The comparison of the output voltage predicted by the ANFIS model with the experimental data is shown in Figure 3.7. This plot shows that the ANFIS model is able to predict the different trends of output with reasonable accuracy. Figure 3.8 demonstrates that the ANFIS model is able to capture and predict the hysteretic behavior of the displacement with voltage applied across the length of the SMA wire.

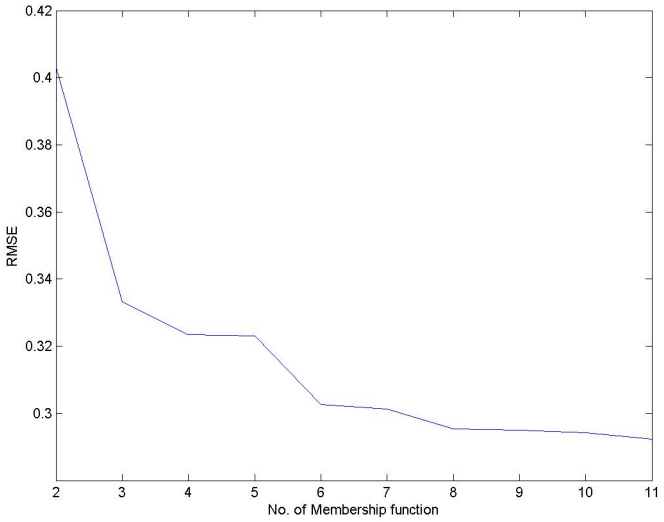

Figure 3.5: Effect of membership functions on single loop ANFIS displacement vs. voltage model

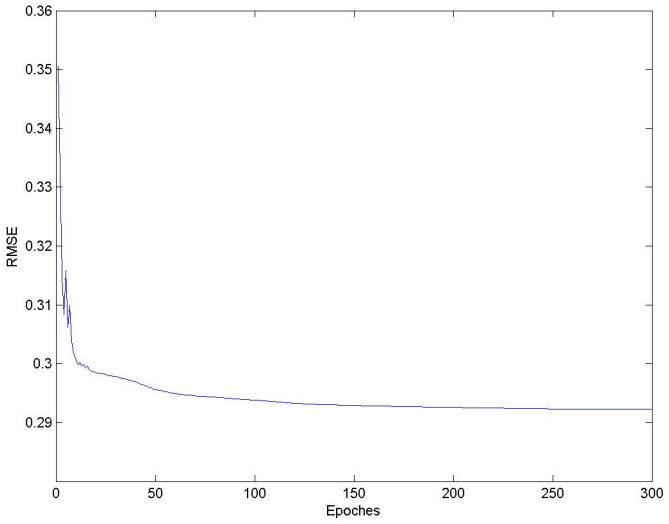

Figure 3.6: Variation of RMSE with epoches for single loop ANFIS displacement vs. voltage model

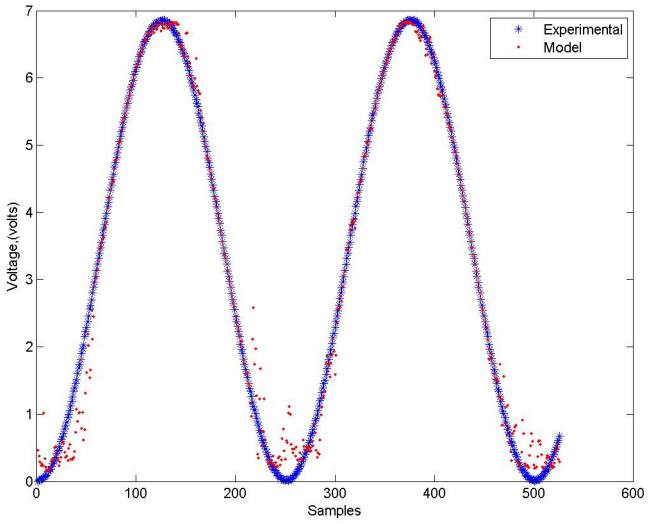

Figure 3.7: Comparison of experimental voltage with single loop ANFIS predicted voltage

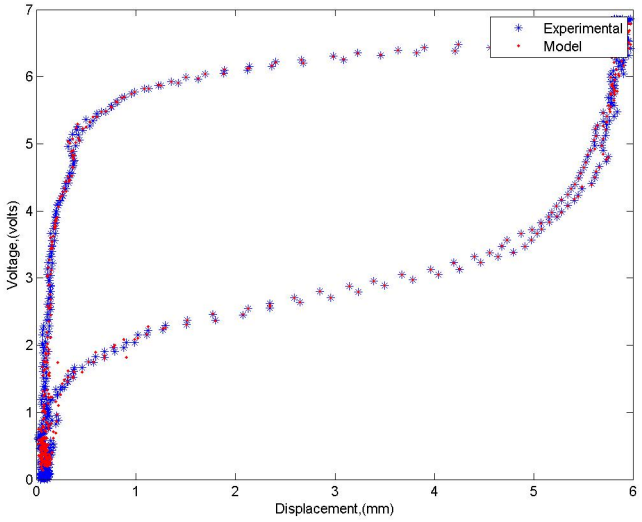

Figure 3.8: Single loop displacement vs. output voltage hysteresis

3.4.1.2 Neural Networks model

The input-output data sets employed in the previous subsection for the ANFIS model is utilized to build an ANN model. A feed-forward, back-propagation network with ten hidden neurons, model a single-loop hysteresis system. The variation of error with iteration is shown in Figure 3.9. In this figure, it is seen that there is an initial drop of a RMSE value from 0.55 to 0.35, but as the number of iterations increases, the RMSE value fluctuates between 0.35 to 0.46. The ANN predicted voltage values in Figure 3.10 follow and track the experimental data. At low voltages, this model is unable to predict accurately and has a lot of noise in the prediction. The hysteresis prediction of this model is displayed in Figure 3.11. The capabilities of ANN to predict nonlinear hysteretic relations is seen in this figure.

The same data utilized for making the ANFIS model is also employed for this model. A feed-forward, back-propagation network is created based on the input-output data sets. Fifteen hidden neurons have been used to make this model. For this single -loop system, a neural network is able to capture the dynamics of the system.

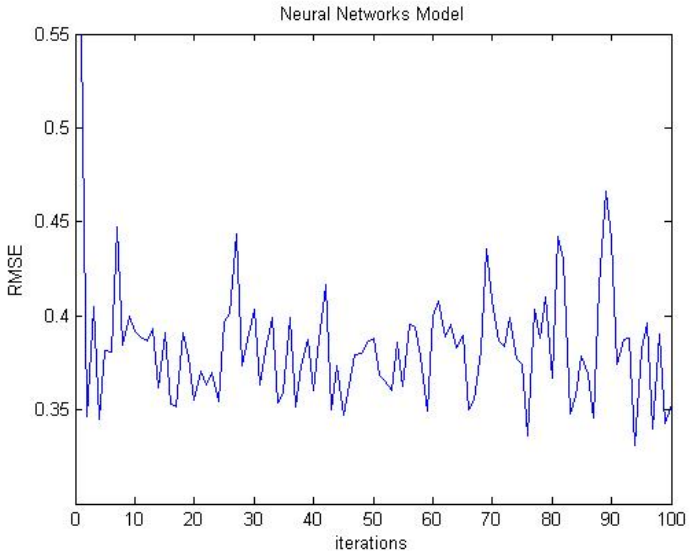

Figure 3.9: Variation of RMSE with iterations for a single -loop ANN displacement vs. voltage model

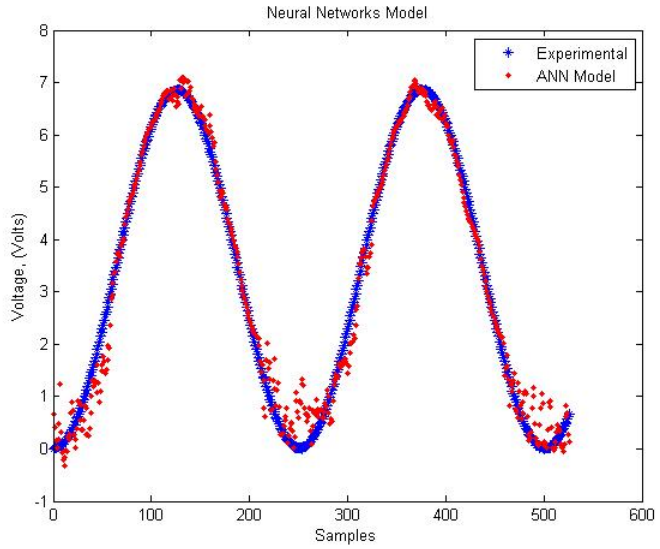

Figure 3.10: Comparison of experimental voltage with single -loop ANN predicted voltage

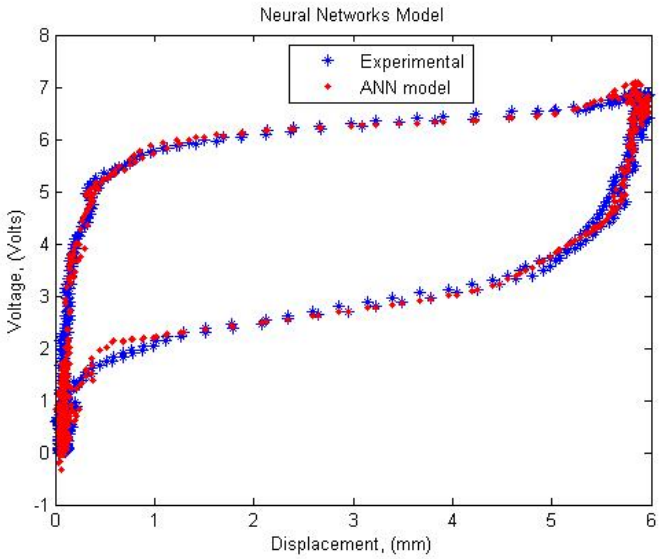

Figure 3.11: Single loop displacement vs. output voltage hysteresis

3.4.2 Feedback Temperature vs. Displacement Model

A temperature vs. displacement model appears in the feedback line of the closed-loop system and predicts the position of the weight. As explained before, the displacement of the weight suspended on an SMA wire is due to the temperature-induced phase transformation. As the voltage in the SMA wire increases, the temperature of the wire increases and the SMA wire contracts. The temperature of the SMA wire is recorded by the SMA-Constantan thermocouple previously developed. In this model the relationship between this temperature and the displacement of the pendulum is established. The experimental data recorded is both path-dependent and time-dependent. Thus, in order to track the path of the system, time history has to be utilized. To predict the position of the pendulum at a time t it is assumed to be related to the temperatures at time t and *t-1*. ANFIS and ANN models have been constructed based on the experimental data and their predictive capabilities are compared.

3.4.2.1 ANFIS model

The first step of building a neuro-fuzzy model is to construct membership functions. For this set of data points, a grid partitioning method is used to determine the initial membership functions. The change in RMSE with number of membership functions is shown in Figure 3.12. As the distribution of data points is crucial in determining the initial fuzzy membership function, a nonlinear sampling is employed in feeding inputs into the model and is shown in Figure 3.13. The initial membership functions are prepared based on these input data sets by using the genfis1 function in MATLAB. Using 10 membership functions and 100 fuzzy rules, the initial model is prepared. After 300 epoches, the RMSE error has reached a value of 0.043, as seen in Figure 3.14. This model is able to predict the displacement of the pendulum based on the inputs of temperature histories. The model tracking the actual experimental data is seen in Figure 3.15. The ANFIS model is able to capture the nonlinear path dependence of displacement with temperature. This trend is shown in Figure 3.16.

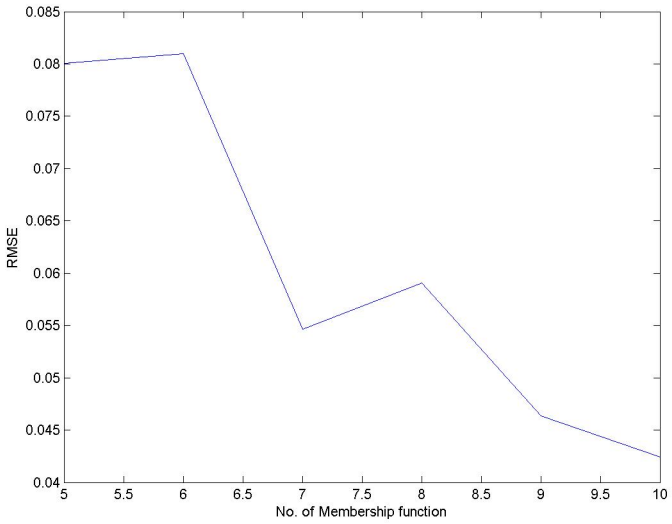

Figure 3.12: Effect of membership functions on single loop ANFIS temperature vs. displacement model

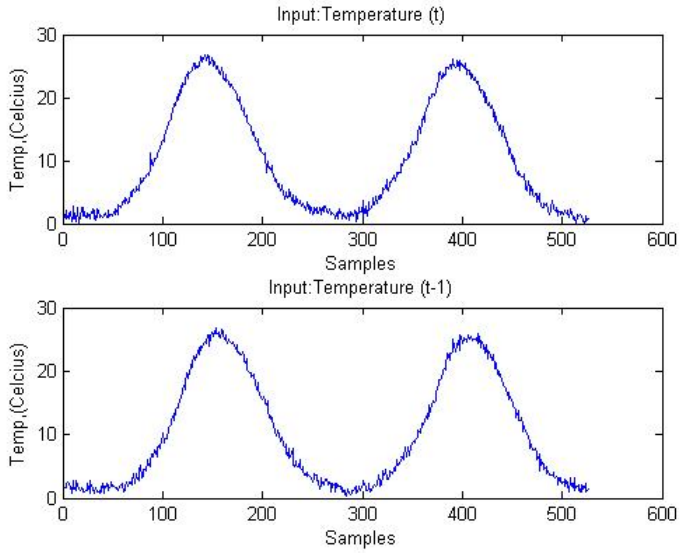

Figure 3.13: Input vectors to predict displacement for single loop hysteresis models

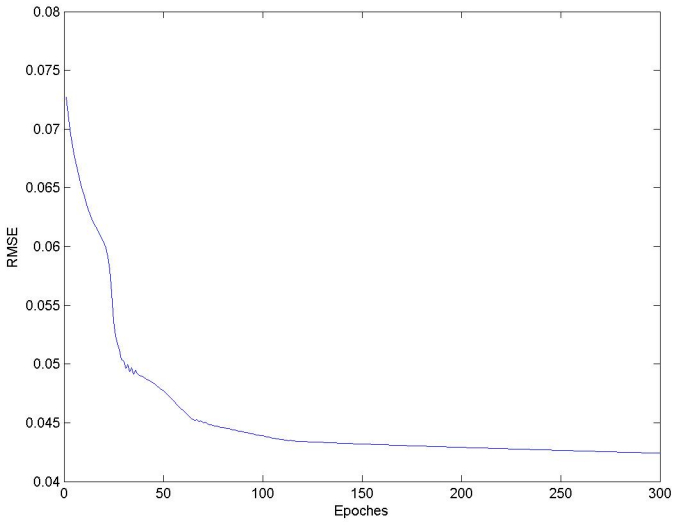

Figure 3.14: Variation of RMSE with epoches for single loop ANFIS temperature vs. displacement model

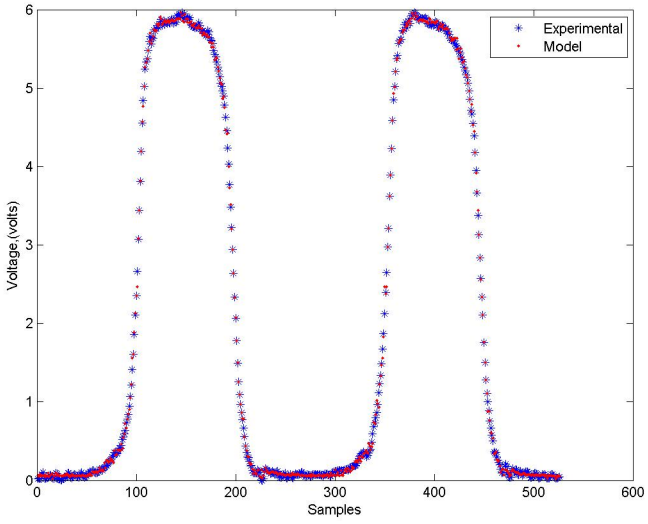

Figure 3.15: Comparison of experimental displacement with single loop ANFIS predicted displacement

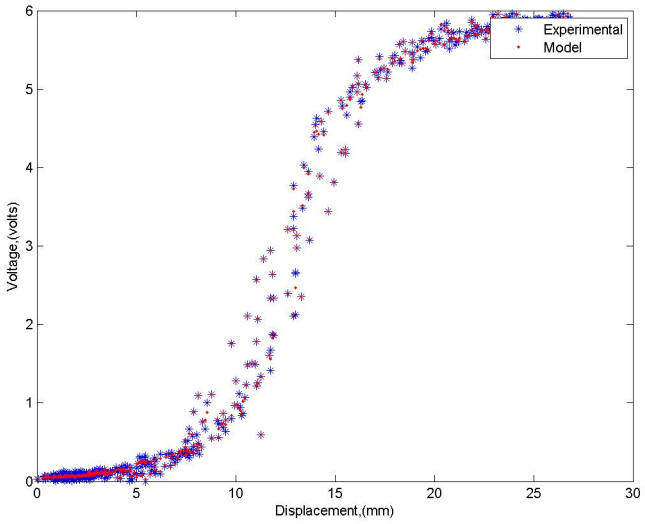

Figure 3.16: Single loop temperature vs. displacement model hysteresis

3.4.2.2 Neural Networks model

To study the prediction capabilities of artificial neural networks, a temperature vs. displacement relationship is modeled in this subsection using experimentally obtained data. A feed-forward back-propagation network is created based on the input-output data sets prepared for the ANFIS model in the last subsection. Ten hidden neurons have been used to make this model. The variation of error with iteration is shown in Figure 3.17. This plot shows that the RMSE is not consistent; i.e., it is neither increasing nor decreasing with iterations. Figure 3.18 points out that the ANN predicted displacement lies on top of the experimental data. The predicted data of this model is able to track the experimentally obtained hysteresis curve. This trend is evident in Figure 3.19.

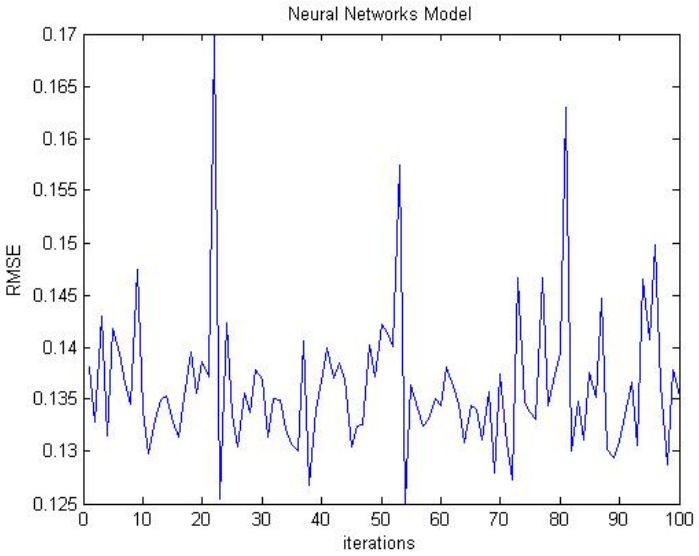

Figure 3.17: Variation of RMSE with iterations for a single loop ANN temperature vs. displacement model

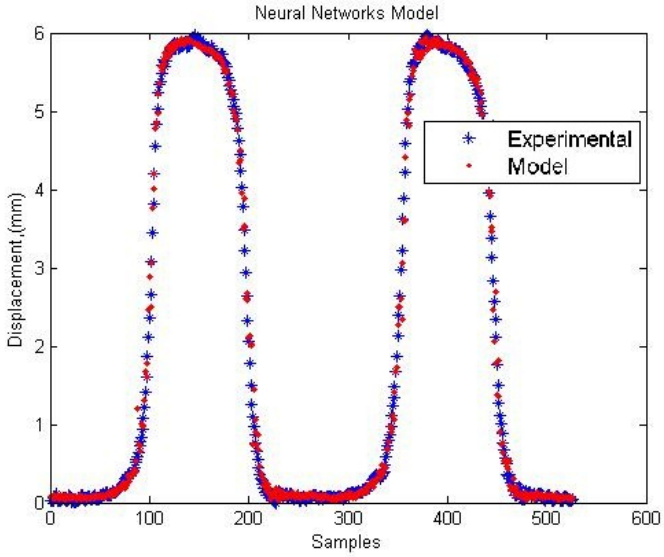

Figure 3.18: Comparison of experimental displacement with single loop ANN predicted displacement

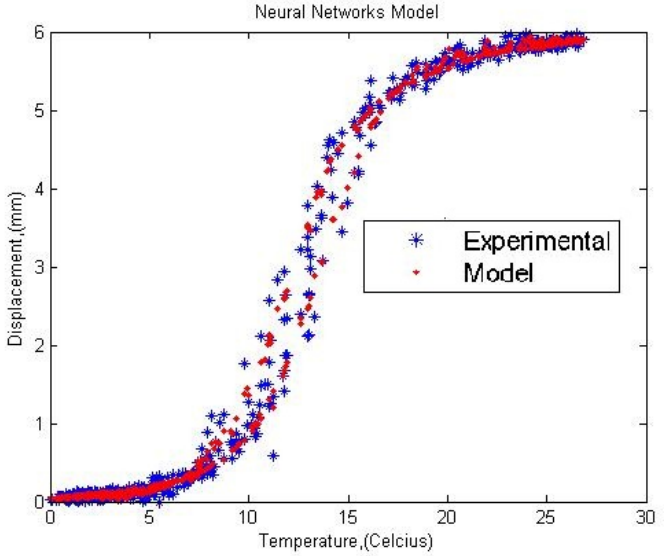

Figure 3.19: Single loop temperature vs. displacement hysteresis

3.5 Multi-loop characteristics - Amplitude variation

As seen in the previous sections, soft-computing techniques like ANFIS and ANN have been employed to model the nonlinear behavior of a single-looped hysteretic curves. Comparing the ANFIS displacement vs. voltage model with the ANN model, it is observed that both these models are able to capture and predict the nonlinear hysteretic behavior of a single-loop system with reasonable accuracy. It is observed that both ANN and ANFIS temperature vs. displacement models are able to track the position of the weight with temperature as the feedback variable. It is noted that in both single loop hysteresis cases, the RMSE of ANFIS models reduce with iterations while no consistent behavior is seen for the ANN models. Taking the prediction capabilities of all these models into consideration, it is noted that both the ANFIS and the ANN techniques are able to capture nonlinear dynamics of a single-loop system.

In this section, the learning capabilities of these soft-computing methods have been verified for single-loop hysteretic curves; using these methods, multi-loop hysteresis curves will be modeled. Firstly, the effect of the amplitude of voltage on the hysteresis is studied, then the response of an SMA due to the variation of frequency, is studied. During numerous experiments, sinusoidal voltage signals with different amplitudes and constant frequency is applied to the terminals of the SMA wire. Although the amplitude of the voltage signal is varied from 6 to 10 volts in different experiments, the frequency is kept constant at 0.05 Hz. Displacement of the pendulum, the Seebeck voltage of the SMA-Constantan thermocouple and the output voltage measurements are recorded using LABVIEW and NI-DAQ system. A part of the experimental data is selected for training these soft-computing methods. The modeling techniques employed using these techniques are discussed in this section.

3.5.1 Desired Displacement vs. Output Voltage Model

Similar to the previous models, this model also assumes that the voltage applied to the SMA wire is dependent on the time-shifted displacement signal. This, for the pendulum to be at a required position at time t, the voltage to be applied to the system at time t is dependent on the future position of the pendulum, i.e. its position at time $t+1$. Experimental data points used as input vectors to train the soft-computing models are plotted in Figure 3.20. As the data acquisition system has a uniform sampling rate, and the displacement of the

pendulum is highly nonlinear, the sampling distribution of the data points experimentally collected is also nonlinear. Nonlinear distribution of data points results in undue importance at a particular portion of the data set, which results in a unreliable model. To avoid this, a complex re-sampling method is employed to uniformly distribute data points throughout its domain. The distortion in shape of the inputs is due to this sampling method.

3.5.1.1 ANFIS model

Initial membership functions are obtained by feeding input-output data pairs into a subtractive clustering algorithm. The radius of the cluster is varied in search of an optimum rule base with minimum error. For 4,845 sets of data points, a cluster radius of 0.07 computes 113 Gauss membership functions using genfis2 function in MATLAB.

The parameters of this set of membership functions are updated using the gradient descent back propagation algorithm. Figure 3.21 displays the transition in root mean squared error (RMSE) with epochs. As expected, the RMSE initially reduces with epochs and finally reaches a plateau to 0.294. The comparison of the output voltage predicted by the ANFIS model with the experimental data is shown in Figure 3.22. This plot shows that the ANFIS model is able to predict the different trends of output with reasonable accuracy.

Figure 3.23 shows the hysteretic behavior of the displacement when the voltage is applied across the length of an SMA wire. It is noted that for each cycle, the model is able to learn the non-linearity of the output. Although the model works for training data, what is more important is the model's ability to generalize the fuzzy rules and interpolate this behavior to other data. The interpolation capabilities of this black box system are validated by testing the model with a data set corresponding to an output voltage of 6.5 volts. This data set has not been used in building and training the parameters of the model. The experimental results are plotted along with the ANFIS predicted points in Figure 3.24 for this data set. The predictions from the model accurately track the experimental results. This ability of the model to predict and generalize the fuzzy rules for any data validates the learning capabilities of the model.

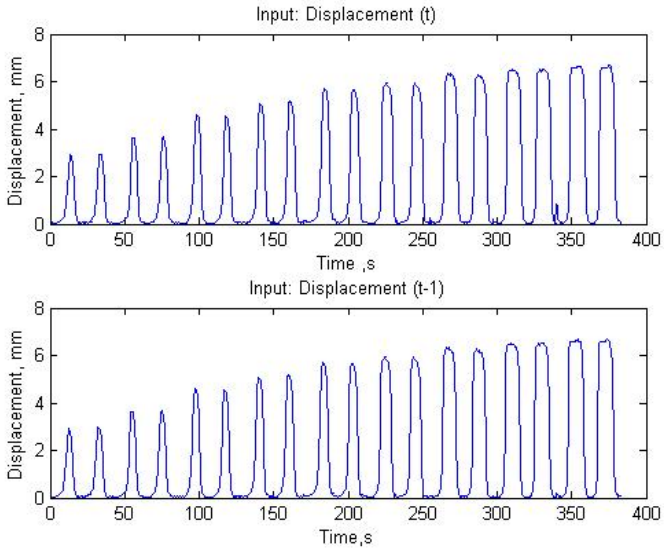

Figure 3.20: Input vectors to predict voltage for multi-loop hysteresis models

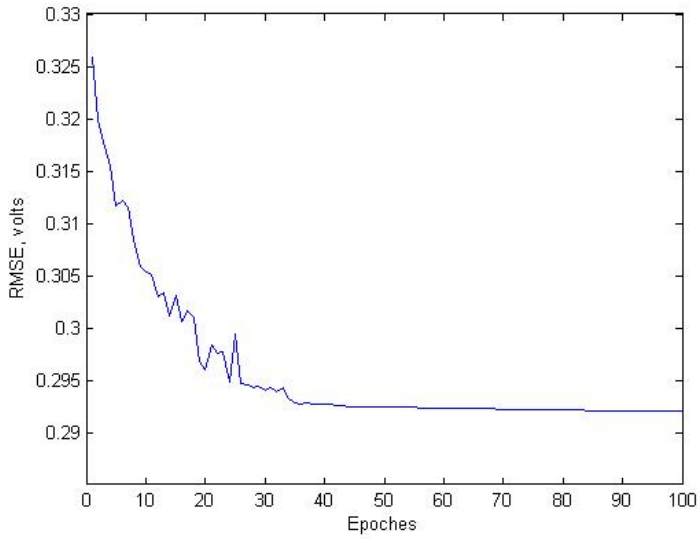

Figure 3.21: Variation of RMSE with epoches for multi-loop ANFIS displacement vs. voltage model

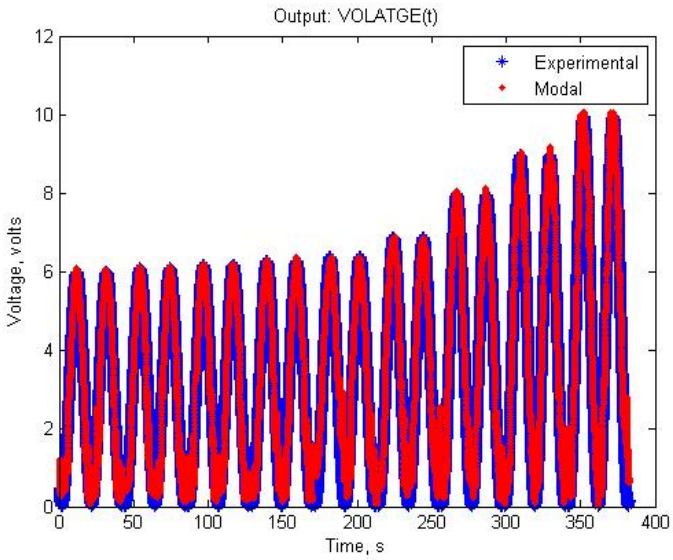

Figure 3.22: Comparison of experimental voltage with multi-loop ANFIS predicted voltage

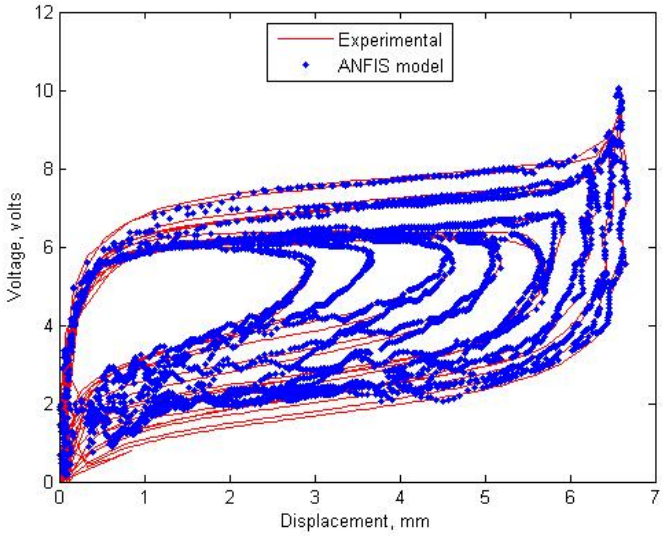

Figure 3.23: Hysteresis multi-loop displacement vs. voltage model

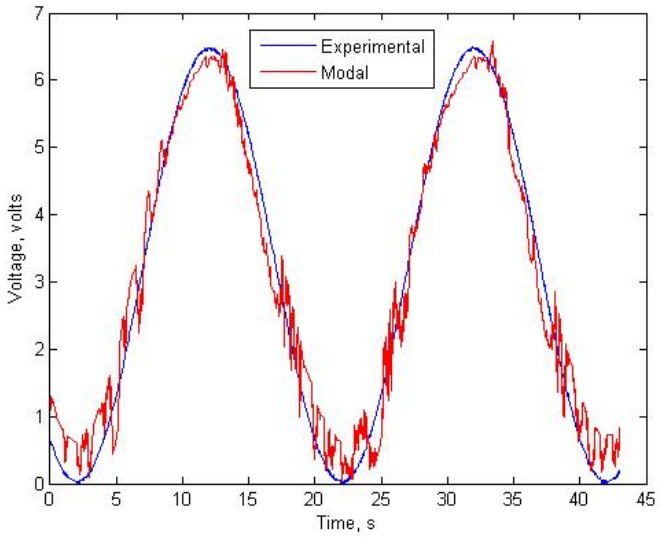

Figure 3.24: Validation of multi-loop ANFIS predicted Voltage

3.5.1.2 Neural Networks model

Artificial neural networks uses experimental data points to train its parameters to develop a model capable of understanding and learning the nonlinearities present in this system. The data set with nonlinear sampling, previously used, is also used to build a fifteen hidden neuron model. The RMSE varies from a value of 0.65 to 0.9 volts with iterations, which is plotted in Figure 3.25. The voltage predicted by this model with displacement as input is compared with the actual experimental data in Figure 3.26. This model is able to capture the peaks of voltage at lower amplitudes. ANN is unable to predict the variation of strain dynamics of SMAs with a voltage. The hysteresis prediction of this model is shown in Figure 3.27. This plot shows that the ANN model is able to detect the presence of inner loops, but it is unable to track the exact path of the pendulum.

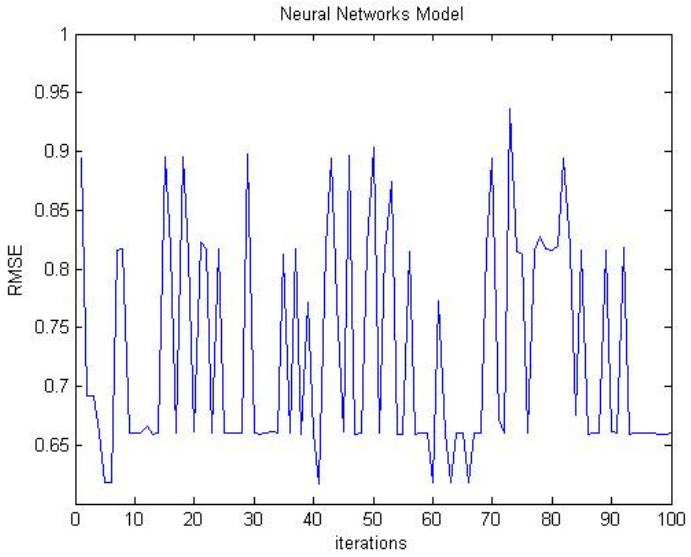

Figure 3.25: Variation of RMSE with iterations for a multi-loop ANN displacement vs. voltage model

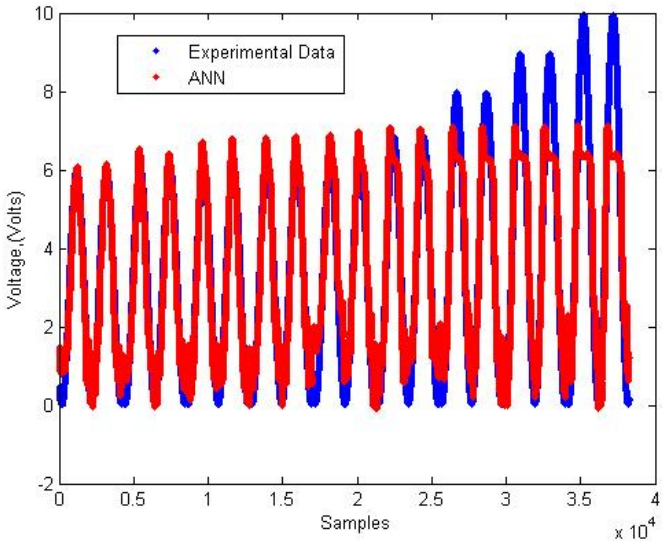

Figure 3.26: Comparison of experimental voltage with multi- loop ANN predicted voltage

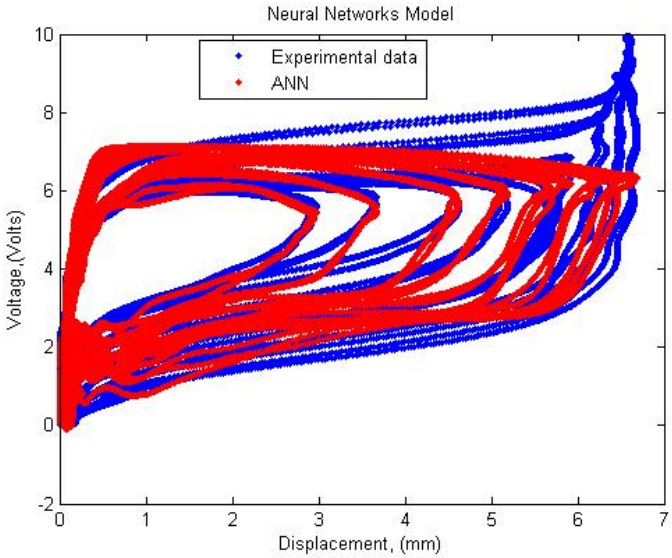

Figure 3.27: Multi-loop displacement vs. output voltage hysteresis

3.5.2 Feedback Temperature vs. Displacement Model

In the last experiment, the voltage required for the pendulum to track a desired path is modeled. In this subsection, a model is developed to monitor the kinematics of the pendulum. Multi input-single-output models with temperatures at time t and t-1, as the inputs and the displacement at time t as the output are developed in this section. The nonlinear change of position of the pendulum gives rise to a nonlinear sample distribution. Such data also attributes to poor prediction capabilities of the resultant model. As before, a nonlinear re-sampling method is employed to uniformly distribute the data points throughout its domain. The distortion of the shape of the inputs is due to this sampling method. The variation of temperature corresponding to the amplitude of the voltage signal is evident from Figure 3.28.

3.5.2.1 ANFIS model

An initial model of 140 rules is developed using a subtractive clustering algorithm in MATLAB. These rules are tuned into an ANFIS model by training with 4,232 data points. The RMSE reduces with epoches and reaches a steady value of 0.056 mm after 200 epoches. The change in RMSE with epochs is plotted in Figure 3.29. The ANFIS model predicted displacement is compared with the experimental data in Figure 3.30. As seen from this figure, the corelation between the model and experimental data is approximately one. The ANFIS model predicts and tracks the experimentally obtained displacement signal with reasonable accuracy. The previously made assumption of displacement having a time history dependence on temperature is correct. The nonlinear behavior of displacement with temperature is seen in Figure 3.31. As before the generalization and interpolation characteristics of this nonlinear model is tested by feeding the experimentally obtained temperature path data in ANFIS model. From the results shown in Figure 3.32, it can be inferred that the model is able to track the path followed by the pendulum with a temperature history of any new data with good accuracy.

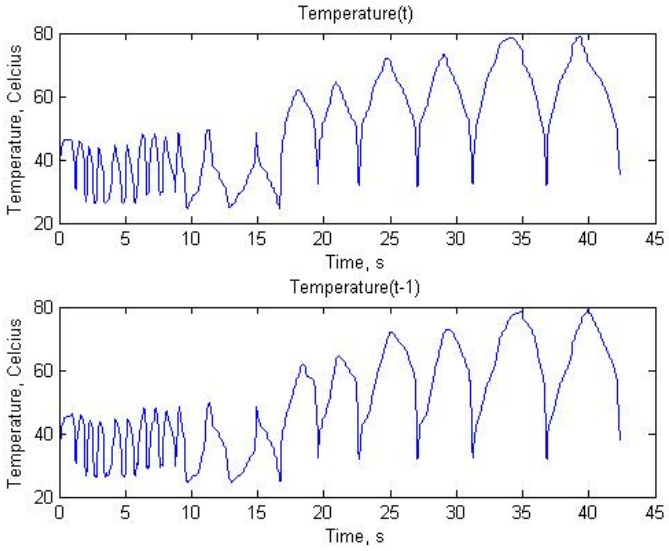

Figure 3.28: Input vectors to predict displacement for multi-loop hysteresis models

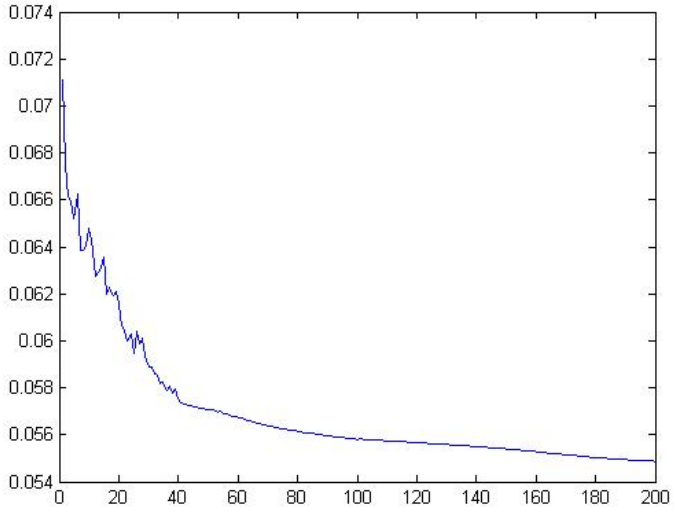

Figure 3.29: Variation of RMSE with epoches for multi-loop ANFIS displacement vs. voltage

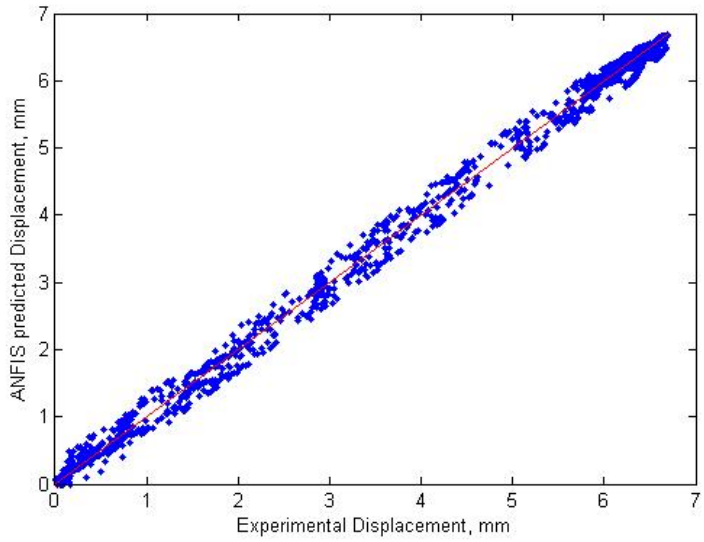

Figure 3.30: Comparison of experimental voltage with multi-loop ANFIS predicted displacement

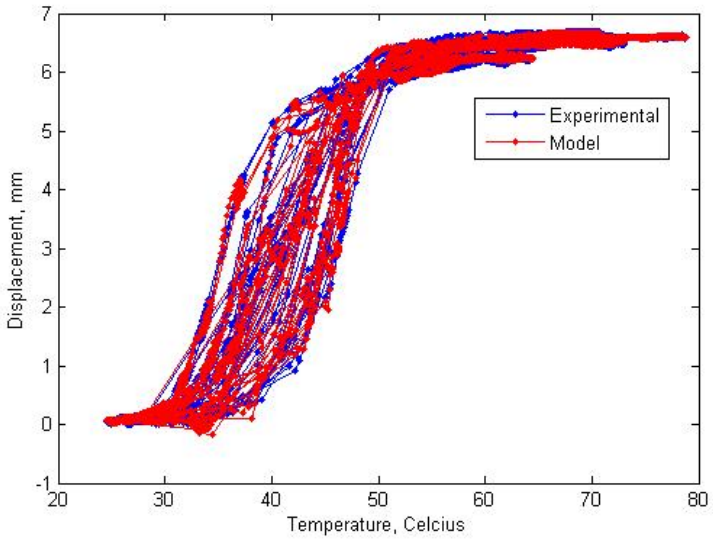

Figure 3.31: Multi-loop temperature vs. displacement hysteresis

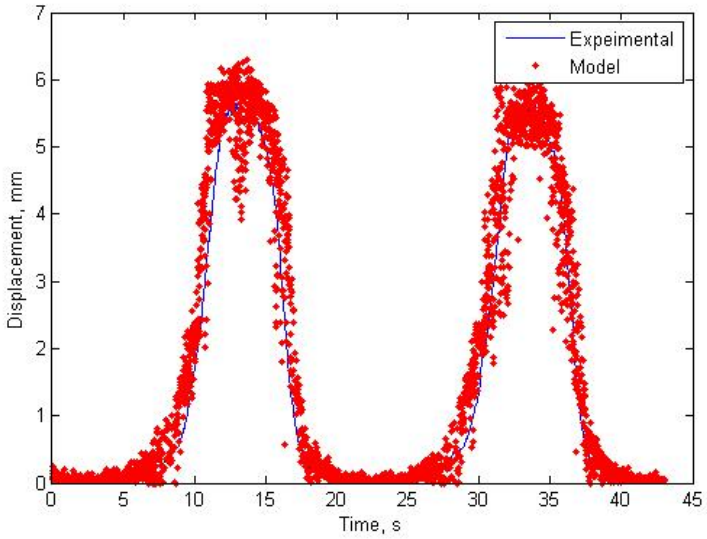

Figure 3.32: Validation Multi-loop ANFIS temperature vs. displacement model

3.5.2.2 Neural Networks model

Multi-loop experimental data is used to build an ANN model which learns and predicts the hysteretic nonlinearities present in the displacement characteristics of the pendulum. A feed-forward back-propagation network is created based on the temperature and displacement of the input-output data sets prepared for the last model. Fifteen hidden neurons have been used to develop this model. The variation of error with iteration is presented in Figure 3.33. The RMSE for this data oscillates between 0.094 to 0.106 mm and it does not converge to a specific value. The displacement predicted by the ANN model is compared with the experimental values in Figure 3.34. The ANN predicted data has followed and captured the higher amplitude peaks in this case. From the hysteresis plot shown in Figure 3.35, it is observed that although the model is able to capture maximum displacements of the pendulum, it is unable to track the path followed by the pendulum.

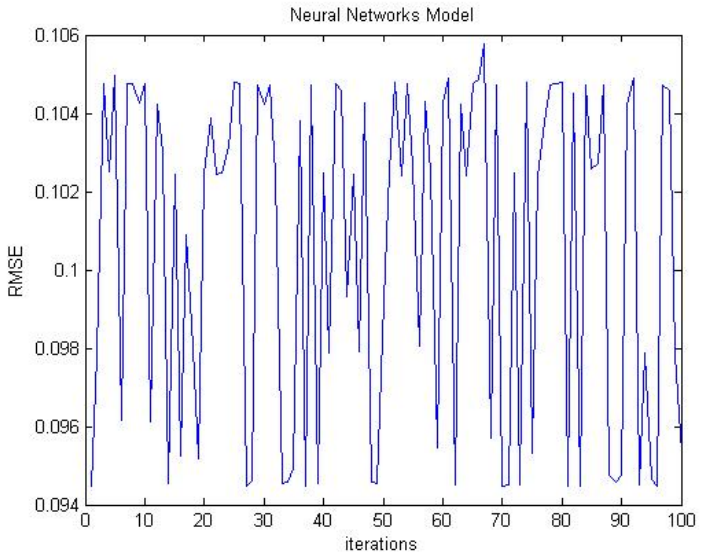

Figure 3.33: Variation of RMSE with epoches for ANN temperature vs. displacement model

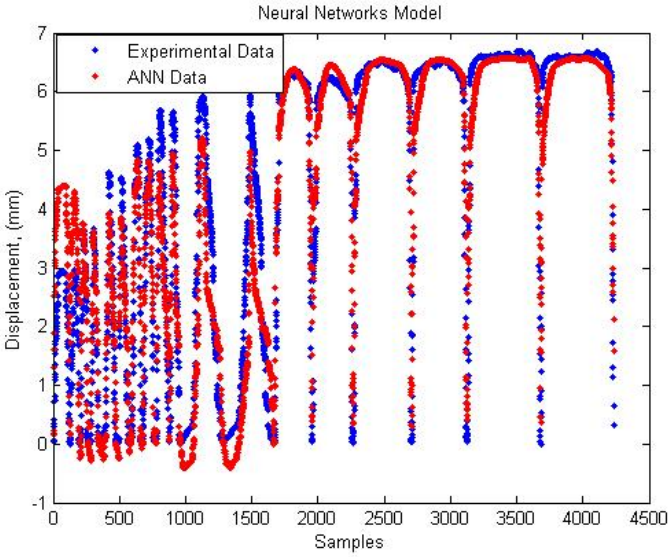

Figure 3.34: Comparison of experimental displacement with multi-loop ANN predicted displacement

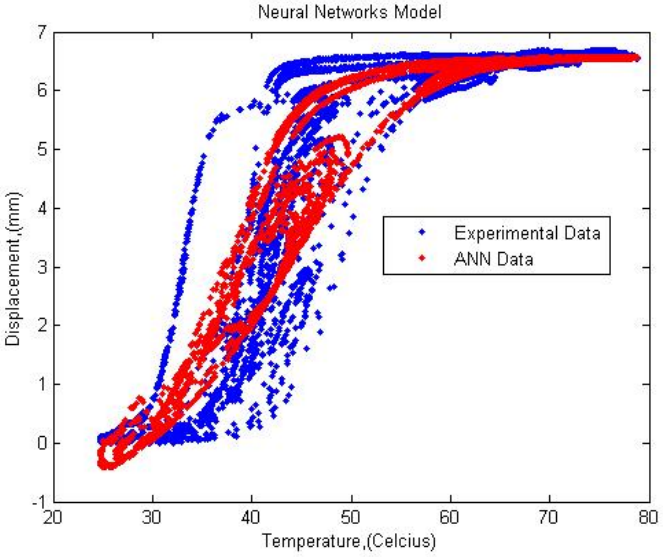

Figure 3.35: Multi-loop temperature vs. displacement hysteresis

3.6 Multi-loop characteristics - Frequency variation

In this section, the influence of frequency on strain characteristics of the system is studied. During different experiments, sinusoidal voltage with varying frequencies and constant amplitude is applied to the terminals of an SMA wire. Although the frequency of the voltage signal is varied from 0.01Hz to 0.2 Hz in different experiments, the amplitude is kept constant at 8 volts. Displacement of the pendulum, the Seebeck voltage of the SMA-Constantan thermocouple, and the output voltage measurements are recorded using LABVIEW and NI-DAQ system. A part of the experimental data is selected for training these soft-computing methods. The modeling techniques employed using these techniques are discussed in this section.

3.6.1 Desired Displacement vs. Output Voltage Model

Similar to the previous models, this model also assumes that the voltage applied to the SMA wire is dependent on the time shifted displacement signal. This model assumes that displacement at time t and $t+1$ are sufficient to predict the voltage signal at a time t. Based on this assumption ANFIS and ANN models have been created using the experimental input shown in Figure 3.36. Similar to previously developed models a nonlinear re-sampling method is engaged to uniformly sample the data.

3.6.1.1 ANFIS model

As previously discussed, the first step in setting up an ANFIS model is to build membership functions. Initial membership functions are obtained by feeding input-output data pairs into a Fuzzy -C Clustering method. For 4,501 sets of data points a rule base of 256 rules is created using 16 membership functions of each input. The parameters of this rule-base are tuned to fit the data by neural networks. The change in RMSE with epoches is plotted in Figure 3.37. The RMSE value is initially high; however with epoches the error reduces and converges to a value of 0.058 volts. The output voltage predicted by the ANFIS model is compared with the experimental data in Figure 3.39. This plot demonstrates that the ANFIS model is able to capture and predict the hysteretic behavior of the displacement when a voltage is applied across the length of the SMA wire.

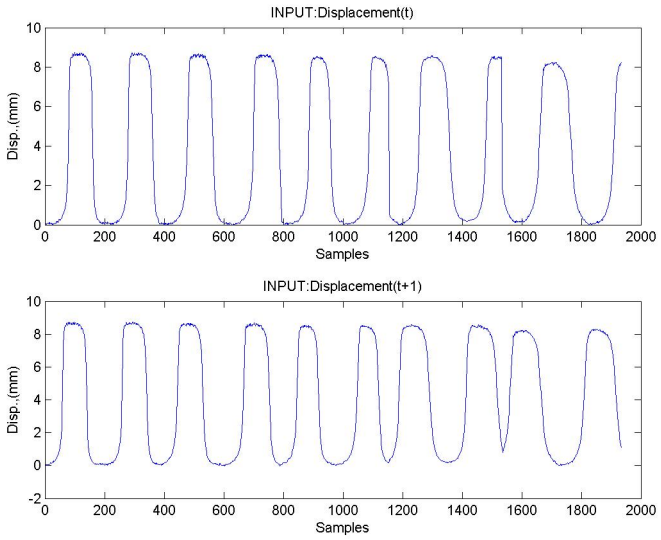

Figure 3.36: Input vectors to predict voltage for multi-loop hysteresis models

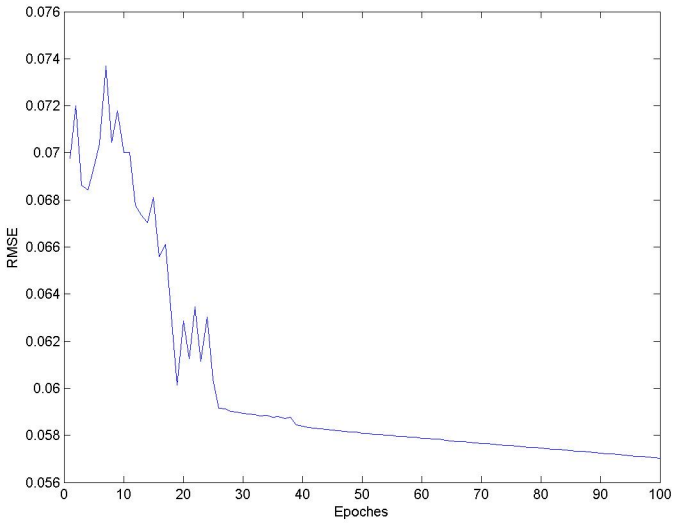

Figure 3.37: Variation of RMSE with epoches for multi-loop ANFIS displacement vs. voltage model

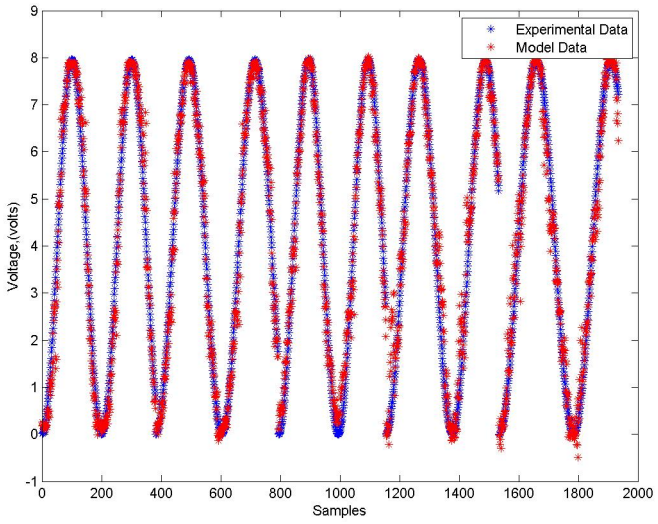

Figure 3.38: Comparison of experimental voltage with multi-loop ANFIS predicted voltage

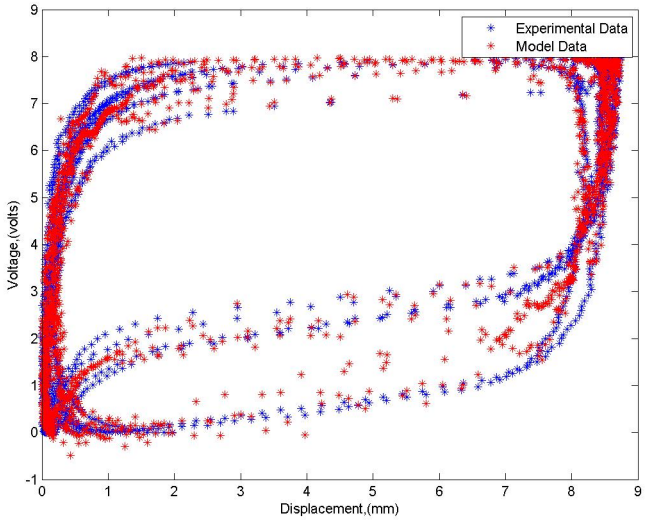

Figure 3.39: Hysteresis multi-loop displacement vs. voltage model

3.6.1.2 Neural Network

The input-output data sets employed in the previous subsection for the ANFIS model is utilized for building an ANN model. A feed-forward back-propagation network with fifteen hidden neurons models a single-loop hysteresis system. The variation of error with iteration can be seen in Figure 3.40. The RMSE valve varies with each iteration but lies in the range of 0.96 to 1.12 volts. The voltage predicted by this model with displacement as input is compared with the actual experimental data in Figure 3.41. This model is unable to capture the peaks of the voltage at any frequency. The ANN is unable to predict the variation of strain dynamics of SMAs with frequency. The hysteresis prediction of this model is plotted in Figure 3.42. This plot shows that the ANN model is able to detect the presence of multiple loops, but it is unable to track the exact path of the pendulum. The complexity of this ANN model is unable to predict the voltage required by an SMA to track a specific path.

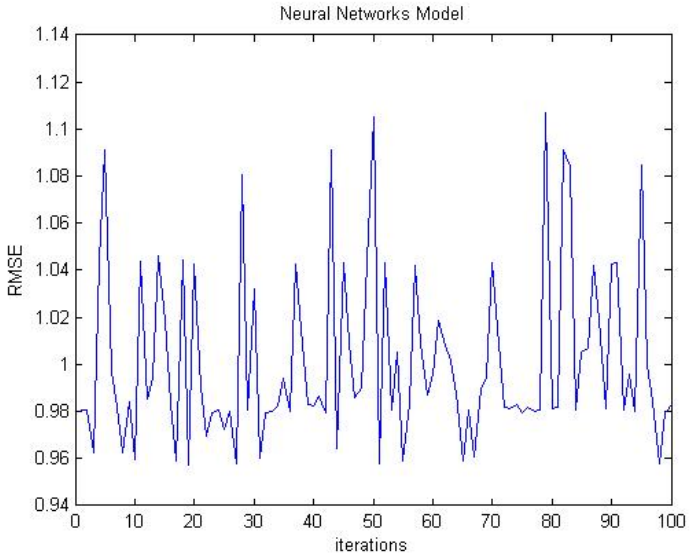

Figure 3.40: Variation of RMSE with iterations for a multi-loop ANN displacement vs. voltage model

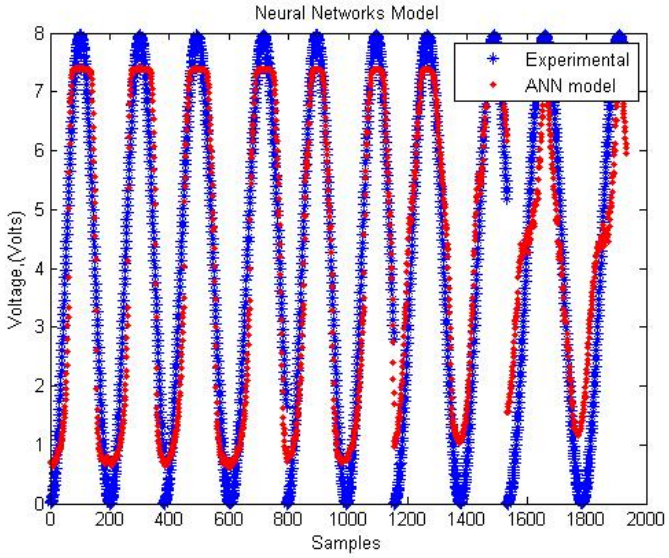

Figure 3.41: Comparison of experimental voltage with multi-loop ANN predicted voltage

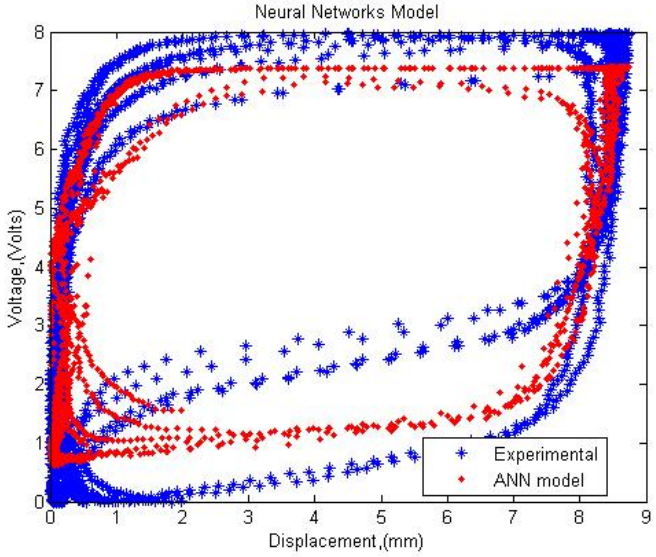

Figure 3.42: Multi-loop displacement vs. output voltage hysteresis

3.6.2 Feedback Temperature vs. Displacement Model

In this section, the relationship between the feedback temperature of the system and the displacement of the pendulum is studied. As explained in previous sections, the temperature - displacement models assume that it is a multi-input single-output model, where temperatures at time *t* and *t-1* are the inputs and displacement at time *t* is the output. The experimentally recorded data points are re-sampled to achieve uniform distribution of training data, resulting in the distortion of the shape of the inputs plotted in Figure 3.43. Using experimental data, both the ANFIS and ANN models have been developed in this subsection.

3.6.2.1 ANFIS model

An initial fuzzy model of 144 rules is developed using Fuzzy-C clustering algorithm in MATLAB. These rules are tuned into an ANFIS model by training it with 4,501 sets of data points. The RMSE values reduce with each epoch and settle at a value of 0.74mm at the end of 100 epoches as shown in Figure 3.44. The results of the ANFIS model are compared with experimental values of the displacement of the pendulum in Figure 3.45.The model predicts and tracks the experimentally obtained displacement signal with reasonable accuracy. The previously made assumption of displacement having a time-history dependence on temperature is proven to be correct. The nonlinear behavior of displacement with temperature is seen in Figure 3.45. The model is able to track the path followed by the pendulum using temperature history of the SMA wire as inputs with good accuracy.

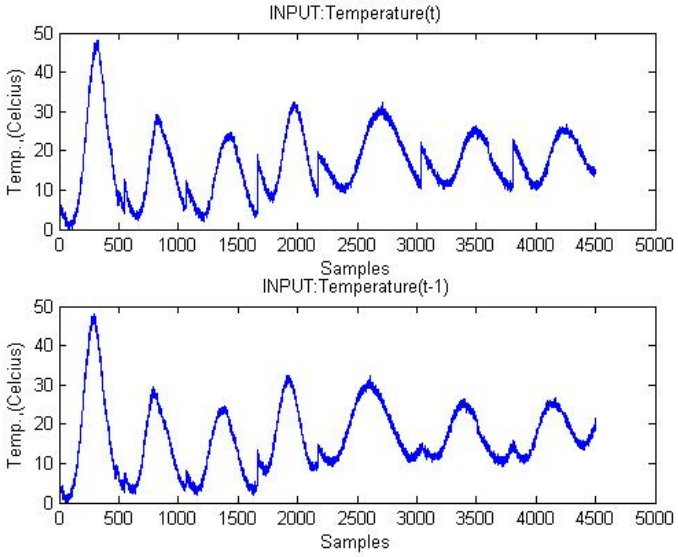

Figure 3.43: Input vectors to predict voltage for multi-loop hysteresis models

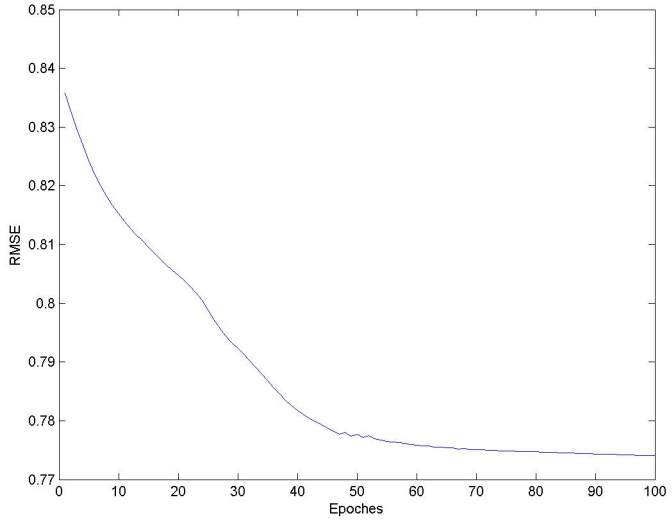

Figure 3.44: Variation of RMSE with epoches for multi-loop ANFIS temperature vs. displacement model

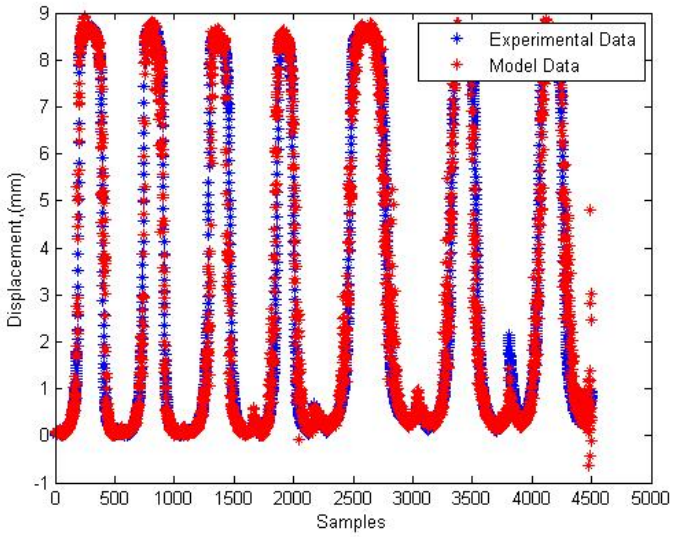

Figure 3.45: Comparison of experimental displacement with multi-loop ANFIS predicted displacement

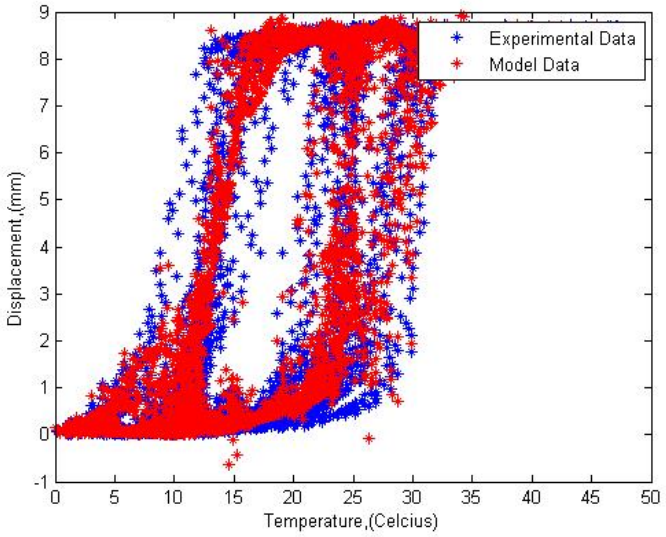

Figure 3.46: Multi-loop temperature vs. displacement hysteresis

3.6.2.2 Neural Network model

Multi-loop experimental data is used to build an ANN model that learns the hysteretic nonlinearities which are required to predict the position of the pendulum. A feed-forward back-propagation network is created based on the temperature and displacement input-output data sets prepared for the last model. Fifteen hidden neurons have been used to make this model. The variation of error with iteration is presented in Figure 3.47. The RMSE for this data oscillates between 1.06 to 1.14 mm and is much higher than the ANFIS model. The displacement predicted by the ANN model is compared with the experimental values in Figure 3.48. This plot shows that the ANN predicted data has followed and captured peaks and troughs in the experimental data. From the hysteresis plot shown in Figure 3.49, it is observed that although the model is able to capture maxima and minima of the displacement response, it is unable to track the precise path followed by the pendulum.

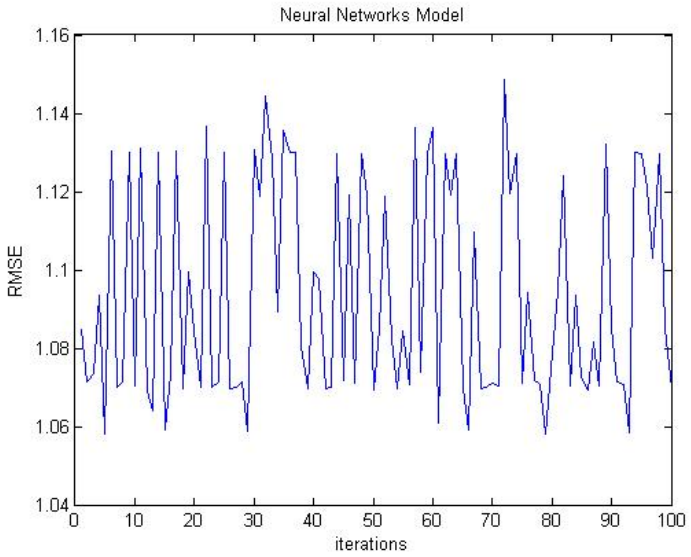

Figure 3.47: Variation of RMSE with iterations for a multi-loop ANN temperature vs. displacement model

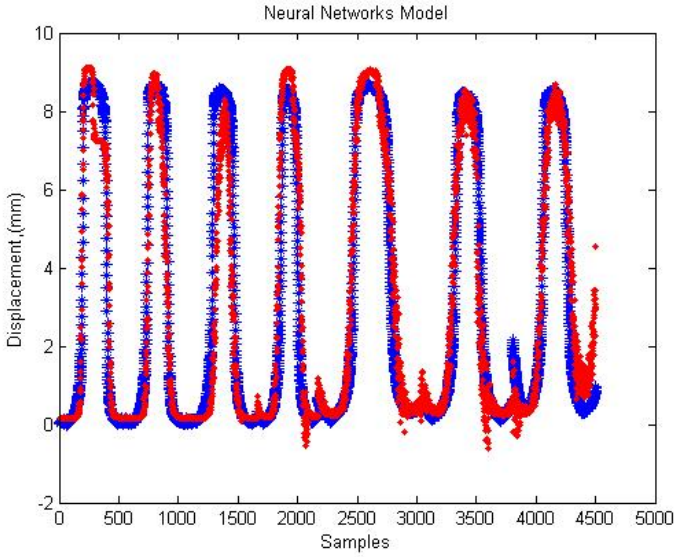

Figure 3.48: Comparison of experimental displacement with multi-loop ANN predicted displacement

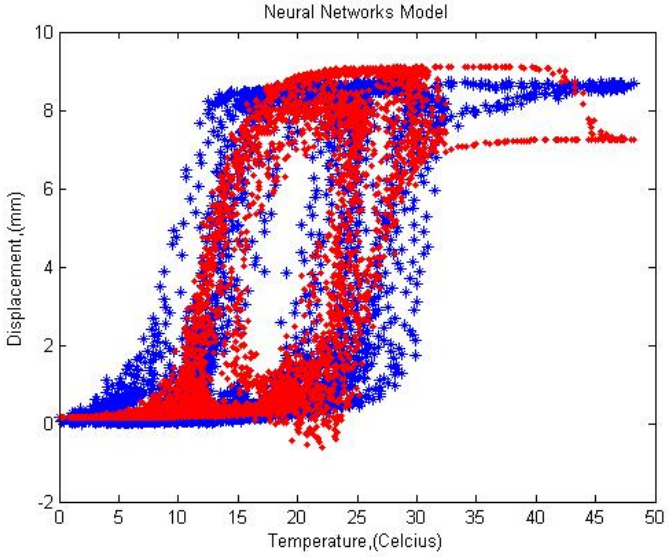

Figure 3.49: Multi-loop temperature vs. output displacement hysteresis

3.7 Conclusions

This chapter focuses on the development of soft-computing models like ANFIS and ANN models to capture and predict the nonlinear hysteretic behavior of displacement-voltage relationship and temperature-displacement relationship. Initially, to verify the applicability of these techniques, single-looped hysteresis curves have been modeled. Both ANFIS and ANN models were able to capture and predict these curves with good accuracy. Results of these models have shown that the learning algorithm of soft-computing methods is sufficient to predict its properties.

In the later part of this chapter, multi-loop hysteresis curves have been modeled. The influence of frequency and amplitude of the voltage signal on the strain characteristics of SMA wires is studied with the help of ANFIS and ANN models. In general, it is observed that the ANFIS model was able to train and predict with higher correlation towards experimental data than the ANN models. The ANN models were unable to predict these nonlinear hysteretic curves, while the ANFIS models have captured these trends.

Chapter 4

Effect of Time-Shift on ANFIS Modeling

4.1 Introduction

In the last chapter, single and multi-loop hysteresis of strain characteristics have been modeled based on inputs storing information with one-second shift. These models have shown that ANFIS has the ability to learn and adapt its parameters to these nonlinearities and model them. In modeling these path dependent behaviors, it is assumed that for predicting voltage, displacement at times t and $t+1$ are required as inputs, and temperature at times t and $t-1$ are required to predict displacements of the pendulum. Initial models present in the last chapter prove the concept that the time-shift analysis is able to capture the complex strain characteristics of SMAs. This chapter studies and verifies if the time-shift value of this system has any effect on the prediction capabilities of the ANFIS model.

To study these nonlinearities, the time-shift of the variables is generalized as seen in Figure 4.1. The displacement vs. voltage model assumes that the positions of the pendulum at time t and $t+n$ are needed to predict the voltage required by the SMA wire. In this case, as the trajectory of the pendulum is pre-determined, the value of n can vary in both negative and positive domains. This means that if the pendulum has to track a specific path then the positive time indicates the future position of the pendulum and the negative time indicates the past position of the pendulum. Similarly, the temperature vs. displacement model requires temperatures at times t and $t+m$ to predict the position of the pendulum. As this model is positioned in the feedback line, the value of m can only be negative.

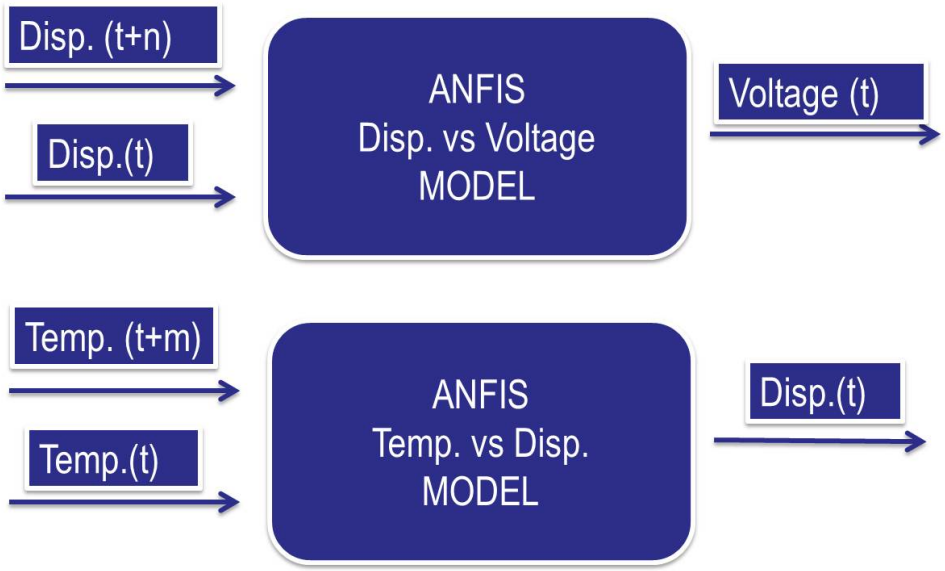

Figure 4.1: Time-shift inclusion in ANFIS models

4.2 Time-Shift effect on Single Loop Hysteresis

The effect of time-shift on the prediction capabilities of ANFIS model will be first studied for single loop hysteresis curves. As previously explained, based on the data collected from various experiments, ANFIS models with different time-shift values are built. The performance characteristic of these models is studied and analyzed in this section.

4.2.1 ANFIS Desired Displacement vs. Output Voltage Model

Experimentally collected time-series data is used to predict the potential difference that is required to actuate the pendulum to a desired position. This multi-input single-output system has two inputs; one is the displacement at time t and the other at time $t+n$. In this case, the value of n is varied from -3.7 sec to 4 sec in steps of 0.1 sec. For each value of n twenty Gauss membership functions are created using the Fuzzy-C clustering method. Data collected in an experiment in which a sinusoidal voltage signal with 0.05 Hz frequency and 8 volts amplitude is applied to the SMA wire. Each model is iterated untill the error value reaches a steady value. The effect of time-shift and the number of memebrship functions is explained in Appendix A. It is observed that in 300 epochs all the parameters of the

membership functions are optimized. Figure 4.2 shows that at time $t=0$, the RMSE of the model is maximum and its prediction capabilities are minimum. As the value of n is shifted from zero, the error slowly reduces untill it reaches a minimum value. If the time is shifted further it is observed that the error starts increasing again. The RMSE at the optimum time-shift value of 2.2 sec is 0.1457 volts. The input displacement signals at this time-shift are plotted in Figure 4.3.

The prediction capabilities of this ANFIS model are optimized by varying the number of MFs and fuzzy if-then rules present in the system. New membership functions are created using the grid partitioning type of clustering method. The effect of membership functions on the predictive capabilities of this model is plotted in Figure 4.4. Finally an ANFIS model with 196 fuzzy if-then rules and 14 membership functions has the lowest RMSE of 0.0778 volts. Voltage predicted by this model is compared with the actual voltage signal in Figure 4.5. This plot shows that the ANFIS model is able to capture and learn the nonlinearities present in the displacement vs. voltage relationship. The corresponding hysteretic curve is plotted in Figure 4.6.

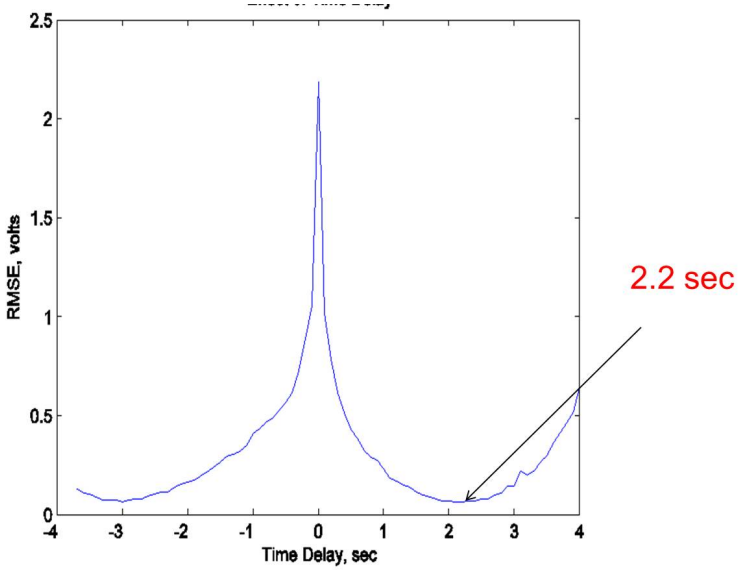

Figure 4.2: Effect of time-shift on single loop ANFIS displacement vs. voltage model

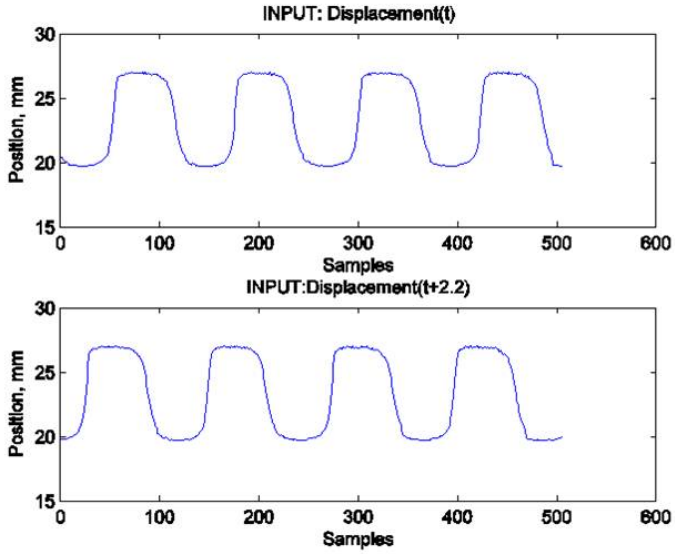

Figure 4.3: Inputs of optimized single loop ANFIS displacement vs. voltage model

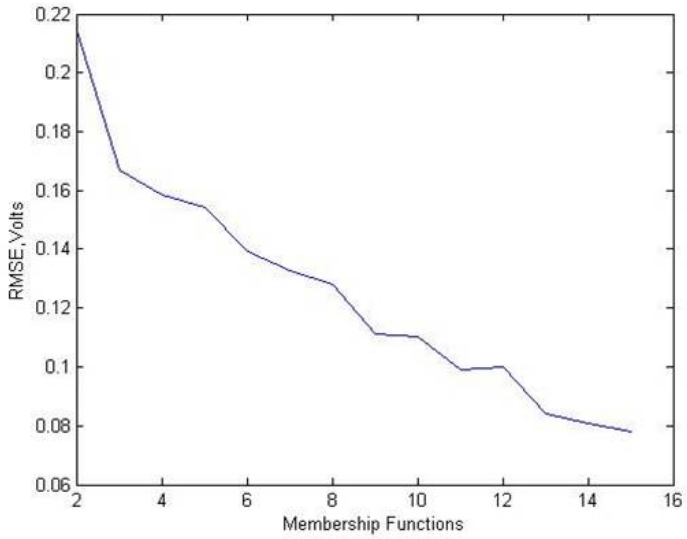

Figure 4.4: Influence of membership functions on single loop ANFIS displacement vs. voltage model

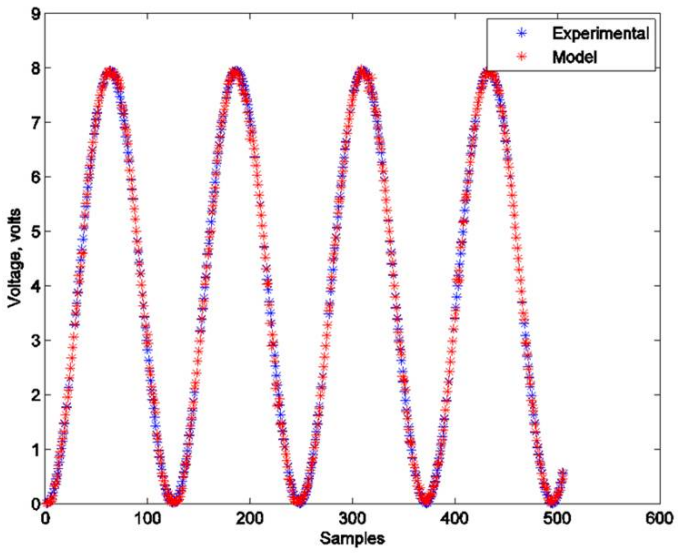

Figure 4.5: Comparison of ANFIS predicted voltage with experimental data

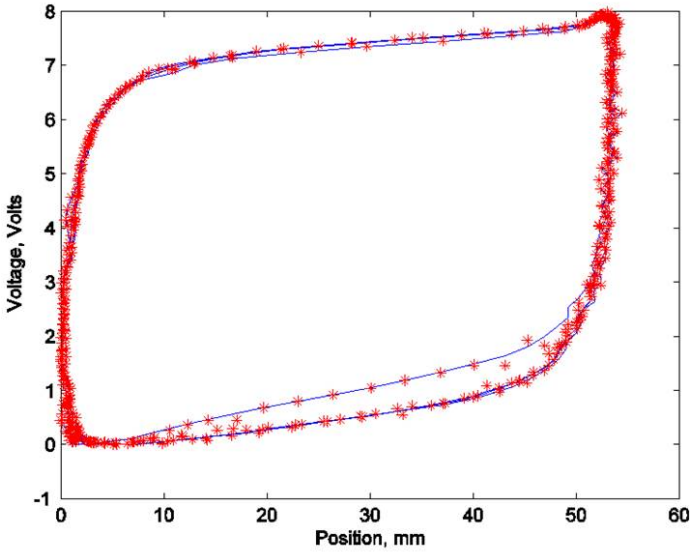

Figure 4.6: Single loop displacement vs. output voltage hysteresis

4.2.2 ANFIS Feedback Temperature vs. Displacement Model

In the feedback loop of the proposed closed-loop system, it is essential that the temperature-displacement model predicts the position of the pendulum precisely. To achieve better learning and generalizing capabilities, the time-shift value is varied and numerous models are prepared from experimentally obtained data. The prediction capabilities of these models are compared with each other and the optimum value of the time-shift is determined. In this case, as temperature is a feedback variable, the value of m is varied from 0 sec to -3.7 sec in steps of 0.1 sec. For each value of m, twenty Gauss membership functions are created using the Fuzzy-C clustering algorithm. Each model with different values of time-shift is trained and the RMSE after 300 epochs is noted and compared. A sample ANFIS program is present in Appendix B. Figure 4.7 shows the effect of time-delay on the error of different models. Although, at time $t=0$ the RMSE is highest, as time-delay is further increased the RMSE sharply falls and reaches pleatue. The minimum value in this plot is observed to occur when the time-shift reaches a value of -0.8 sec. Corresponding to this time-delay value, input temperatures at time t and $t\text{-}0.8$ is plotted in Figure 4.8. Similar to previous models, the influence of membership functions on errors is studied in Figure 4.9. An ANFIS model with sixteen membership functions and 256 Fuzzy if-then rules, produces a RMSE value of 0.05 mm. The ANFIS predicted displacement is compared with the experimental displacement values in Figure 4.10. This model is able to capture and learn the nonlinearities present in the temperature vs. displacement relationship. The corresponding hysteretic curve is plotted in Figure 4.11.

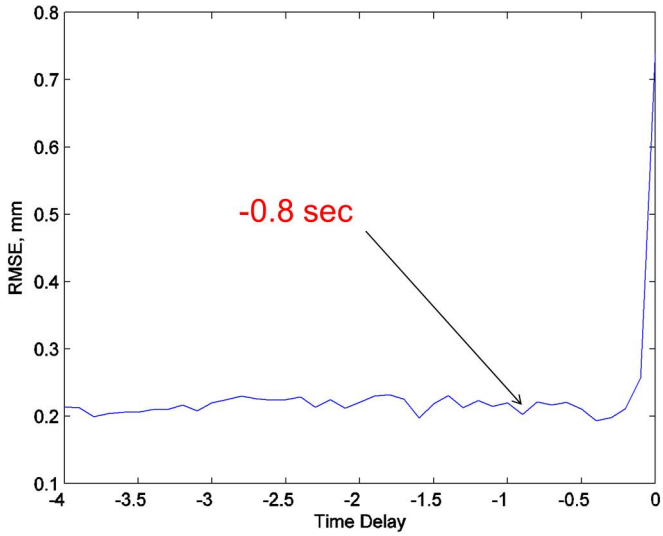

Figure 4.7: Effect of time-shift on single loop ANFIS temperature vs. displacement model

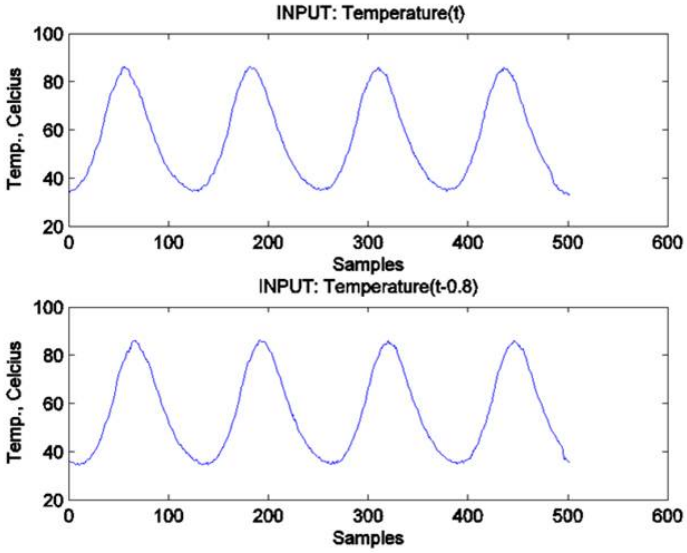

Figure 4.8: Inputs of optimized single loop ANFIS temperature vs. displacement model

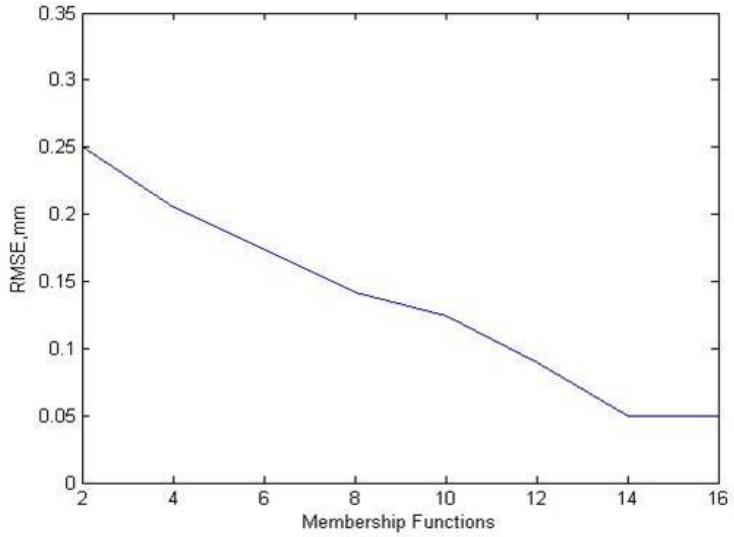

Figure 4.9: Influence of membership functions on single loop ANFIS temperature vs. displacement model

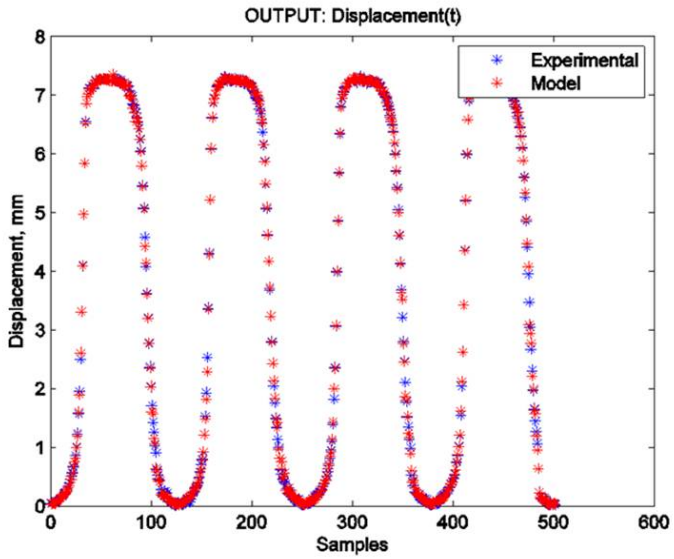

Figure 4.10: Comparison of ANFIS predicted displacement with experimental data

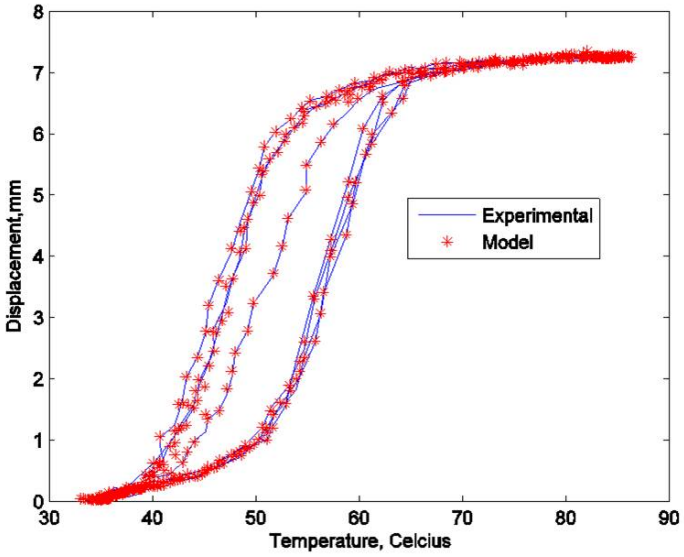

Figure 4.11: Single loop displacement vs. output displacement hysteresis

4.3 Effect of Time-Shift on Multi-Loop Hysteresis - Amplitude variation

Major and minor hysteresis loops are experimentally obtained by driving the experimental setup at various amplitudes of voltage signal supplied to the system. To represent the complete dynamics of the input-output space, input data sequences are selected from a large pool of data sets. The ANFIS models in previous sections have shown that for a single-looped system, time-shift has a greater effect on the displacement-voltage model than the temperature-displacement model. A smart choice of time-shift value results in a better predictive model for single-loop hysteresis systems. Does this time-shift value depend on driving amplitude or frequency? ANFIS models with different time-shift values are modeled for a system in which the driving frequency is constant, but the amplitude is varied. ANFIS displacement-voltage model and ANFIS temperature-displacement models are presented in this section.

4.3.1 ANFIS Desired Displacement vs. Output Voltage Model

An optimum displacement-voltage ANFIS model includes an input with an optimum time-shift stamp. Although optimum models require many steps, the first step is to create large data sets with different time-shift values. Each data set has two inputs; one is the displacement at time t and the other at time $t+n$. By intuition, the domain of the time-shift value is assumed to lie in an interval of [-4 4]. For all the models with different time-shift values, twenty initial membership functions and a corresponding rule base is created by a Fuzzy C-clustering algorithm in MATLAB. The parameters of all these models were tuned by training them with the experimental data sets and the final error of each of these models is noted. The RMSE of these models is plotted in Figure 4.12. This plot shows that the ANFIS model with a time-shift value of 2.6 sec has a minimum error. The input data with optimum value of time-shift is plotted in Figure 4.13.

The next step is to optimize the number of membership functions required to model this hysteretic system. In general, with a greater number of membership functions, the error of the model is reduced and predictive properties are increased, but at the same time, the interpolation properties are also degraded. Thus, to develop a better predictive model, a grid clustering method is employed to reduce the number of membership functions, and at

the same time, increase the number of fuzzy if-then rules. As the behavior of this data set is determined by Fuzzy-C clustering method, it is safe to use any other clustering method to optimize the number of rules and membership functions. The effect membership functions on the RMSE of the model is plotted in Figure 4.14. The results of an ANFIS model with 15 membership functions and 225 rules is plotted in Figure 4.15 and Figure 4.16. The results of the model for a new validation data set is plotted in Figure 4.17. This plot ascertains the number of membership functions and the interpolation properties of this model.

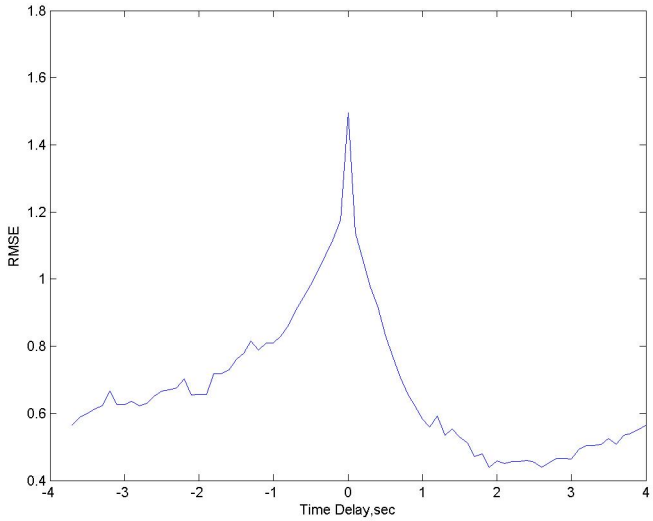

Figure 4.12: Effect of time-shift on multi-loop ANFIS displacement vs. voltage model

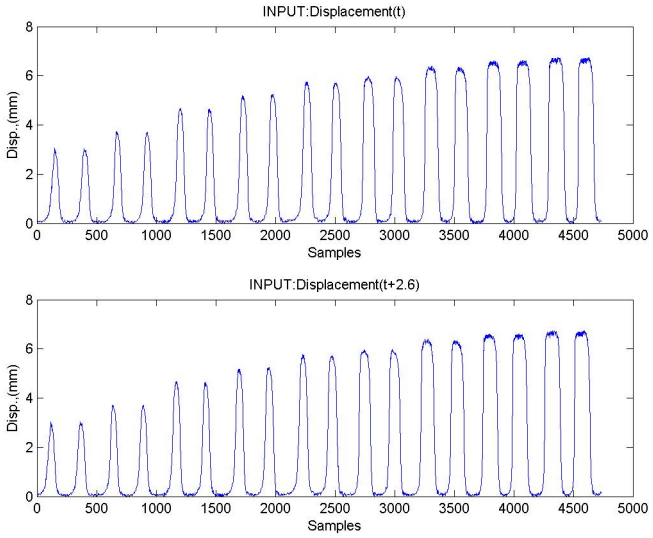

Figure 4.13: Inputs of optimized multi-loop ANFIS displacement vs. voltage model

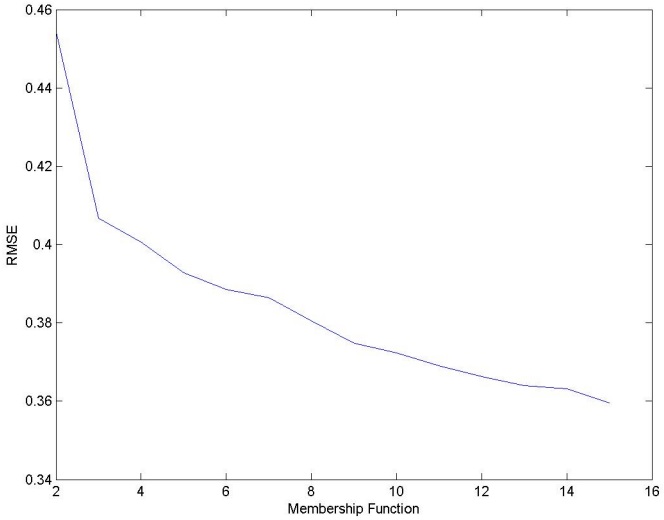

Figure 4.14: Influence of membership functions on multi-loop ANFIS displacement vs. voltage model

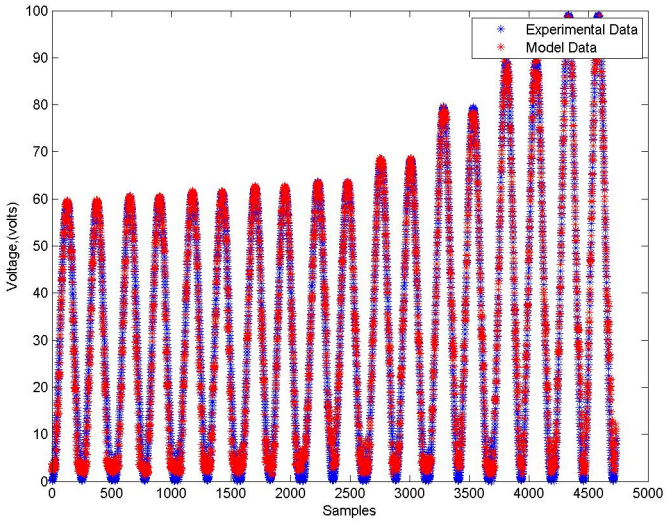

Figure 4.15: Comparison of ANFIS predicted voltage with experimental data

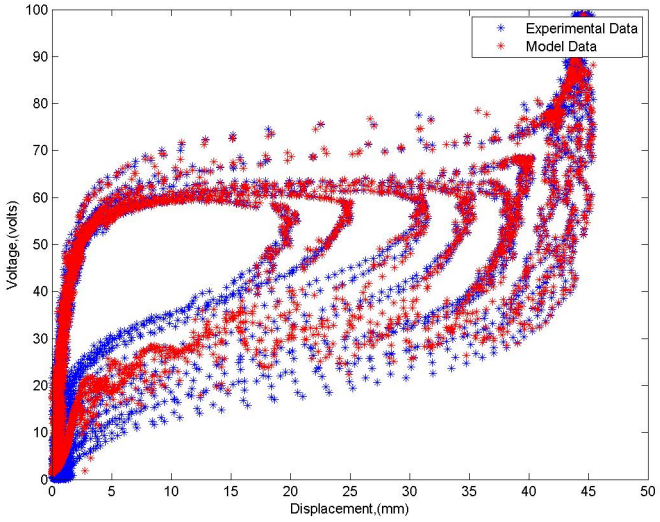

Figure 4.16: Multi-loop displacement vs. output voltage hysteresis

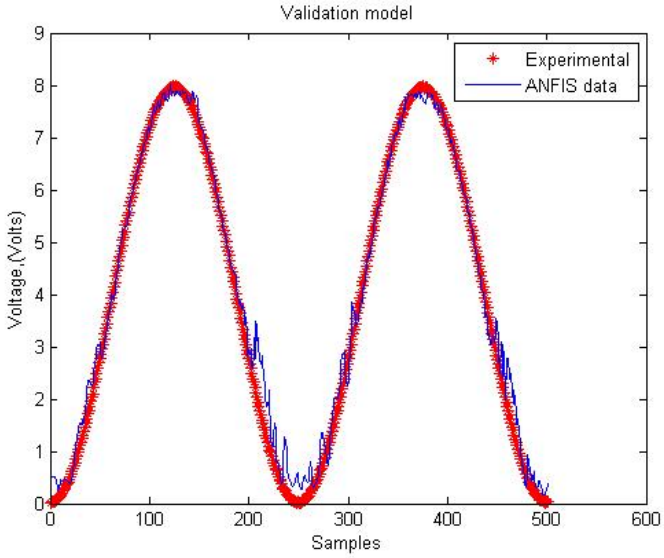

Figure 4.17: Validation of multi-loop ANFIS displacement vs. voltage model

4.3.2 ANFIS Feedback Temperature vs. Displacement Model

A similar procedure is followed in obtaining the temperature-displacement model. Initially various data sets are created for different time-delay values. As this is model is stationed in the feedback line, the time-shift values are chosen to be in a domain of $[-4\ 0]$ sec. Initial fuzzy membership functions are created using Fuzzy-C clustering algorithm. The predictive nature of these models is plotted in Figure 4.18. The RMSE error of different models decreases as time-delay increases from 0 to 4 sec. The time-shift value corresponding to a minimum error model is chosen. Input temperature vectors time-shifted by 3.4 sec is plotted in Figure 4.19. The next step is to optimize the number of membership functions and a fuzzy rule-base. Using a grid partitioning algorithm in MATLAB, a variation of RMSE with MFs is computed and those results are shown in Figure 4.20. An ANFIS model with 225 fuzzy if-then rules and 15 membership functions has a RMSE of 0.34 mm after 150 epochs. The ANFIS predicted displacement is compared with the experimental displacement values in Figure 4.21. This model is able to capture and learn the nonlinearities present in the temperature- displacement relationship. The hysteretic curve is plotted in Figure 4.22. The results of the model for a new set of validation data points is plotted in Figure 4.23. This plot ascertains the choice of number of membership functions and the interpolation properties of this model.

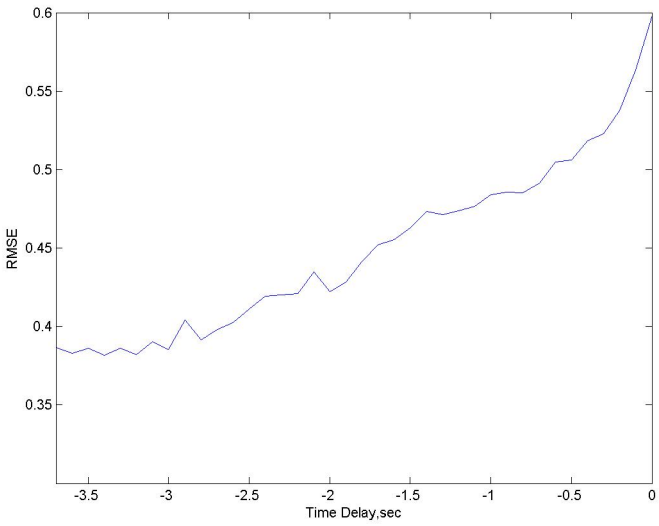

Figure 4.18: Effect of time-shift on multi-loop ANFIS temperature vs. displacement model

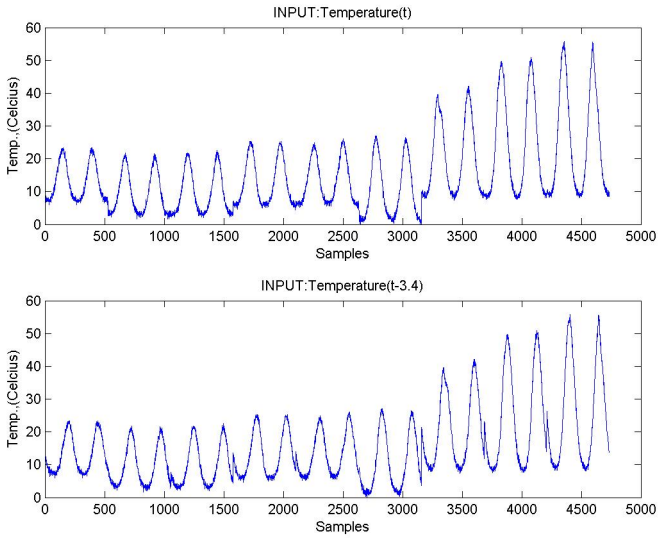

Figure 4.19: Inputs of optimized multi-loop ANFIS temperature vs. displacement model

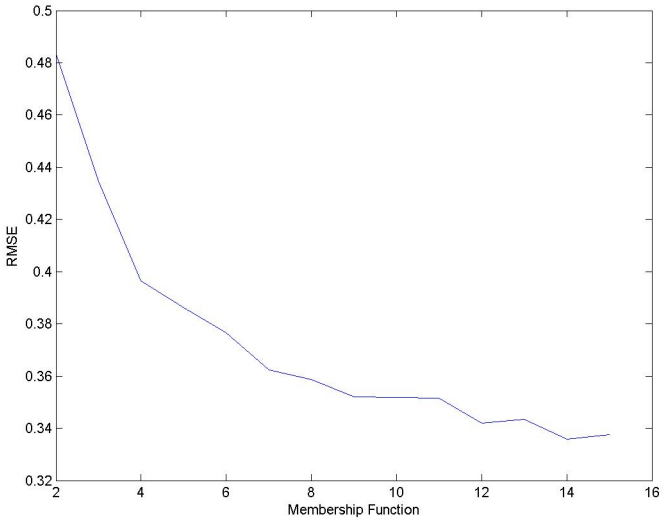

Figure 4.20: Influence of membership functions on multi-loop ANFIS temperature vs. displacement model

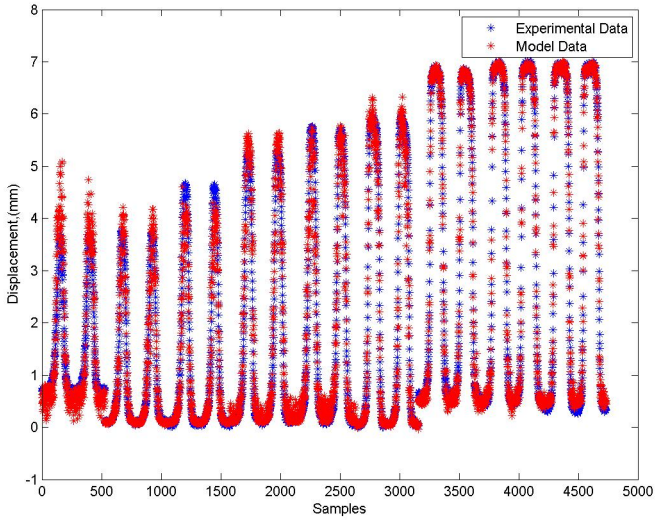

Figure 4.21: Comparison of ANFIS predicted displacement with experimental data

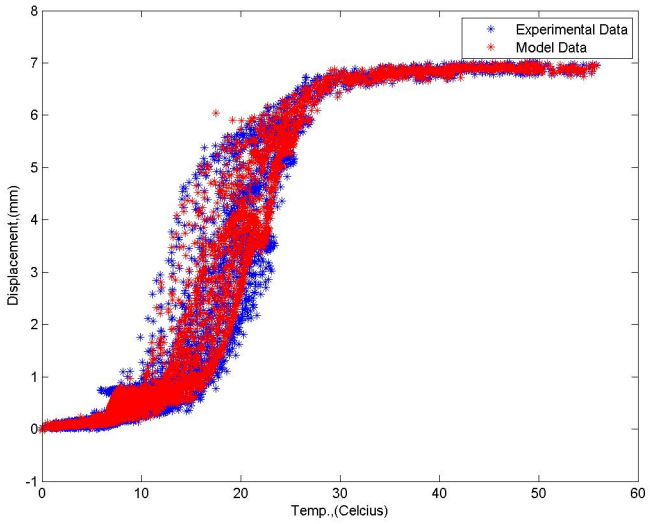

Figure 4.22: Multi-loop displacement vs. output displacement hysteresis

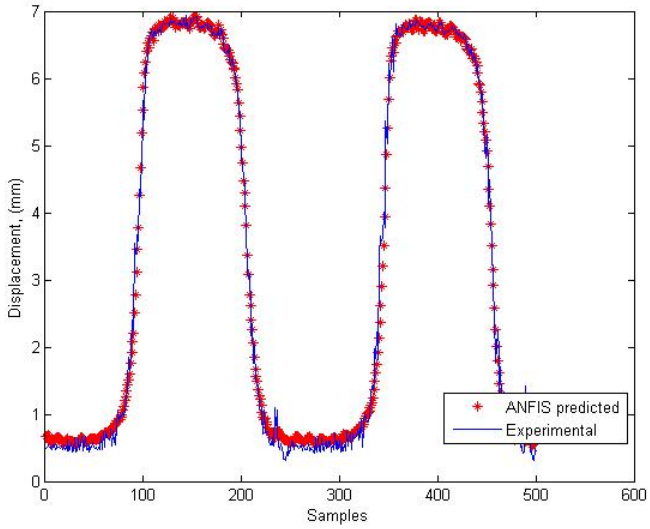

Figure 4.23: Validation of multi-loop ANFIS temperature vs. displacement model

4.4 Effect of Time-Shift on Multi-Loop Hysteresis - Frequency variation

Multiple hysteresis curves are experimentally obtained by driving the experimental setup at various frequencies of a voltage signal supplied to the system. To represent the complete dynamics of the input-output space, data sequences are selected from a large pool of experimental data. Previous ANFIS models have shown that a smart choice of the time-shift value results in a better predictive model. ANFIS models with different time-shift values are modeled for a system in which the driving frequency is varying and the amplitude is constant. An ANFIS displacement - voltage model and an ANFIS temperature - displacement models are presented in this section.

4.4.1 ANFIS Desired Displacement vs. Output Voltage Model

A similar modeling procedure is followed in order to determine the optimum time-shift value for the displacement-voltage model. The errors recorded for different time-shift models are plotted in Figure 4.24. This plot shows that the displacement signal time shifted by 0.8 sec gives the best model with the lowest RMSE. Using this value, the input vectors based on which ANFIS model is developed are plotted in 4.25. As the frequencies of these systems are different, the width of each of these pulses is different. RMSE reduces as the parameters of this ANFIS model with 15 membership functions and 225 fuzzy if-then rules are tuned. The variation of RMSE with iterations is plotted in Figure 4.26. ANFIS predicted voltage signal is plotted along with the experimental data points in Figure 4.27. This trained ANFIS model is able to track and capture the dynamics between displacement and voltage. Although the ANFIS predicted data is able to track the hysteretic curve shown in Figure 4.28, some amount of noise is seen at the lower voltage ranges. This is due to the large density of data points at the lower ranges of voltage than when the pendulum is in motion.

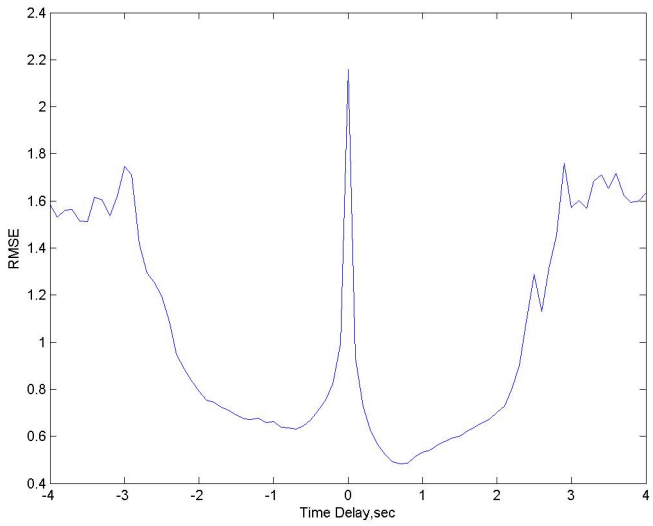

Figure 4.24: Effect of time-shift on multi-loop ANFIS displacement vs. voltage model

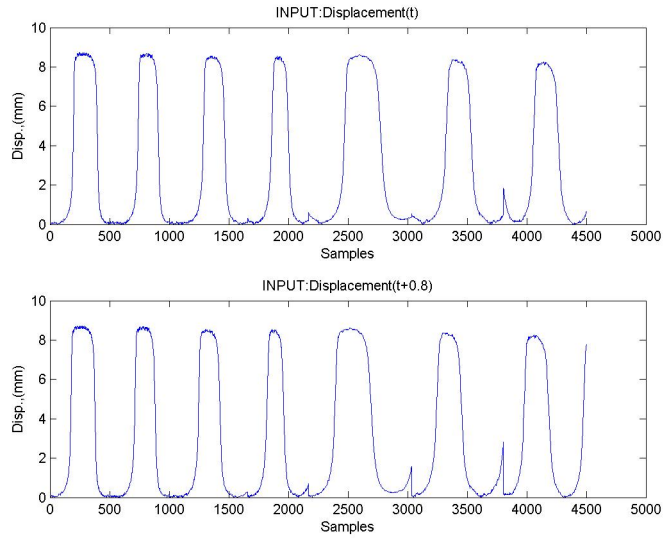

Figure 4.25: Inputs of optimized multi-loop ANFIS displacement vs. voltage model

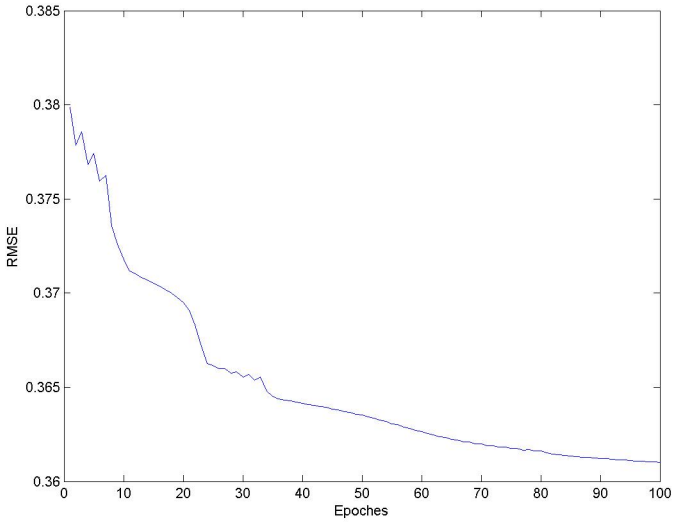

Figure 4.26: Influence of epochs on multi-loop ANFIS displacement vs. voltage model

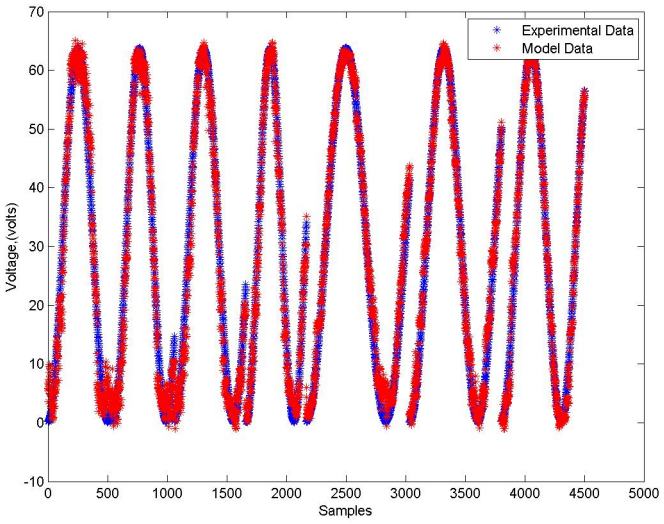

Figure 4.27: Comparison of ANFIS predicted voltage with experimental data

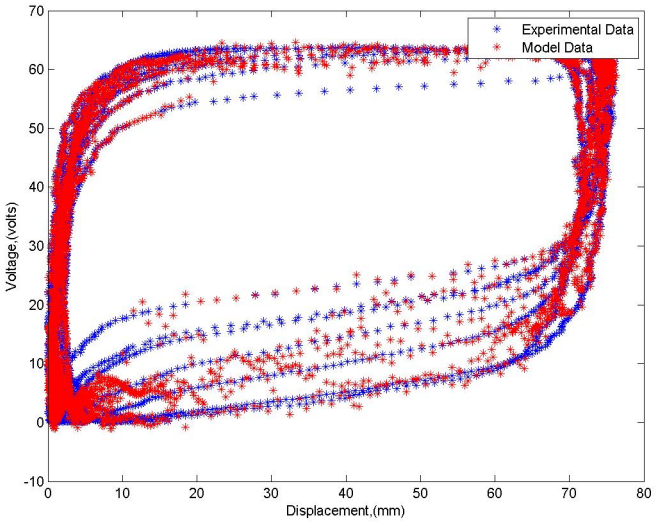

Figure 4.28: Multi-loop displacement vs. output voltage hysteresis

4.4.2 ANFIS Feedback Temperature vs. Displacement Model

As explained in previous models, the amplitude of the voltage signal is kept constant during generation of the data required by this model. Multi-input-single-output models with time-delayed temperature signals are used as inputs to predict the displacement of the pendulum. The optimum time-shift values are obtained by creating and evaluating numerous ANFIS models. The influence of time-delay on the prediction capabilities of this model is displayed in Figure 4.29. This plot shows that an optimum ANFIS model is possible when the input temperature signals are -1.1 sec apart. This time-delay value is used to build an optimum temperature-displacement model with 196 fuzzy if-then rules and fourteen membership functions. The predictions of this optimum temperature–displacement model are displayed in Figure 4.32 and Figure 4.33. This ANFIS model is able to track and predict the path followed by the pendulum using temperature histories of the SMA wire as inputs with reasonably good accuracy.

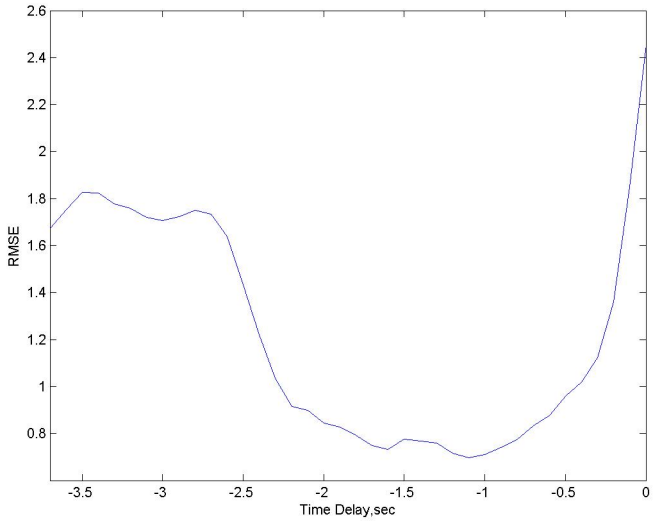

Figure 4.29: Effect of time-shift on multi-loop ANFIS temperature vs. displacement model

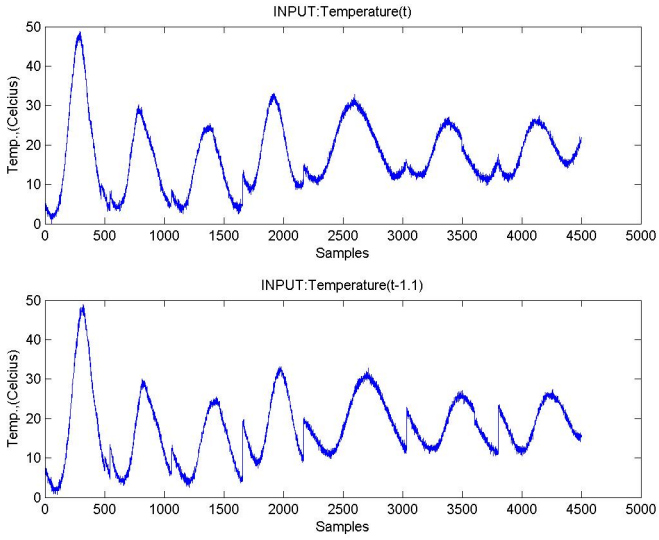

Figure 4.30: Inputs of optimized multi-loop ANFIS temperature vs. displacement model

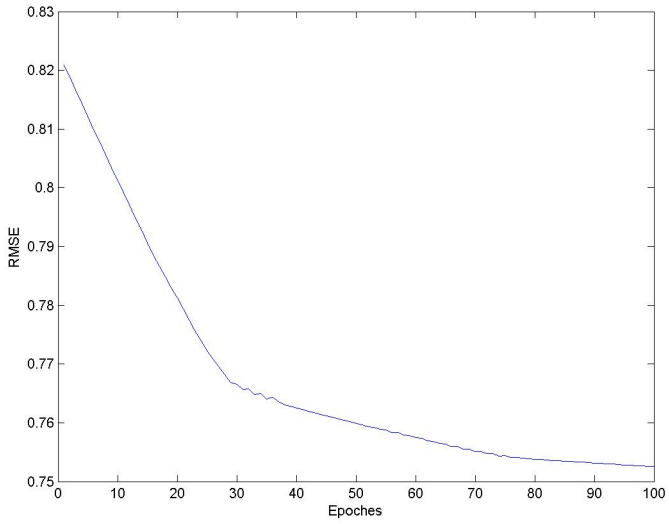

Figure 4.31: Influence of epoches on multi-loop ANFIS temperature vs. displacement model

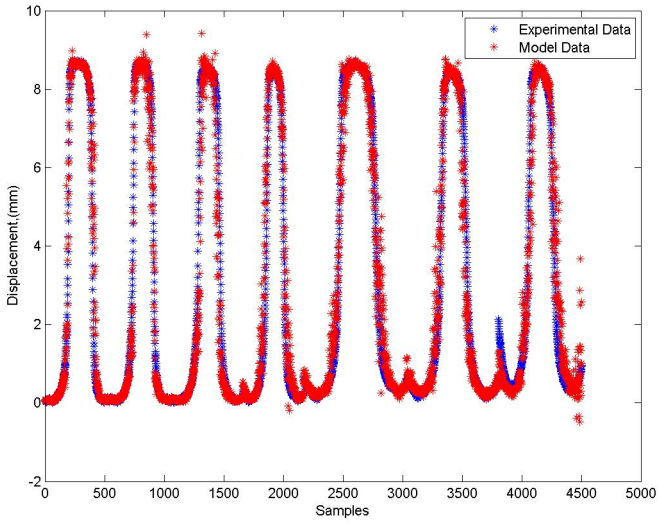

Figure 4.32: Comparison of ANFIS predicted displacement with experimental data

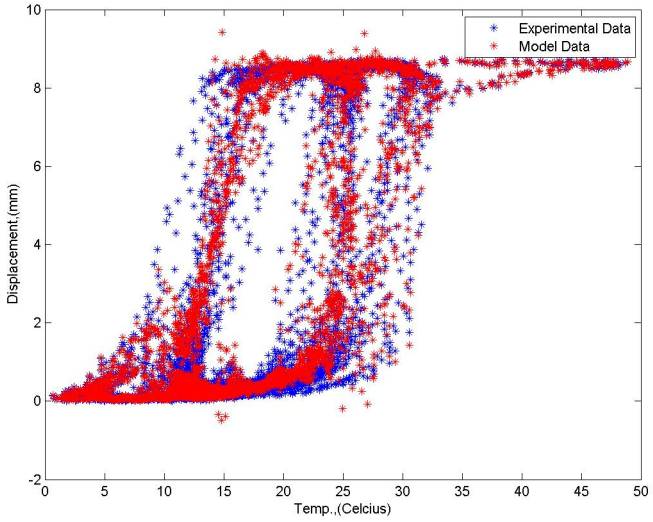

Figure 4.33: Multi-loop displacement vs. output displacement hysteresis

4.5 Experimental Validation of ANFIS Models

In order to validate the ANFIS approach of modeling hysteresis, an experiment based on the developed ANFIS models is conducted to track a path of the pendulum. As a first step, an open-loop position tracking experiment is performed. In this experiment the pendulum is required to follow the trajectory shown in Figure 4.34. Based on this trajectory and the developed optimal single-loop ANFIS displacement vs. voltage model the output voltage required to actuate the SMA wires is computed. For the inputs plotted in Figure 4.35, the output voltage is given by Figure 4.36. This voltage signal is supplied to the SMA wire.

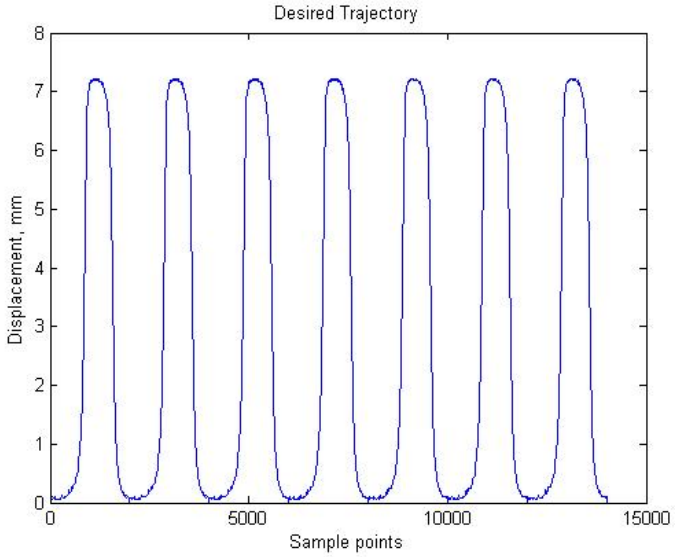

Figure 4.34: Desired trajectory of the pendulum

The change in temperature of this SMA wire is measured by an SMA-Constantan thermocouple and the actual displacement of the pendulum is determined. The actual displacement of the pendulum is compare with the desired trajectory in Figure 4.37. The correlation coefficient of this experimental data is 0.9849 . In another experiment, a PI controller is included in the feedback line to accurately track the desired trajectory. Using an auto-tuning program in LABVIEW, the proportional gain and the integral time are obtained to be 8.320 and 0.103 respectively. The bandwidth of the output voltage of the PI controller is maintained at $\pm$ 0.5 volts. The actual trajectory and the desired trajectory are plotted in Figure 4.38. The correlation coefficient of this experimental data is given by 0.9903. These results

show that a PI controller is able to improve the tracking capabilities of the an open-loop system.

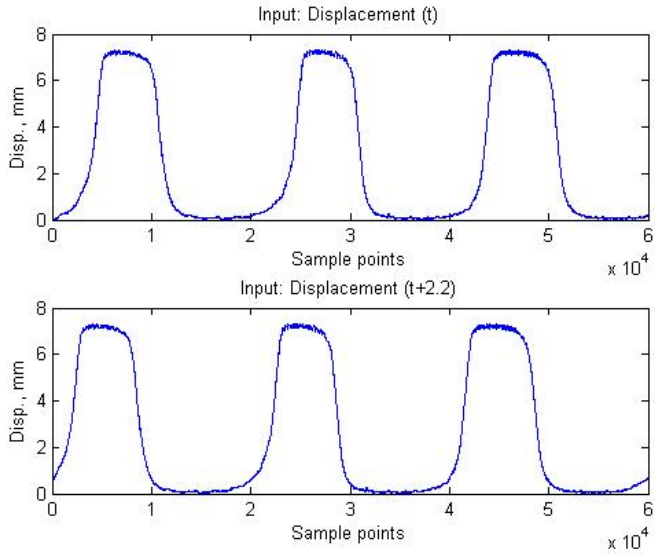

Figure 4.35: Inputs to determine voltage to the SMA wire

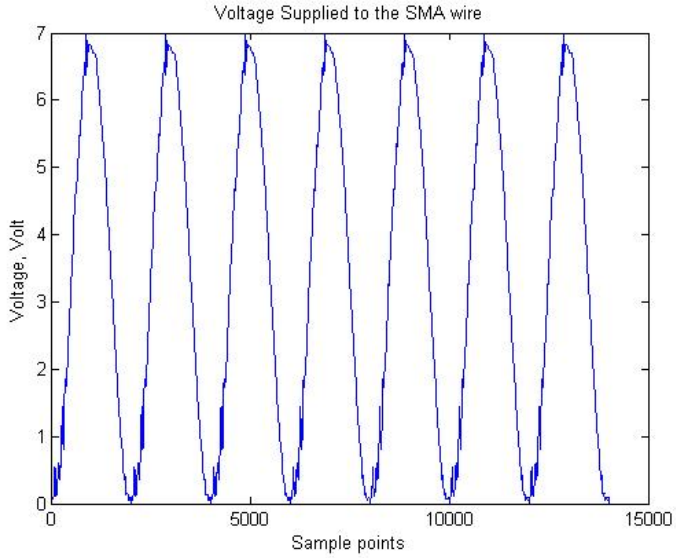

Figure 4.36: Voltage supplied to the SMA wire

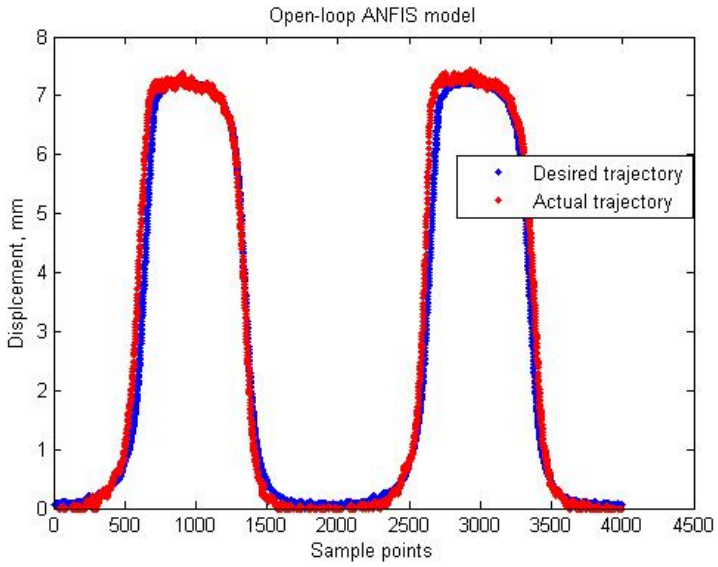

Figure 4.37: Resuts of open-loop ANFIS model

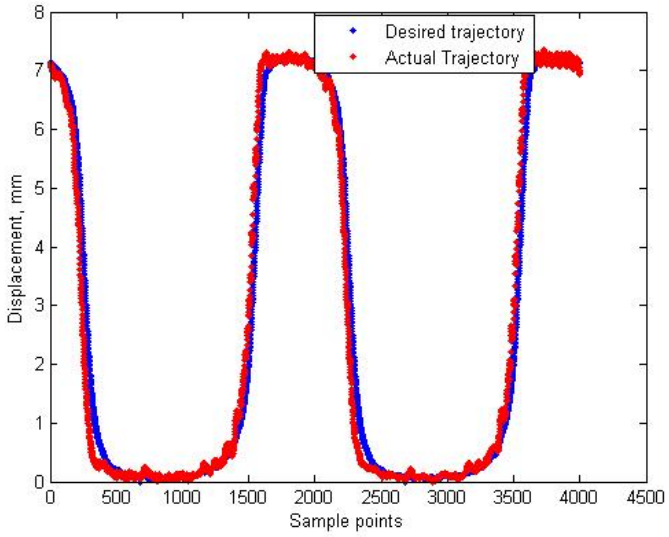

Figure 4.38: Resuts of the closed-loop ANFIS - PI model

4.6 Conclusion

Results of all the models developed in this chapter have been tabulated in Table 4.1. The striking point of this table is that for all these cases, the optimum model has a better predictive capability and a lower RMSE value than the initial one-second time-shift commonly used in ANFIS modeling.

ANFIS model	Type of model	Time-Shift	RMSE
Displacement vs. Voltage model	Amplitude variation	1 sec	0.5824 volts
		2.6 sec	0.4284 volts
	Frequency variation	1 sec	0.5317 volts
		0.8 sec	0.4863 volts
Temperature vs. Displacement model	Amplitude variation	-1 sec	0.484 mm
		-3.4 sec	0.3818 mm
	Frequency variation	-1 sec	0.7105 mm
		-1.1 sec	0.6973 mm

Table 4.1: Effect of time-shift on different ANFIS models

The optimum time-shift value for the amplitude variation models is farther from the initial guess of one second than the frequency variation models. The error improvement on modeling amplitude variation is much higher than the frequency variation. These results suggest that the time-shift has higher influence on the amplitude variation models than the frequency variation models.

Chapter 5

Conclusions

5.1 Summary and Conclusions

The principle objective of this study is to develop a sensor capable of detecting the multi-phase transformations of this material, and correlate this crystallographic change with the non-linear hysteretic response of SMA wires. A simple bi-material junction of SMAs and Constantan wires, senses temperature due to its relative thermoelectric properties. More importantly, this work has shown that an SMA-Constantan thermocouple is a capable feed-back sensor that directly measures the temperature of the system. This work established that Seebeck voltage is an able variable to detect the degree of phase transformations of the system. As Constantan is an alloy of nickel and copper, it can be welded to any nickel based SMA wire. As the present work is not specific to the composition of an SMA wire, the work can be extended for any Ni-Ti composition of an SMA wire. Similar black box modeling techniques can be utilized to study the hysteretic behavior of SMA wires of different Ni-Ti compositions. Throughout this work, the usefulness of implementing ANFIS models to study the nonlinearities of SMAs was shown. It is a black-box method of modeling the hysteretic behavior of strain characteristics of SMAs. This final chapter will give a brief overview of the research presented in this thesis and address how this work extends into self-sensing actuator.

Chapter 1 provided the motivation for this research, an overview of soft-computing methods and a brief literature survey of modeling techniques used to study the hysteresis of SMAs. Several researchers have used various techniques to model and predict the nonlinearities of

SMAs. However, each of these methods has its advantages and disadvantages and none of these methods is applicable for any mode of actuation of SMAs.

In Chapter 2, wires of SMA and Constantan were brought together to form a novel thermocouple. The Seebeck voltage developed across the thermocouple due to change in tip temperature is characterized using a linear relationship at a constant room temperature. The dependence of room temperature on the Seebeck voltage tip temperature relationship is modeled. The output of the ANFIS model developed shows a good correlation with the experimental data. An inverse model is developed to simplify the setup required to use this sensor.

Chapter 3 focused on experimentally studying the strain characteristics of SMAs. The adaptive capabilities of soft-computing methods like ANFIS and ANN to model complex path dependent data sets are tested. The ANFIS and ANN models are able to capture the relationship between the temperature history data and nonlinear strain characteristics for single-loop hysteresis curves of SMA wires. The influence of amplitude and frequency of voltage signal applied to actuate an SMA wire is thoroughly explored in this chapter. ANFIS and ANN techniques model the multi-loop hysteresis cures generated by actuation of an SMA wire. The predictive capabilities of these techniques are compared to each other. An ANFIS approach showed to be more versatile in the modeling the response for all cases.

Chapter 4 explores the effect of time-shift on the predictive capabilities of various ANFIS models. The displacement vs. voltage model assumes that the positions of the pendulum at time t and t+n, are required to predict the voltage needed to actuate an SMA wire. Similarly, the temperature vs. displacement model requires temperatures at times t and t+m to predict the position of the pendulum. An optimum time-shift value is discovered for both single and multi-loop hysteretic relationships. Using this value, input vectors are created to develop the models that optimally train their properties. Finally, chapter 4 concluded by discussing the various plots of the results generated by all these optimum models.

In the present investigation, the hysteretic behavior of thin SMA wires with respect to temperature is studied. In this work, the stress of the SMA wires is maintained constant by suspending a fixed load on the SMA wire. The different models developed in this thesis do

not consider the effect of variation of stress in the SMA. Similarly, the force characteristics of an SMA wire at constant strain conditions can be modeled by utilizing the various soft-computing techniques described in this work. It is also possible to use these techniques to build hybrid strain models that include the effects of varying temperature and stress of the SMA wire. A hybrid model that predicts the strain of the system would require the stress and temperature of the SMA wire as its inputs.

5.2 Future Work

In this work, it has been shown that an SMA-Constantan thermocouple is a capable sensor and can be used in real-time applications. A nonlinear relationship has been established between the tip temperature and the Seebeck voltage. Using this relation, an SMA can be used to sense temperature when coupled with Constantan. The principle idea in eliminating an external sensor can be explained with an example of a bi-morph cantilevered (clamped-free) beam configuration as illustrated in Figure 5.1.

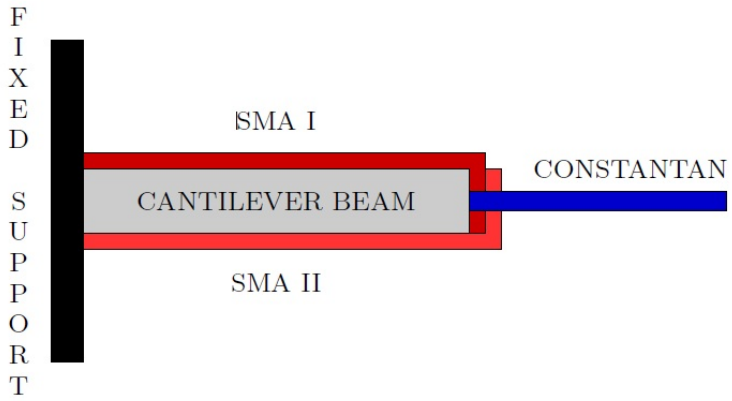

Figure 5.1: Cantilevered beam bimorph configuration

The thin layers of Shape Memory Alloy (SMA I and SMA II) cover the cantilever beam on either side, such that the cantilever and the SMAs are electrically insulated from each

other. The three layers are mechanically fastened with each other, i.e. activation of any SMA layer results in the actuation of the cantilever beam along with the other SMA layer. At the free end of the cantilever, SMA I and SMA II are in thermal contact with each other. A Constantan wire is implanted at this end of the cantilever to have an electrical contact with each SMA. This configuration allows each SMA to form two bi-material junctions with a Constantan. This bi-morph configuration, along with the linear relationship of a Seebeck voltage and Temperature, is presented as a sensorless control configuration strategy. Application of the Seebeck Voltage Temperature relation to the cantilever bi-morph is described with a flowchart in Figure 5.2.

To activate SMA I, a voltage is applied across both its ends as shown in Figure 5.3B. The resistive heating of the SMA I leads to the rise of temperature of this layer and the actuation of the cantilever beam. The change in temperature of SMA I is sensed at the SMA II-Constantan bi-material junction.

The displacement of the cantilever beam is in direct relation with the phase transformation in SMA I. The phase transformation of SMA I can be detected by measuring the temperature of SMA I. The SMA II-Constantan thermocouple pair senses the temperature change in SMA I at the free-end of the cantilever. An internal electrical field developed in the SMA II layer and the Constantan wire is due to a temperature gradient developed across the junctions. This field results in a thermoelectric emf across the free-end of the Constantan and the SMA II. The developed voltage is measured and the temperature of SMA I is obtained from the linear relation of the SMA-Constantan thermocouple pair. Using the temperature of SMA I, the SMA displacement and temperature relationship, the displacement of the cantilever beam can be determined using the system model.

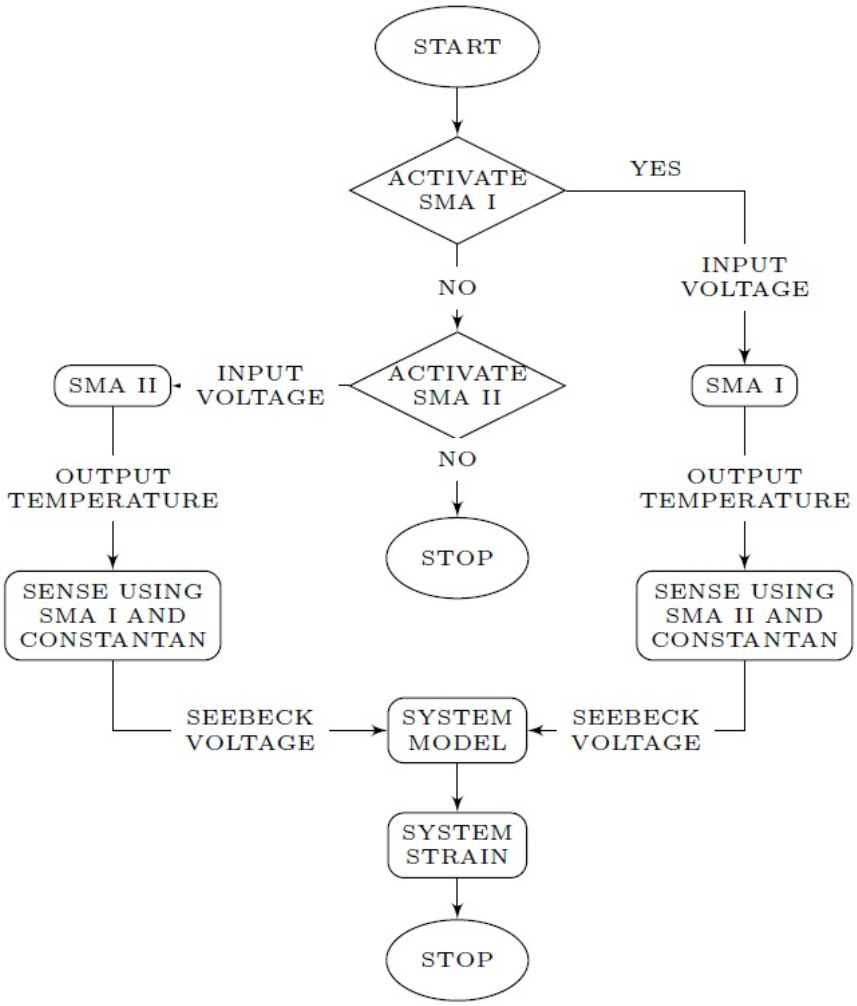

Figure 5.2: Flowchart for actuating Cantilevered beam bi-morph

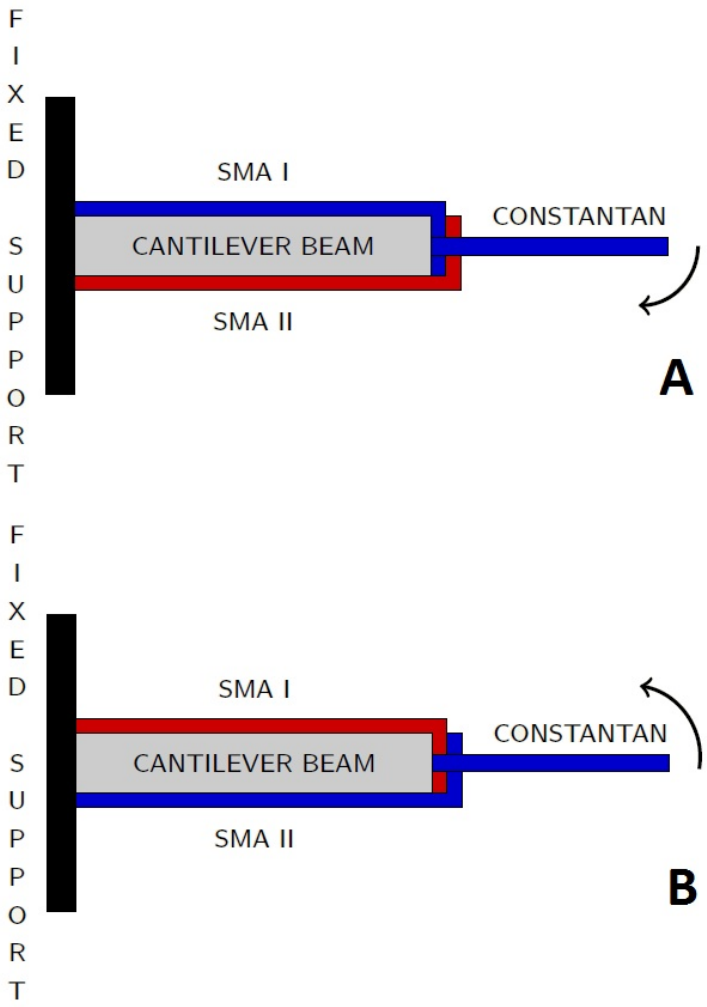

Figure 5.3: Actuator-Sensor duality of Cantilevered beam bi-morph

Appendix A

Effect of time-shift and number of memebership functions

In Chapter 4 the effect of time-shift is studied for different ANFIS models. In modelling of different hystersis curves, the optimal time-shift value is determined for fixed number of membership functions. Then, at this time-shift value the optimum mebership function is determined. This type of analysis assumes that the effect of number of membershift functions on the RMSE is near linear. This assumption is justified by studying the time-

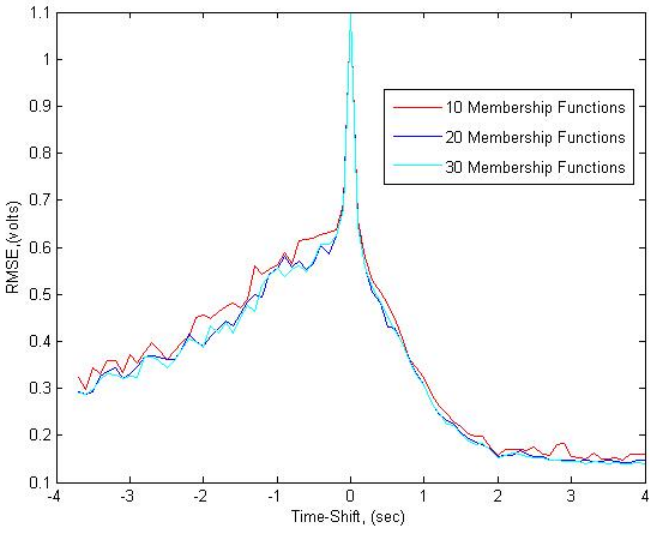

Figure A.1: Variation of RMSE time-shift and memebership functions for a single loop ANFIS displacement vs. voltage model

shift vs. RMSE relationship at different number of membership functions. Figure A.1 shows tht time-shift vs. RMSE relationship, at different memebrship functions, for a single

-loop displacement -voltage model. In this figure it can be seen that the time-shift value has a higher effect than the number of membership functions. By changing the number of memebrship functions the model is fine tuned. The trends in this figure also show that the global minimum of earch curve occurs at the same position; this showns that there is a litte effect of the number of memebrship functions on the optimum time-shift value.

Appendix B

ANFIS program

clear all

clc

close all

% ====== Input File ==========================

$names = ['Voltage06.9\_f0.05'];$

% ======Initialize Variables ======================

$INPUT1 = [];$

$INPUT2 = [];$

$OUTPUT = [];$

$INPUT = [];$

$INPUT\_1 = [];$

$OUTPUT\_1 = [];$

ii=1;

%======Time History Inputs and Output ======================

for i=1:size(names,1)

$load(name\_data(i,:))$

$[peakLoc, peakMag] =$ peakfinder($-Voltage\_select$);

$cycle\_start = peakLoc(1,1);$

$[peakLoc, peakMag] =$ peakfinder(-$Voltage\_select$);

$cycle\_end$=peakLoc(1,3)+200;

$INPUT\_11$=$Displacement\_select(1, cycle\_start : cycle\_end) - min(Displacement\_select(1, cycle\_$

$cycle\_end));$

$OUTPUT\_11 = Voltage\_select(1, cycle\_start : cycle\_end);$

aa=$resampling\_uniform(500, INPUT\_11)$;
% here the experimental data points are uniformly resampled
$ifmax(aa) > size(Voltage\_select)$
$[yyzz] = max(aa)$;
$aa(zz) = aa(zz) - 1$;
end
$INPUT\_1 = INPUT\_11(aa)$;
$OUTPUT\_1 = OUTPUT\_11(aa)$;
$INPUT1 =$ [INPUT1 INPUT_1];
$OUTPUT =$ [OUTPUT OUTPUT_1];
$INPUT = []$;
end
$INPUT2 = []$;
ii=1;
% time-shift value is defined here
$time\_shift = 1$;
$INPUT22 = Displacement\_select(1, cycle\_start+aa-1+time\_shift*100)-min(Displacement\_sel$
$aa - 1 + time\_shift * 100))$;
$INPUT2 = [INPUT2; INPUT22]$;
end
end
$INPUT =$ [INPUT INPUT2];
% plot inputs
plot(INPUT1)
hold on
plot(INPUT2,'r')
$trn\_data = [INPUT; OUTPUT]'$;
$chk\_data = trn_data$;
%======ANFIS program ======================

$min\_Input = min(min(input))$;
$min\_Output = min(min(output))$;
$input = input - ones(size(input)) * min\_Input$;

$output = output - ones(size(output)) * min\_Output;$
$max\_Input = max(max(input));$
$max\_Output = max(max(output));$
$Input = input/max\_Input;$
$Output = output/max\_Output;$
trnINPUT=Input;
trnOUTPUT=Output;
$trnDATA = [InputOutput];$
chkINPUT=Input;
chkOUTPUT=Output;
$chkDATA = [InputOutput];$
% number of memebrship functions
numMFs=20;
mfType = 'trimf';
fismatsmatemp = genfis1(trnData,numMFs,mfType);
plotfis(fismatsmatemp)
numEpochs =300;
$err\_goal = 0;$
$in\_step = 0.1;$
$step\_dec = 0.3;$
$step\_inc = 1;$
$[fismatsmatemp1, trnErr, ss, fismatsmatemp2, chkErr] = anfis(trnDATA, fismatsmatemp, [num$
trnout = evalfis(trnINPUT,fismatsmatemp2);
trnRMSE = norm(trnout-trnOUTPUT)/sqrt(length(trnout))

Bibilography

Dragan Avirovik, Ashok Kumar, Robert J Bodnar, and Shashank Priya. Remote light energy harvesting and actuation using shape memory alloy—piezoelectric hybrid transducer. *Smart Materials and Structures*, 22(5):052001, 2013. 2

S Barbarino, Salvatore Ameduri, Leonardo Lecce, et al. Wing shape control through an sma-based device. *Journal of Intelligent Material Systems and Structures*, 20(3):283–296, 2009. 3

Richard E Bellman and Lotfi Asker Zadeh. Decision-making in a fuzzy environment. *Management science*, 17(4):B–141, 1970. 10

A Bertram. Thermo-mechanical constitutive equations for the description of shape memory effects in alloys. *Nuclear engineering and design*, 74(2):173–182, 1983. 5

Victor Birman. Review of mechanics of shape memory alloy structures. *Applied Mechanics Reviews*, 50:629, 1997. 5

LC Brinson. One-dimensional constitutive behavior of shape memory alloys: thermomechanical derivation with non-constant material functions and redefined martensite internal variable. *Journal of intelligent material systems and structures*, 4(2):229–242, 1993. 5

William J Buehler, JV Gilfrich, and RC Wiley. Effect of low-temperature phase changes on the mechanical properties of alloys near composition tini. *Journal of Applied Physics*, 34 (5):1475–1477, 1963. 1

Vishalini Bundhoo, Edmund Haslam, Benjamin Birch, and Edward J Park. A shape memory alloy-based tendon-driven actuation system for biomimetic artificial fingers, part i: design and evaluation. *Robotica*, 27(01):131–146, 2009. 1

Yves Chemisky, Arnaud Duval, Etienne Patoor, and T Ben Zineb. Constitutive model for shape memory alloys including phase transformation, martensitic reorientation and twins accommodation. *Mechanics of Materials*, 43(7):361–376, 2011. 5

MF Chen, XJ Yang, RX Hu, ZD Cui, and HC Man. Bioactive niti shape memory alloy used as bone bonding implants. *Materials Science and Engineering: C*, 24(4):497–502, 2004. 1

Sheng Chen, CFN Cowan, and PM Grant. Orthogonal least squares learning algorithm for radial basis function networks. *Neural Networks, IEEE Transactions on*, 2(2):302–309, 1991. 9

Daniel Christ and Stefanie Reese. A finite element model for shape memory alloys considering thermomechanical couplings at large strains. *International Journal of solids and Structures*, 46(20):3694–3709, 2009. 5

Corneliu Craciunescu and Manfred Wuttig. Extraordinary damping of ni–ti double layer films. *Thin Solid Films*, 379(1):173–175, 2000. 3

Kathryn J De Laurentis and Constantinos Mavroidis. Mechanical design of a shape memory alloy actuated prosthetic hand. *Technology and Health Care*, 10(2):91–106, 2002. 1

Sonia Degeratu, P Rotaru, Gh Manolea, HO Manolea, and A Rotaru. Thermal characteristics of ni–ti sma (shape memory alloy) actuators. *Journal of thermal analysis and calorimetry*, 97(2):695–700, 2009. 15

Dynalloy. Technical characteristics of flexinol actuator wires, 2011. URL `http://www.dynalloy.com/pdfs/TCF1140.pdf`. 16

Jeffrey L Elman. Finding structure in time. *Cognitive science*, 14(2):179–211, 1990. 9

Dana M Elzey, Aarash YN Sofla, and Haydn NG Wadley. A shape memory-based multifunctional structural actuator panel. *International Journal of solids and Structures*, 42 (7):1943–1955, 2005. 3

Ehsan Tarkesh Esfahani and Mohammad H Elahinia. Developing an adaptive controller for a shape memory alloy walking assistive device. *Journal of vibration and control*, 16(13): 1897–1914, 2010. 1

TL Grigorie and RM Botez. New adaptive controller method for sma hysteresis modelling of a morphing wing. *Aeronautical Journal*, 114(1151):1, 2010. 6

François Guély and Patrick Siarry. Gradient descent method for optimizing various fuzzy rule bases. In *Fuzzy Systems, 1993., Second IEEE International Conference on*, pages 1241–1246. IEEE, 1993. 12

MM Gupta and DH Rao. On the principles of fuzzy neural networks. *Fuzzy sets and systems*, 61(1):1–18, 1994. 10

Martin T Hagan and Mohammad B Menhaj. Training feedforward networks with the marquardt algorithm. *Neural Networks, IEEE Transactions on*, 5(6):989–993, 1994. 9

DJ Hartl and Dimitris C Lagoudas. Aerospace applications of shape memory alloys. *Proceedings of the Institution of Mechanical Engineers, Part G: Journal of Aerospace Engineering*, 221(4):535–552, 2007. 1

Mohammed R Hassan, Fabrizio L Scarpa, and Nik Abdullah Mohamed. Shape memory alloys honeycomb: design and properties. In *Proceedings of SPIE: Smart Structures and Materials*, pages 557–564, 2004. 3

Donald Olding Hebb. *The organization of behavior: A neuropsychological theory*. Psychology Press, 2002. 7

Shigeo Hirose, Koji Ikuta, and Yoji Umetani. Development of shape-memory alloy actuators. performance assessment and introduction of a new composing approach. *Advanced Robotics*, 3(1):3–16, 1988. 2

JJ Hopfield. Neural Networks And Physical Systems With Emergent Collective Computational Abilities. *Proceedings Of The National Academy Of Sciences Of The USA-Biological Sciences*, 79(8):2554–2558, 1982. ISSN 0027-8424. doi: {10.1073/pnas.79.8.2554}. 9

S-i Horikawa, Takeshi Furuhashi, and Yoshiki Uchikawa. On fuzzy modeling using fuzzy neural networks with the back-propagation algorithm. *Neural Networks, IEEE Transactions on*, 3(5):801–806, 1992. 10

J-SR Jang. Anfis: Adaptive-network-based fuzzy inference system. *Systems, Man and Cybernetics, IEEE Transactions on*, 23(3):665–685, 1993. 10

Jyh-Shing Roger Jang, Chuen-Tsai Sun, and Eiji Mizutani. Neuro-fuzzy and soft computing-a computational approach to learning and machine intelligence [book review]. *Automatic Control, IEEE Transactions on*, 42(10):1482–1484, 1997. 10

Atilla Kilicarslan, Gangbing Song, and Karolos Grigoriadis. Anfis based modeling and inverse control of a thin sma wire. In *The 15th International Symposium on: Smart Structures and Materials & Nondestructive Evaluation and Health Monitoring*, pages 69260H–69260H. International Society for Optics and Photonics, 2008. 6

Atilla Kilicarslan, Gangbing Song, and Karolos M Grigoriadis. Modeling and hysteresis compensation in a thin sma wire using anfis methods. *Journal of Intelligent Material Systems and Structures*, 22(1):45–57, 2011. 6

M Kohl, D Dittmann, E Quandt, and B Winzek. Thin film shape memory microvalves with adjustable operation temperature. *Sensors and Actuators A: Physical*, 83(1):214–219, 2000. 2

Peter Krulevitch, Abraham P Lee, Philip B Ramsey, James C Trevino, Julie Hamilton, and M Allen Northrup. Thin film shape memory alloy microactuators. *Microelectromechanical Systems, Journal of*, 5(4):270–282, 1996. 3

Akihiko Kumagai, Paul A Hozian, and Michael Kirkland. Neurofuzzy-model-based feedback controller for shape memory alloy actuators. In *SPIE's 7th Annual International Symposium on Smart Structures and Materials*, pages 291–299. International Society for Optics and Photonics, 2000. 6

Dimitris C Lagoudas, Pavlin B Entchev, Peter Popov, Etienne Patoor, L Catherine Brinson, and Xiujie Gao. Shape memory alloys, part ii: Modeling of polycrystals. *Mechanics of Materials*, 38(5):430–462, 2006. 5

Jinoh Lee, Maolin Jin, and Kyoung Kwan Ahn. Precise tracking control of shape memory alloy actuator systems using hyperbolic tangential sliding mode control with time delay estimation. *Mechatronics*, 2013. 6

K. Levenberg. A method for the solution of certain nonlinear problems in least squares. *Quarterly of Applied Mathematics 2*, pages 164–168, 1944. 7

Valery I Levitas and Istemi B Ozsoy. Micromechanical modeling of stress-induced phase transformations. part 1. thermodynamics and kinetics of coupled interface propagation and reorientation. *International Journal of Plasticity*, 25(2):239–280, 2009. 5

Chen Liang and CA Rogers. One-dimensional thermomechanical constitutive relations for shape memory materials. *Journal of intelligent material systems and structures*, 1(2): 207–234, 1990. 5

Richard Lippmann. An introduction to computing with neural nets. *ASSP Magazine, IEEE*, 4(2):4–22, 1987. 7

N Ma, G Song, and HJ Lee. Position control of shape memory alloy actuators with internal electrical resistance feedback using neural networks. *Smart materials and structures*, 13 (4):777, 2004. 6

Shigeo Maeda, Kazuhiro Abe, Keisuke Yamamoto, Osamu Tohyama, and Hirotaka Ito. Active endoscope with sma (shape memory alloy) coil springs. In *Micro Electro Mechanical Systems, 1996, MEMS'96, Proceedings.'An Investigation of Micro Structures, Sensors, Actuators, Machines and Systems'. IEEE, The Ninth Annual International Workshop on*, pages 290–295. IEEE, 1996. 2

Ebrahim H Mamdani and Sedrak Assilian. An experiment in linguistic synthesis with a fuzzy logic controller. *International journal of man-machine studies*, 7(1):1–13, 1975. 10

Donald W Marquardt. An algorithm for least-squares estimation of nonlinear parameters. *Journal of the Society for Industrial & Applied Mathematics*, 11(2):431–441, 1963. 9

MATWORKS. Matlab user's guide. *Inc., Natick, MA*, 5, 1998. 20

Warren S McCulloch and Walter Pitts. A logical calculus of the ideas immanent in nervous activity. *The Bulletin of Mathematical Biophysics*, 5(4):115–133, 1943. 7

A Menciassi, Jong H Park, S Lee, S Gorini, P Dario, and Jong-Oh Park. Robotic solutions and mechanisms for a semi-autonomous endoscope. In *Intelligent Robots and Systems, 2002. IEEE/RSJ International Conference on*, volume 2, pages 1379–1384. IEEE, 2002. 2

A Menciassi, S Gorini, G Pernorio, and P Dario. A sma actuated artificial earthworm. In *Robotics and Automation, 2004. Proceedings. ICRA'04. 2004 IEEE International Conference on*, volume 4, pages 3282–3287. IEEE, 2004. 2

NB Morgan. Medical shape memory alloy applications—the market and its products. *Materials Science and Engineering: A*, 378(1):16–23, 2004. 1

Robert K Morgan and John R Yaeger. Self-regulated actuator, June 18 1985. US Patent 4,524,343. 2

Etienne Patoor, Dimitris C Lagoudas, Pavlin B Entchev, L Catherine Brinson, and Xiujie Gao. Shape memory alloys, part i: General properties and modeling of single crystals. *Mechanics of Materials*, 38(5):391–429, 2006. 5

H Petryk and S Stupkiewicz. Interfacial energy and dissipation in martensitic phase transformations. part i: Theory. *Journal of the Mechanics and Physics of Solids*, 58(3):390–408, 2010. 5

Peter Popov and Dimitris C Lagoudas. A 3-d constitutive model for shape memory alloys incorporating pseudoelasticity and detwinning of self-accommodated martensite. *International Journal of Plasticity*, 23(10):1679–1720, 2007. 5

AD Price, A Jnifene, and HE Naguib. Design and control of a shape memory alloy based dexterous robot hand. *Smart Materials and Structures*, 16(4):1401, 2007. 1

F. Rosenblatt. *Principles of neurodynamics: perceptrons and the theory of brain mechanisms*. Report (Cornell Aeronautical Laboratory). Spartan Books, 1962. URL `http://books.google.ca/books?id=7FhRAAAAMAAJ`. 7

Carl F Ruoff. Memory metal actuator, November 19 1985. US Patent 4,553,393. 38

Danuta Rutkowska. *Neuro-fuzzy architectures and hybrid learning*, volume 85. Physica Verlag, 2002. 12

Jorma Ryhänen. *Biocompatibility evaluation of nickel-titanium shape memory metal alloy.* Oulun yliopisto, 1999. 1

Brian Selden, Kyujin Cho, and H Harry Asada. Segmented shape memory alloy actuators using hysteresis loop control. *Smart materials and structures*, 15(2):642, 2006. 3

Nagahico Shinjo and Geoffrey W Swain. Use of a shape memory alloy for the design of an oscillatory propulsion system. *Oceanic Engineering, IEEE Journal of*, 29(3):750–755, 2004. 1

G Song, V Chaudhry, and C Batur. A neural network inverse model for a shape memory alloy wire actuator. *Journal of intelligent material systems and structures*, 14(6):371–377, 2003a. 6

G Song, V Chaudhry, and C Batur. Precision tracking control of shape memory alloy actuators using neural networks and a sliding-mode based robust controller. *Smart materials and structures*, 12(2):223, 2003b. 6

Nguyen Trong Tai and Kyoung Kwan Ahn. A hysteresis functional link artificial neural network for identification and model predictive control of sma actuator. *Journal of Process Control*, 22(4):766–777, 2012. 6

Xiaobo Tan and John S Baras. Adaptive identification and control of hysteresis in smart materials. *Automatic Control, IEEE Transactions on*, 50(6):827–839, 2005. 6

Kikuaki Tanaka. A thermomechanical sketch of shape memory effect: one-dimensional tensile behavior. *Res Mech.*, 18(3):251–263, 1986. 5

J Uchil, KP Mohanchandra, KK Mahesh, and K Ganesh Kumara. Thermal and electrical characterization of r-phase dependence on heat-treat temperature in nitinol. *Physica B: Condensed Matter*, 253(1):83–89, 1998. 6

CM Wayman, I Cornelis, and K Shimizu. Transformation behaviour and the shape memory in thermally cycled tini. *SCR METALL*, 6(2):115–122, 1972. 6

Bernard Widrow and Michael A Lehr. 30 years of adaptive neural networks: perceptron, madaline, and backpropagation. *Proceedings of the IEEE*, 78(9):1415–1442, 1990. 9

I Yoshida, T Ono, and M Asai. Internal friction of ti–ni alloys. *Journal of alloys and compounds*, 310(1):339–343, 2000. 15, 16

Lotfi A Zadeh. Outline of a new approach to the analysis of complex systems and decision processes. *Systems, Man and Cybernetics, IEEE Transactions on*, 3(1):28–44, 1973. 10

Lotfi Asker Zadeh. Fuzzy sets. *Information and control*, 8(3):338–353, 1965. 10

Lotfi Asker Zadeh. The concept of a linguistic variable and its application to approximate reasoning—i. *Information sciences*, 8(3):199–249, 1975. 10

A Ziolkowski. Three-dimensional phenomenological thermodynamic model of pseudoelasticity of shape memory alloys at finite strains. *Continuum Mechanics and Thermodynamics*, 19(6):379–398, 2007. 5